博士論文

Design of a Novel Load Frequency Controller for EV Aggregators

(EV アグリゲーターのための新たな系統負荷周波数制御手法の設計)

令和 3 年 6 月 1 日提出

指導教員　松橋　隆治教授

東京大学大学院工学系研究科

電気系工学専攻

37-187181

蔡　思楠

THE UNIVERSITY OF TOKYO

DOCTORAL DISSERTATION

Design of a Novel Load Frequency Controller for EV Aggregators

---

Author:
Sinan CAI

Supervisor:
Prof. Ryuji MATSUHASHI

A dissertation submitted in fulfillment of the requirements for the degree of Doctor of Philosophy

in the

Matsuhashi Laboratory
Department of Electrical Engineering and Information Systems

August 6, 2021

Declaration of Authorship

I, Sinan CAI, declare that this dissertation titled, "Design of a Novel Load Frequency Controller for EV Aggregators" and the work presented in it are my own. I confirm that:

- This work was done wholly or mainly while in candidature for a research degree at this University.
- Where any part of this dissertation has previously been submitted for a degree or any other qualification at this University or any other institution, this has been clearly stated.
- Where I have consulted the published work of others, this is always clearly attributed.
- Where I have quoted from the work of others, the source is always given. With the exception of such quotations, this thesis is entirely my own work.
- I have acknowledged all main sources of help.
- Where the dissertation is based on work done by myself jointly with others, I have made clear exactly what was done by others and what I have contributed myself.

Date: May 31st, 2021

Abstract

In recent years, a large amount of renewable energy sources (RES) has been installed into power systems. However, the large integration of RES generation tends to cause frequency stability problems in power systems. To deal with these problems, power systems around the world are prompted to create or reform the ancillary market for frequency regulation to invite additional regulation resources, especially from the system demand side.

The utilization of electric vehicles (EVs) is one of the most prospective solutions in frequency regulation especially in the load frequency control (LFC) domain because of the fast-response characteristics of the EV batteries. Since the power level of a single EV is small, the EVs must be aggregated to participate in LFC. The EV aggregator is expected to receive a control signal sent by the control center of the local system operator and dispatch the signal to every single EV in the aggregation. There are two problems for the EV aggregator under this operation: firstly, the transmission and processing of the single will cause communication delay; secondly, how to dispatch the received LFC signal to the aggregated EVs.

The novel load frequency control scheme for EV aggregators proposed in this dissertation consists of two parts: delay compensation control and optimal dispatching control. The former aims at compensating for the communication delay of LFC signal in a power system, while the latter is to search for an optimal dispatching control strategy that maximizes the revenue from the LFC regulation market. An adaptive control scheme is used to generate a delay-compensated control signal, and the optimal dispatching control strategy is obtained with a novel modified genetic algorithm. The two parts are bonded together in a model predictive control scheme with a SARIMA prediction model on LFC market price for real-time operation. With the proposed control scheme, the performance of EV aggregators in LFC can be improved. The EV aggregators could earn more benefits and become more competitive in the frequency regulation market, while the system frequency stability could be better secured.

Keywords: Electric vehicle (EV), frequency regulation, load frequency control (LFC), renewable energy, communication delay, vehicle to grid (V2G) control.

Acknowledgements

First and foremost, I would like to express my deepest and most sincere gratitude to my supervisor, Prof. Ryuji Matsuhashi, for his kind instructions and invaluable advice. The research works in this dissertation would not have been accomplished successfully without his continuous help and guidance. Being able to work and study under his supervision was a great privilege and honor.

I would like to extend my heartfelt appreciation to all the lab members, secretaries, and staffs for providing great assistance to my researches: Furuta-san, Nishiura-san, Wang-san, Xie-san, Tien-san, Sunny-san, Okina-kun, Iwamoto-kun, Onoda-kun, Yoneda-kun, Okuyama-kun, Zhang-kun, Matsubara-kun, Matsufuji-kun, Liu-kun, Rahul-kun, Watanabe-san, Matsumoto-san, Fukushima-san, and Nishigawa-san. It was a great pleasure to have them by my side during the long period of studying and researching.

Besides, I am genuinely grateful to my family and old friends for their support, encouragement, and company.

Moreover, I wish to express my thanks to all the members of FGA, for showing me how fun and passionate life can be. The energy and friendship I received from FGA have always been my driving force.

Finally, my special thanks go to CHiCO, the vocalist of my favorite band CHiCO with HoneyWorks. Her voice pulled me through the hardest time and lighted up my darkest night. I could not have come this far without all the courage and strength she gave to me.

All in all, this is the best three years of my life.

Contents

List of Figures

List of Tables

List of Abbreviations

ACE	**A**rea **C**ontrol **E**rror
ACF	**A**auto**c**orrelation **F**unction
AGC	**A**uto **G**eneration **C**ontrol
AR	**A**rea **R**equirement
BESS	**B**attery **E**nergy **S**torage **S**ystem
CCP	**C**apability **C**learing **P**rice
DR	**D**emand **R**esponse
EDC	**E**conomic **D**ispatch **C**ontrol
EV	**E**lectric **V**ehicle
FERC	**F**ederal **E**nergy **R**egulatory **C**ommission
FFC	**F**lat **F**requency **C**ontrol
GA	**G**enetic **A**lgorithm
GHG	**G**reen**h**ouse **G**as
GTCC	**G**as **T**urbine **C**ombined **C**ycle
HIL	**H**ardware-**I**n-the-**L**oop
HVDC	**H**igh **V**oltage **D**irect **C**urrent
ICT	**I**nformation **C**ommunication **T**echnology
IoT	**I**nternet **o**f **T**hings
ISO	**I**ndependent **S**ystem **O**perator
LFC	**L**oad **F**requency **C**ontrol
LNG	**L**iquefied **N**atural **G**as
LOC	**L**ost **O**pportunity **C**osts
LPF	**L**ow **P**ass **F**ilter
LTI	**L**inear **T**ime-**I**nvariant
MILP	**M**ixed **I**nteger **L**inear **P**rogramming
MPC	**M**odel **P**redictive **C**ontrol
PACF	**P**artial **A**autocorrelation **F**unction
PCP	**P**erformance **C**learing **P**rice
PFC	**P**rimary **F**requency **C**ontrol
POP	**P**referred **O**perating **P**oint
PV	**P**hoto**v**oltaic
RES	**R**enewable **E**nergy **S**ource

RMS	**R**oot **M**ean **S**quare
RMCP	**R**egulation **M**arket **C**learing **P**rice
SACE	**S**moothed **A**rea **C**ontrol **E**rror
SARIMA	**S**easonal-**A**uto**r**egressive-**I**ntegral-**M**oving-**A**verage
SISO	**S**ingle-**I**nput-**S**ingle-**O**utput
SOC	**S**tate **O**f **C**harge
TBC	**T**ie-line **B**ias **C**ontrol
UC	**U**nit **C**ommitment
V2G	**V**ehicle-to(**2**)-**G**rid

Nomenclature

a	high pass filter coefficient	
a_i	numerator parameters of the actual transfer function	
a'_i	numerator parameters of the estimated transfer function	
b	high pass filter coefficient	
b_i	denominator parameters of the actual transfer function	
b'_i	denominator parameters of the estimated transfer function	
Cap	the provided LFC regulation capacity	MW
Cap_{bid}	the bidding LFC regulation capacity	MW
Cap_k^{EV}	the LFC regulation capacity provided by the k^{th} EV	kW
d	the number of the delayed sample	
d'	the estimated number of the delayed sample	
df	frequency measurement noise	Hz
E	energy capacity of the EV battery	kWh
f	system frequency	Hz
f_0	nominal or rated system frequency	Hz
I	Identity matrix	
K	system constant	
K_p	proportional gain of PI controller	
K_i	integral gain of PI controller	
l	number of sets of equations in the least-squares model	
LFC_k	the delayed LFC signal dispatched to the k^{th} EV	kW
LFC'_k	the reconstructed LFC signal dispatched to the k^{th} EV	kW
$LFC_{req}(t_m)$	the total system fast LFC capacity requirement	MW
$LFC_{Signal_{EV}}$	the LFC signal dispatched to the EV aggregator	MW
$LFC_{Signal_{Fast}}$	the fast LFC signal	MW
m	numerator degree of the actual transfer function	
m'	numerator degree of the estimated transfer function	
n	denominator degree of the actual transfer function	
n'	denominator degree of the estimated transfer function	
n_{EV}	the number of aggregated EVs	
n_{reg}	the number of the resources participating in LFC regulation	
P	the gain matrix for adaptive parameter estimation	

$Price$	the LFC market price	\$/ΔMW
P_A	system capacity in Area A	MW
P_B	system capacity in Area B	MW
P_T	tie-line flow power	MW
P^{charge}	EV's charging power output	kW
P^{max}	EV's maximum charging power	kW
P^{reg}	EV's regulation power output	kW
P^{tot}	EV's total power output	kW
p	the participation factor	
$pole_i$	pole of the estimated transfer function	
p^{leave}	the leaving probability of an EV	
$p^{promise}$	the probability that an EV does not leave earlier	
R	droop parameter	%
$ramp$	ramp rate	p.u. min^{-1}
SOC^{ini}	EV's SOC when plugging in	%
SOC^{req}	EV's SOC requirement when plugging out	%
t^{arrive}	EV's arrival time	s
t^{leave}	EV's departure time	s
u	accuracy determinate factor for linear regression estimation	
x	noise level of the frequency measurement	
$zero_i$	zero of the estimated transfer function	
α	low pass filter coefficient	
ΔE_k^{charge}	energy change in EV battery due to scheduled charging	kWh
ΔE_k^{reg}	energy change in EV battery due to frequency regulation	kWh
Δf	system frequency deviation	Hz
$\Delta f'$	system frequency deviation with manual delay	Hz
ΔP	change in generation power	MW
ΔP_T	tie-line flow bias	MW
ΔT_p	the estimation period of linear regression	s
Δt	LFC signal sampling time	s
Δt_c	time-step of the optimal dispatching control	s
Δt_m	time-step of the LFC market bidding	s
$\Delta\omega$	speed deviation	rad
δ	delay time of the LFC signal	s
θ	estimated parameter vector	
κ	design parameter for adaptive parameter estimation	
σ_p	adjustable variable for linear regression estimation	
σ_z	adjustable variable for linear regression estimation	

ϕ	the regressor vector	
ω_0	nominal or rated speed	rad
ω_{FL}	steady-state speed at full load	rad
ω_{NL}	steady-state speed at no load	rad

Chapter 1

Introduction

1.1 General Background

1.1.1 The Growth of Renewable Energy

The demand for energy around the globe is growing rapidly. As shown in Figure 1.1, the past decade has witnessed an increase of about 10% in world total energy supply, and the trend of growth is expected to continue [1]. Nowadays, most of the energy is supplied by the non-renewable fossil fuels such as coal and oil. Apart from the potential energy crisis caused by the depletion of the fossil fuels in the near future, the burning of them also produces greenhouse gases (GHG) and air pollutions, such as CO_2, NO_x and SO_x. The emission of these GHG damages the earth's atmosphere severely, resulting in the global warming [2,3].

Similar to the total energy supply, a large amount of electricity generation around the world still relies on fossil fuels currently. The global electricity generation mix in 2018 is given in Figure 1.2 [4]. Generation from fossil fuels comprises a total of 64.2% of electricity, and such large-scale use of fossil fuels results in the exponential rise of CO_2 emission.

In contrast to fossil fuels, renewable energy sources (RES) offered clean energy from natural resources that can be constantly replenished. The energy can be produced from RES in an environmental-friendly way without emitting GHG, and more importantly, it is an alternative solution for meeting future energy demands. Generally, the increase of RES generation capacity is favorable for [5]:

- Boosting economic growth and job creation
- Limiting carbon emissions

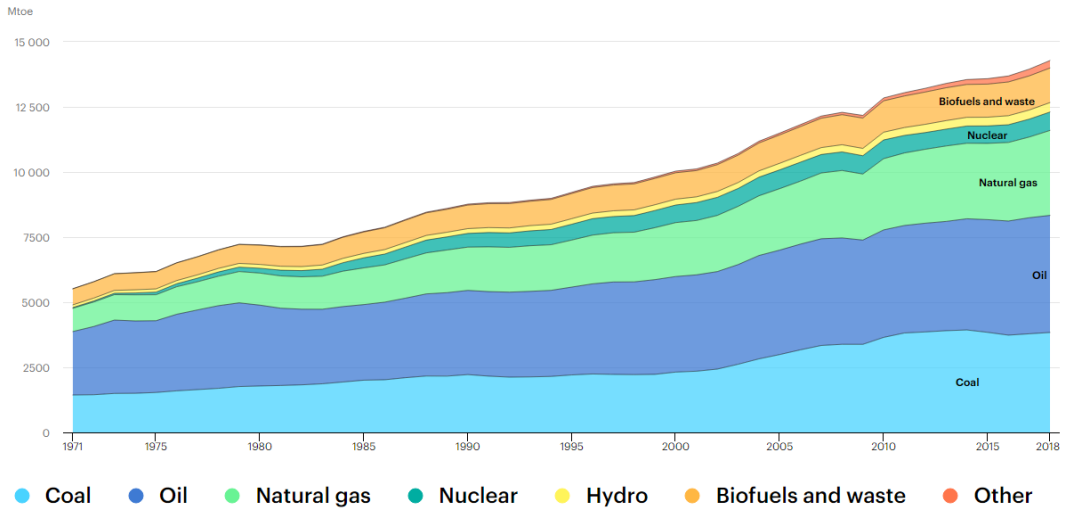

FIGURE 1.1: World total energy supply by source, 1971-2018. [1]

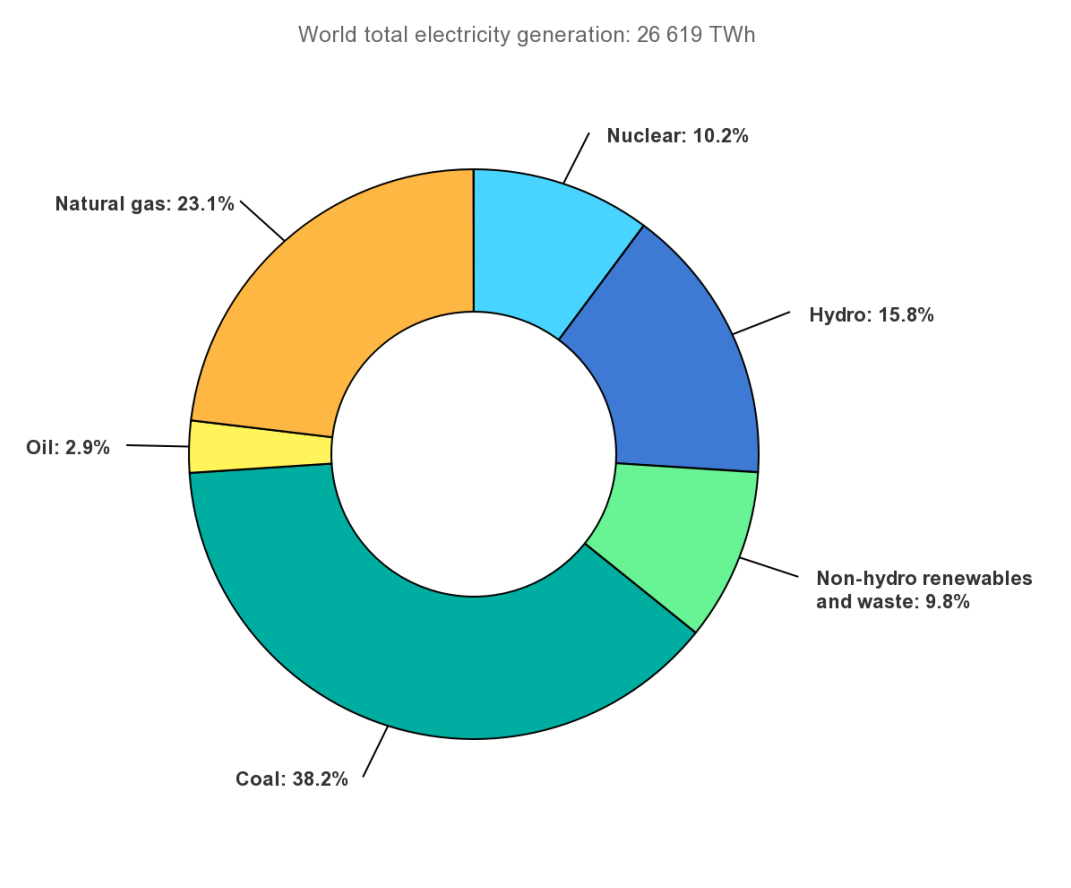

FIGURE 1.2: Global share of total energy supply by source, 2018. [4]

- Reduction of air pollution
- Expansion of energy access

Countries around the world are introducing new policies to promote the use of RES. By the end of 2017, the global RES generation capacity has reached 2,179GW, as reported in [6]. The largest share comes from hydro generation, with an installed capacity of 1,152GW. Most of the remainder is wind and solar generation, with capacities of 514GW and 390GW respectively. The rest are 529MW of marine energy, 109GW of bioenergy, and 13GW of geothermal energy. The new installation of wind energy and solar energy contributes most to the growth of RES capacity. Together, they account for 85% of the RES capacity newly installed.

Regionally, in 2017, the renewable generation has taken up 14.5% of the total electricity generation in Japan [7], and is expected to reach around 22% ~24% in 2030 [8] Meanwhile, the ratio of photovoltaic (PV) and wind generation has also reached 7.2% in the State Grid of China, in 2017, with a 30% increase in the renewable generation capacity [9]. In 2020, the share of non-hydro RES generation reached 12% in the U.S. and is expected to further increase to 16% by 2022 [10].

1.1.2 New Challenges to Power Systems

While RES is regraded essential for future energy-related problems, large integration of RES could also bring new problems to traditional power systems.

The wind turbines and PV generation, as well as some fuel cells, required power electronics, usually a grid-connected inverter, to interface with the power grid. The electric power generated by these RES is in a variable frequency or DC form. The power electronic inverters convert the electricity to AC power so that they could be injected into the grid. However, the fast controls of the power electronic inverters will introduce complex dynamics and possible resonance problems into the system [11–13]. The resonance involving energy exchange between the wind turbines and the grid might cause not only the oscillation and distortion in system voltage and current but also severe damage to the system devices. Moreover, the interfacing

power electronics consume reactive power and could affect the system voltage stability [14].

Another big challenge is the insufficiency of system inertia. The stability of a power system is defined as the ability to return to the steady-state operation after a physical disturbance occurs [15]. System inertia is one of the most important factors when considering system stability. The lower the inertia, the weaker the system stability is, and the more the system is sensitive to disturbance, especially frequency deviations [16]. Conventional thermal power plants can provide inertia to the system because they are synchronous generators with mechanical rotating mass. The wind turbines have a mechanical rotating mass, however, they cannot provide inertia to the power system due to the interfacing power electronics. PV cannot contribute to the power system either because of the lack of rotating mass in their structures [17]. Consequently, as the proportion of RES generation in the system increases, the system inertia decreases.

The most critical challenge that RES brings is the intermittent generation. In a power system, the nominal frequency is maintained by balancing the generation and the demand in real-time. Traditionally, the system operator predicts the future electricity demand and schedules the generation plan for each power plant in the system. The electricity demand is directly related to daily human activities and it is not difficult to obtain a relatively accurate prediction, especially on a large system scale where the accidental personal behavior would be smoothed. The real-time mismatch of generation and demand is compensated by controlling the power output of the generators according to the frequency deviation.

The RES generation highly depending on weather conditions such as wind speed and solar radiation is very unpredictable and uncontrollable. Therefore, when the RES penetration rate is high in a system, it becomes extremely difficult for the power system to maintain the balance between generation and load. A large amount of RES reduces the proportion of thermal plants in the system, which provides frequency regulation capacity for the system. Meanwhile, the sudden changes in RES power output caused by weather conditions result in supply and demand imbalances in a short time period, which requires the frequency regulation resources in the system to have faster ramping abilities.

Many studies have been done to examine how the RES penetration

affects system frequency stability. [18] assesses 3 scenarios of 5%, 10%, and 20% of PV penetration levels while keeping synchronous generators in the system. The simulation results show that the system frequency stability is significantly affected at 20% penetration level. In [19], it is estimated that an increase of 10GW wind capacity installation will require 126~192MW of continuous conventional frequency regulation capacity in the UK power system. Another study for Denmark and Germany shows that 6.6MW of additional regulation capacity should be provided per 1GW of installed wind capacity for maintaining the system nominal frequency [20].

Electrical energy cannot be stored on a large scale economically. When the balance between generation and load cannot be satisfied, for the safe and continuous operation of the system, the RES generation has to be curtailed. The massive amount of RES curtailment is happening worldwide as the penetration rate of RES increases, and the loss is enormous. In 2011, up to 12,300GWh of wind power generation was abandoned in “three-N region” (North, Northeast, and Northwest) windfarms in China. This takes up 16.23% of the total generation of “three-N region” windfarm and causes a loss of 6.6 billion CNY [21]. In Spain, 315GWh of wind energy is curtailed in 2020, and the curtailed electric energy (CEE) of wind energy reached around 45%~50% in Texas, the USA from January to August 2008 [22]. In Kyusyu, Japan, the average solar CEE is 3% with a peak of 13.7% in April 2019. The value of the wasted PV energy was approximately 9.6 billion JPY [23].

Efforts devoted to reducing the RES generation curtailment can be categorized into two perspectives: policies and technologies as followed [24]:

Policies

- Incentive policies for electric grid construction
- Priority dispatch generation
- Policy guidance for a well-functioning market
- Cost allocation

Technologies

- Capability of renewable energy generators

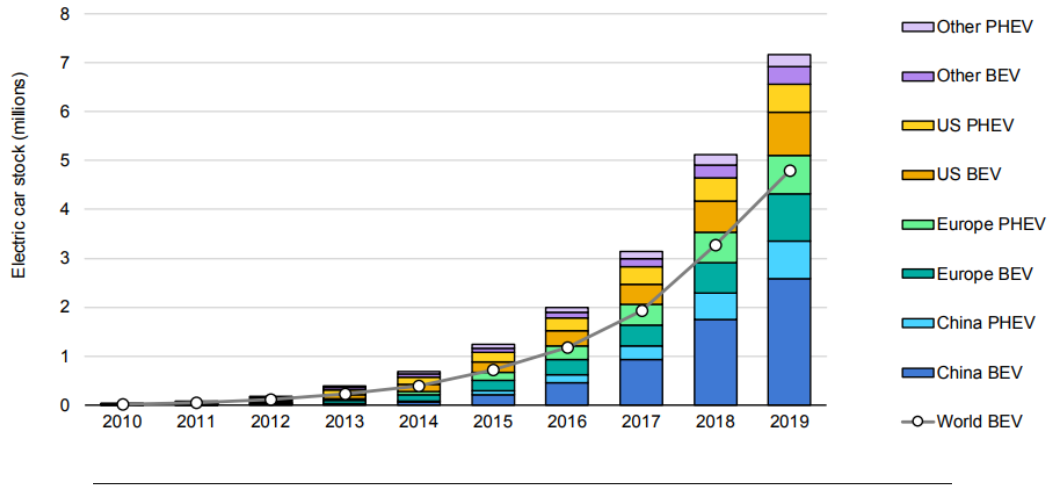

FIGURE 1.3: Global EV stock. [27]

- Power system coordinated scheduling and planning
- Energy storage technologies
- Grid-friendly technologies

1.1.3 Electric Vehicles

At present, the majority of the world's oil production is consumed by vehicles on the road [25]. The conventional internal combustion-based vehicles also contribute 27% of the total GHG emissions [26]. As a result, electric vehicles (EVs) became a popular transport option due to their potential for reducing fossil fuel usage and air pollutions.

While there were only around 17,000 EVs on road globally in 2010, by 2019 the number of EVs on the world's road has swelled to 7.2 million. The stock of plug-in hybrid electric vehicle (PHEV) and battery electric vehicle (BEV) is depicted in Figure 1.3. Even though the majority of the global stocks remain concentrated in China, Europe, and the U.S., the market shares in at least 20 countries also surpass 1% [27].

Despite the tremendous growth in EV sales over the last decade, the number of EVs still only represents 1% of the total vehicles worldwide. The electrification of vehicles is accompanied by the popularity of large and more conventional vehicles in the market. Ambitious targets and policies have been set by the government of different countries to increase the portion of

EVs in total road transportation. The targets and policies are in various forms concerning [27]:

- GHG reduction targets in transportation
- Fuel efficiency or CO_2 emission standard
- EV stock/sale targets/mandates
- Financial support to consumers and the EV industry
- Charging infrastructure deployment support and regulations

The long term vision for EV sales/stock of different countries is given in Table 1.1 [27].

Without the growth of RES generation, the charging demand of EVs will still largely depend on the generation from conventional thermal plants, hence the actual carbon emission of EVs might not be less than that of the traditional vehicles [28]. As mentioned in Section 1.1.2, maintaining generation and load balance under large RES integration is crucial for the future development and utilization of RES generation. Hence, more and faster frequency regulation resources are demanded by the traditional power system. With the certain increase of EVs in the future, the possibility for the idle EVs to provide frequency regulation capacity with their fast-response batteries to the grid as grid-friendly technology has emerged, especially in a well-designed market that welcomes the participation from the demand side. By helping the growth of RES penetration, EVs can truly reduce their carbon emission and contribute to environmental protection.

1.2 Dissertation Objective and Contributions

This dissertation proposed a novel controller design for the EV aggregators who would like to participate in the frequency regulation market. The proposed controller design is to improve the performance of the EV aggregator so that they can be more competitive in the market and receive more payment for providing frequency regulation service. Theoretically, the controller proposed in this dissertation can be implemented by any EV aggregator.

The main contributions of this dissertation can be summarized as the following:

TABLE 1.1: National EV deployment targets.[1] [27]

Country	2025	2030	2040	2050
China	25% EV	-	-	-
Japan	-	30~40% HEV, 20~30% BEV, PHEV	-	100% EV
France	500,000 PHEVs, 660,000 BEVs (2023)	1.8 million PHEVs, 3 million BEVs (2028)	No sales of new vehicles using fossil fuels	-
Germany	-	7~10 million BEV, FCEV	-	All passenger vehicles sales to be ZEV
Spain	-	5 million EVs	100% ZEV sales	-
U.K.	-	50~70% EV	No sales of new ICE vehicles(2035)	-
U.S. (selected states)	3.3 million ZEVs in 11 states	-	-	All passenger vehicles sales to be ZEV in 10 states

- Propose a delay compensation controller to address the communication delay of the frequency regulation signal.
- Propose an optimal dispatching controller to maximize the capacity payment while not violating the EV users' convenience
- Propose to predict the clearing price of the frequency regulation market via time-series analysis
- Precisely, the performance score is improved by the delay compensation controller and the capacity payment is increased by the optimal dispatching controller.

[1] HEV: hybrid electric vehicle; FCEV: fuel cell electric vehicle; ZEV: zero emission vehicle; ICE: internal combustion engine

- The system also benefits from the proposed controller as a better frequency regulation service can be provided by the EV aggregator.

1.3 Dissertation Outline

The outline of the dissertation is organized into six chapters in detail below.

Chapter 2 reviews the frequency regulation techniques in the power system and the relative frequency regulation markets. The advantages and the necessity of the performance-based frequency regulation market mechanisms in power systems with large RES generation penetration are explained. The bidding rules in the target market and the simulation model of the target power system in this dissertation are also introduced in this chapter as well.

Chapter 3 reviews the ideal and the existing researches of using EVs as the demand response to provide frequency regulation. The benefits and potential problems are also pointed out in this chapter. In the end, the business scheme of the target EV aggregator in this dissertation is presented.

Chapter 4 proposes the delay compensation control to increase the performance score of the EV aggregator.

Chapter 5 proposes the optimal dispatching control to increase the capacity payment of the EV aggregator.

Chapter 6 unifies the delay compensation control and the optimal dispatching control into the proposed novel controller.

Chapter 7 gives the conclusion and presents the scope for the future work of this dissertation.

Chapter 2

Load Frequency Control

2.1 Frequency Stability in Power System

For the stable and satisfactory operation of a power system, it is necessary that system frequency remain nearly constant at its rated value. A constant system frequency ensures that all the generators in the system are synchronized and operates at a constant speed, which is crucial for the performance of these generation units. A large frequency deviation in the system could result in high magnetizing currents in the generators and transformers, causing malfunction of the equipment due to overheating or mechanical overstress [29].

Due to the fact that it is very difficult to store a large quantity of electrical power in the power systems, the system frequency depends on real-time active power balance. When the generation is equal to the load demand, system frequency is held at its nominal value. Otherwise, surplus and deficit of generation will lead to the rising or descending of the frequency. Generally, the larger the power system is, the more rigorous its frequency regulation requirement is. The regulation targets of frequency fluctuation of different power systems in different regions are summarized in Table 2.1 [30,31].

In a conventional power system, the active power balance is maintained by controlling the amount of generation to match the load demand. The load fluctuation might seem random, however, it can be decomposed into 3 components in different frequency ranges, namely, cyclic, fringe, and sustained. The decomposition of the load fluctuation is shown in Figure 2.1. These 3 kinds of load fluctuation within different frequency ranges are balanced by different generation controls: Primary Frequency Control (PFC), Load Frequency Control (LFC), Economic Dispatch Control (EDC) and Unit

TABLE 2.1: Frequency regulation targets in different regions [30,31].

Region	Regulation Target of Frequency Fluctuation
Hokkaido	Maximum deviation: $\pm 0.3Hz$
East Japan	Maximum deviation: $\pm 0.2Hz$
West Japan	Maximum deviation: $\pm 0.2Hz$
North America (NERC)	Yearly standard deviation of 1-minute average value Eastern Part: 0.018Hz Western Part: 0.0228Hz ERCOT(Texas): 0.020Hz Hydro Quebec: 0.0212Hz Yearly standard deviation of 10-minute average value Eastern Part: 0.0057Hz Western Part: 0.0073Hz ERCOT(Texas): 0.0073Hz Hydro Quebec: 0.00125Hz
Europe (UCTE)	Staying rate within 50 ± 0.04Hz over 95% Staying rate within 50 ± 0.06Hz over 99%
China	System installed capacity over 3GW: maximum deviation ± 0.2Hz System installed capacity below 3GW: maximum deviation ± 0.5Hz Under any contingency: maximum deviation ± 1Hz

Commitment (UC) as shown in Figure 2.2.

2.1.1 Primary Frequency Control

The cyclic component refers to the load fluctuation within a few minutes. The fluctuation is very random, but generally, it only takes up a small part of the total system load fluctuation. Some load in the system, especially load with mechanical torque such as fans and turbines, has the ability to suppress these fluctuations. For example, when the system generation is higher than load, the system frequency increases, leading to the increase of rotation speed of these loads. An increase of the rotation speed in turn leads to the increase of these loads, given that the load is the product of

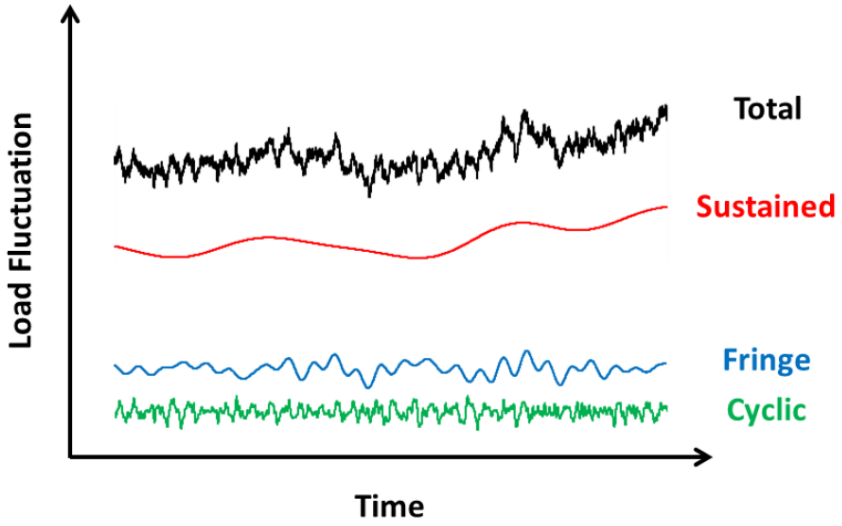

FIGURE 2.1: The load fluctuation in the power system.

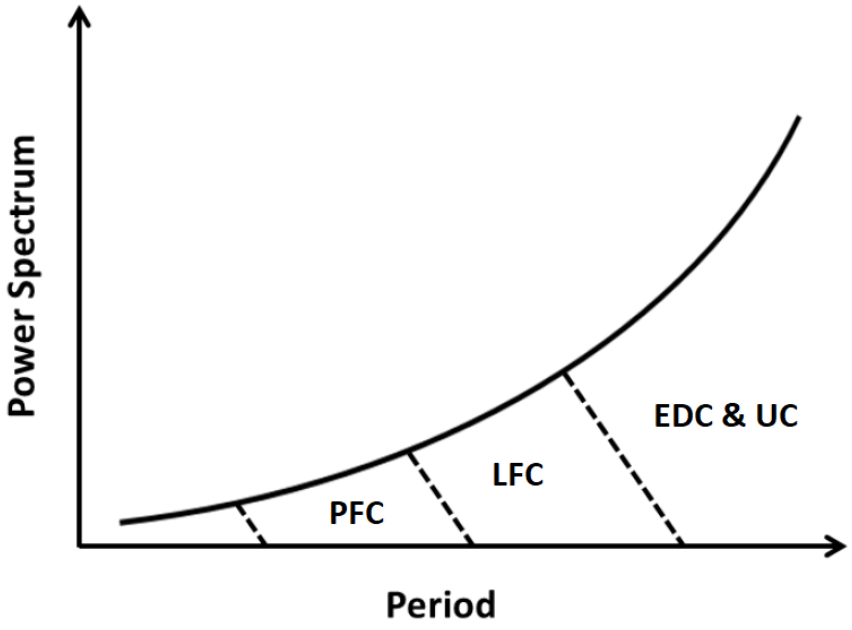

FIGURE 2.2: The distribution of the load fluctuation.

rotation speed and constant mechanical torque. With the load increased, the imbalance between generation and load decreases, and the frequency deviation is also suppressed.

Still, most of the load in the power system like lighting loads are resistive loads, independent of system frequency. Hence, it is not enough to balance the cyclic fluctuation only by the load response to frequency deviation.

The synchronous generators in the system are equipped with a governor with droop speed control. The governor controls the power output of the generator according to the grid frequency. When the system frequency decreases, the governor increases the generation, i.e. changes the position of the valve of a steam turbine, proportionally, and vice versa. An ideal steady-state characteristics of a governor with speed droop is shown in Figure 2.3 [29].

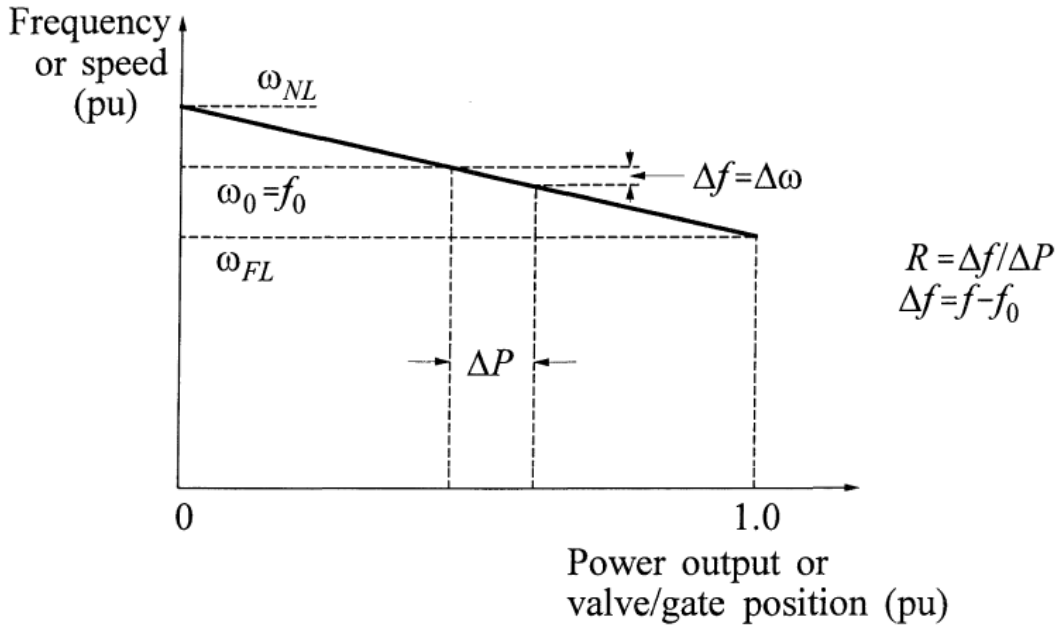

FIGURE 2.3: Ideal steady-state characteristics of a governor with speed droop [29].

The droop parameter R is denoted as a percentage value which is the ratio of percent speedfrequency change over percent power output change. Since the droop alters the generation proportionally to the frequency deviation, R can also be expressed as:

$$R = (\frac{\omega_{NL} - \omega_{FL}}{\omega_0}) \times 100 \tag{2.1}$$

where ω_{NL} and ω_{FL} are the steady-state speed at no load and full load respectively, and ω_0 is the nominal or rated speed. An R% of droop indicates that a R% of frequency deviation will cause 100% change in the valve position of the steam turbine or power output. This automatic control completed by the governor is referred as the PFC.

The speed of PFC is very fast since that each generator directly responds to the system frequency deviation, therefore it is suitable for balancing the cyclic components that are fast and random. Also, PFC is a decentralized control. All the generators adjust their power output separately without a central control signal. Besides balancing instant cyclic frequency fluctuation, PFC is also responsible for recovering the frequency to an acceptable value in contingencies such as a sudden frequency dip due to the loss of a generator. Finally, PFC is a simple proportional control, therefore it cannot bring the frequency back to the exact nominal value.

2.1.2 Load Frequency Control

The frequency deviation caused by the fringe component of load fluctuation, whose time period is around a dozen minutes, is suppressed by LFC. Unlike PFC, LFC is a centralized control, and only some of the generators in the system will participate in LFC. LFC is also mentioned as Auto Generation Control (AGC) or Secondary Frequency Control in some literature.

There are two modes of LFC: Flat Frequency Control (FFC) and Tie-line Bias Control (TBC). The objective of FFC is to bring the frequency in the whole system back to its nominal value based on the real-time frequency deviation. It is usually implemented for a single area system or the main system in a multi-area system. Diversely, besides frequency regulation, the objective of TBC also includes maintaining tie-line power deviation from the scheduled value. The LFC modes of the 10 power systems in Japan is shown in Figure 2.4.

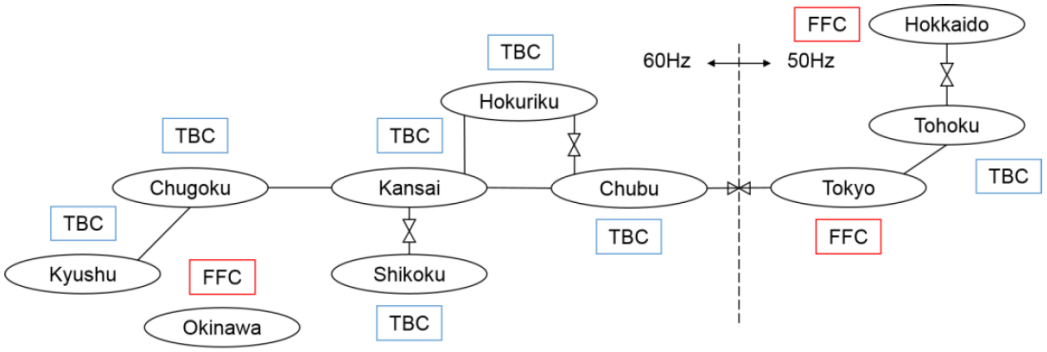

FIGURE 2.4: The LFC modes of the 10 power systems in Japan. [30].

The system operator calculates the Area Control Error (ACE), also referred to as Area Requirement (AR), according to the LFC mode. In FFC, only system frequency deviation is used for deriving ACE, while tie-line bias is combined with system frequency deviation to calculate ACE in TBC. In LFC, the generating units need not respond to the cyclic load fluctuations, since control action for such fast and random variation not only cannot reduce ACE but also causes unnecessary wear and tear on the generator governors and the turbine valves. Hence, normally, a low-pass filter is applied to the ACE to filter out the high-frequency components. The filtered signal called smoothed ACE (SACE) is used to control power output.

A controller then generates the LFC signal using ACE or SACE as the error signal. The LFC signal (also referred to as the AGC signal) indicates how much change in the generation is required for active power balancing. The design methodologies of this LFC controller have been studied and discussed in many literature [32–42]. The most conventional strategy is to take the integral of the ACE signal as the control signal and obtain the desired gain and phase margins through Bode plot, Nyquist diagrams, and root locus. Such design approach is easy and straightforward but suffers from poor dynamic performance due to the parameter variations and nonlinearities of an actual power system [32–34]. The tuning of such controller also requires detailed information from the system, which is large and hard to observe all the dynamics.

More sophisticated methodologies of LFC controller design were then introduced to the industry for better performance. The adaptive control techniques, especially self-tuning regulators, were adopted to make the LFC controller less sensitive to the system parameter changes and un-modeled system dynamics [35–37]. In practice, the operation of the power systems contains many uncertainties and disturbances, and the operation point of the system could also change. To ensure that the LFC controller not only meets the stability criterion in normal operation state but also have sufficient robustness for unknown disturbance, the robust control theories such as H_∞ control was also applied to the design and tuning of the LFC controller [38, 39]. The utilization of intelligent approaches such as artificial neural networks, fuzzy logic, and genetic algorithms in LFC controller design was also proposed to take the nonlinear system dynamics into consideration, which are often omitted or approximated by reduced-order linear models [40–42].

Finally, the system operator dispatches the LFC signal to the generators participating in LFC to adjust their output to match the actual load. There are two common ways for LFC signal dispatching, namely pro-rata and merit-order [43]. In pro-rata dispatch, the LFC signal is dispatched to the regulation resources proportionally by multiplying a participation factor according to the offered capacity. In merit-order dispatch, the regulation resources are sorted into a list. In practice, the list is sorted by the regulation cost of the resources. Firstly, the LFC signal is sent to the first resource on the list. The LFC signal that is over the capacity of the resources is sent to the second resource on the list, and the process goes on until the LFC signal is completely dispatched.

The block diagrams of these two LFC dispatching methods are depicted in Figure 2.5. C_i is the regulation capacity offered by i_{th} regulation resource and p_i is the participation factor calculated as:

$$p_i = \frac{C_i}{\sum_{j=1}^{n_{reg}} C_j} \tag{2.2}$$

where n_{reg} is the number of the resources participating in LFC regulation. For both of the methods, the sum of the dispatched LFC signal will be equal to the original system LFC signal, meaning no additional dynamics is included due to the dispatching method. Pro-rata dispatch is employed in Switzerland, France, and PJM in the U.S. while merit-order dispatch is adopted by power systems in Germany and Italy. The simulation in [43] also points out that merit-order dispatch is more likely to cause violations on generator ramping constraints compared to pro-rata dispatch.

2.1.3 Economic Dispatch Control and Unit Commitment

Contrary to the cyclic and the fringe load fluctuation that is fast and random, the sustained load fluctuation is slow and predictable given that usually human activities have daily and seasonal patterns. The time frame of the sustained fluctuation is generally longer than twenty minutes. The sustained load fluctuation is predicted as a load curve in advance, and the generation is scheduled to provide enough electricity supply at each time slot, typically 30min or 1h.

The schedule of the generation is commonly an optimization problem

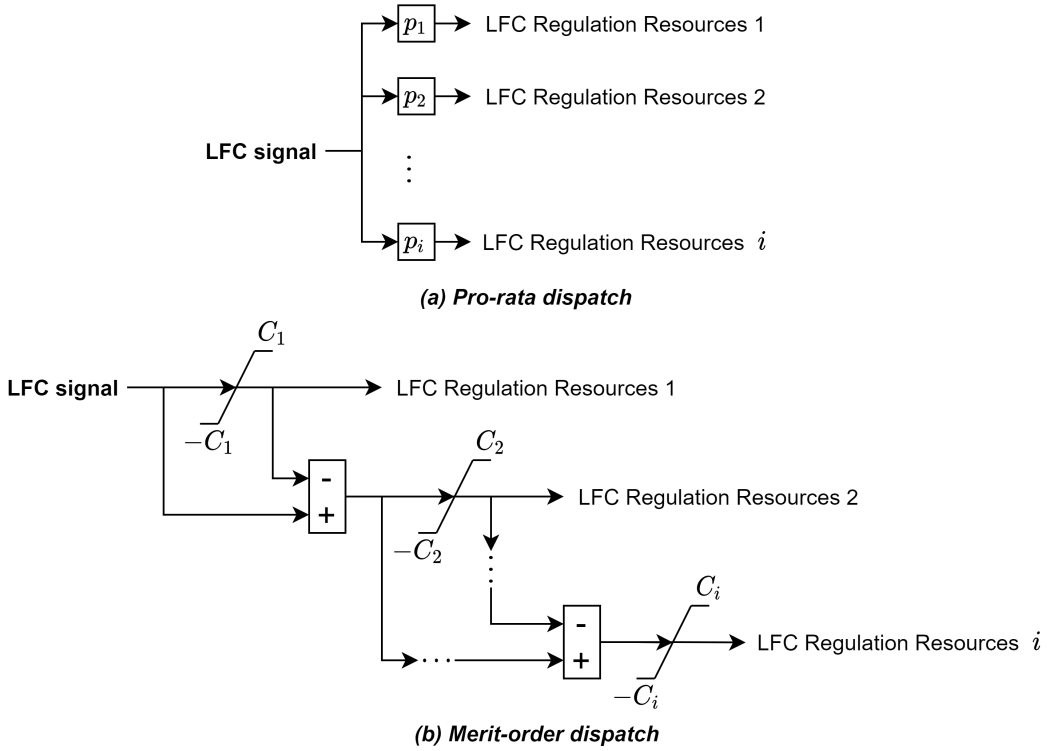

FIGURE 2.5: Two LFC dispatching methods: pro-rata and merit-order.

to minimize the generation cost while meeting the power demand. The optimization is also subject to other operating constraints on generation units such as power output limits, ramping, and minimum on/off times. This optimization problem of searching the optimal mix of different generation units along a certain time span, usually on a daily basis, based on economic criteria is known as the UC problem. Similar to LFC, UC is conducted by the system operator. Different formulations and solutions of UC have been developed and studied. The early methods were based on priority listing and dynamic programming and then evolved into the current most widely used ones based on mixed-integer linear programming [44].

The recent increasing penetration of RES generation has drawn a tremendous amount of attention in refining UC algorithms. In addition to the physical means such as implementing demand-side management and storage devices to increase regulation flexibility, UC algorithms adopting stochastic and probabilistic schemes have also been regarded as a promising method [45]. The uncertainty of RES generation is modeled into scenarios, and the UC schedule is optimized according to the probabilities and distribution of these scenarios [46–48]. Since mostly there is a trade-off between the number

of scenarios and the performance of the algorithm, scenario reduction techniques have been proposed in many studies to limit the number of scenarios without sacrificing the performance too much [49–51].

The predicted generation at each time-step is dispatched to the operating generating units economically. This process is referred to as EDC. While UC determines the on/off state of each generation unit, EDC is applied to determined the precise amount of generation for each generating unit. For thermal power plants, the cost of the fuel can be approximated by a second-order function of the generated power. Typically, the optimization can be solved by the method of Lagrange multipliers. Together, EDC and UC ensure that the system operational cost is minimized and the sustained load fluctuation can be well supplied all the time.

The functional block diagram of a typical frequency control system is shown in Figure 2.6 [29]

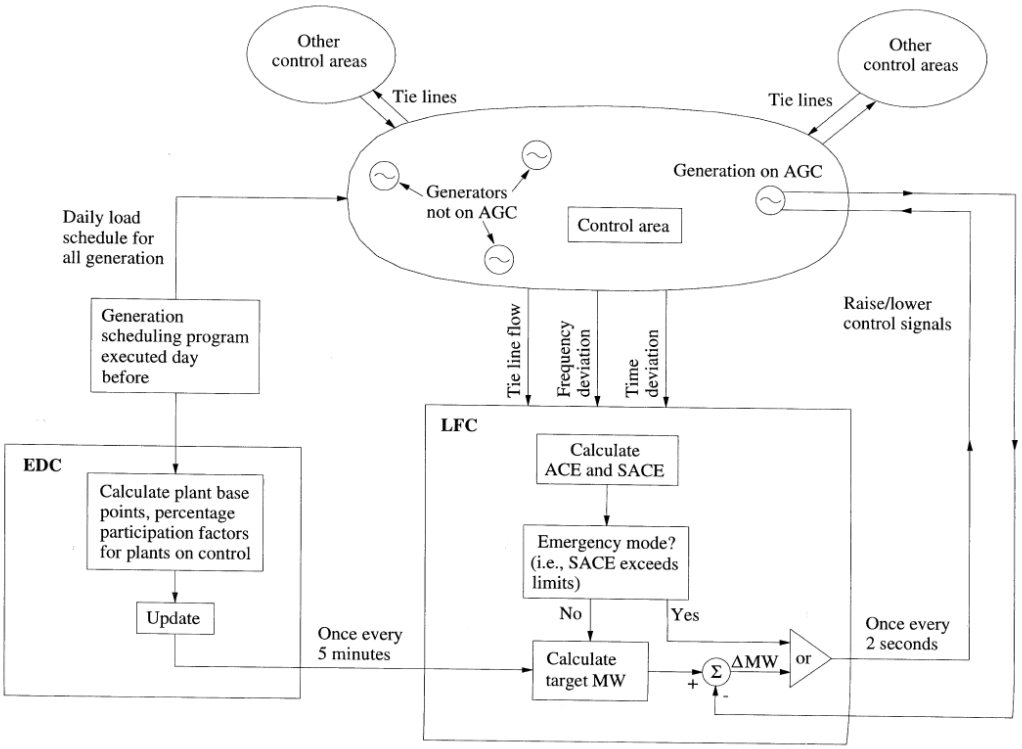

FIGURE 2.6: The functional block diagram of a typical frequency control system [29].

2.2 The Effect of Large Renewable Penetration on Frequency Regulation Reserves

The intermittent and unpredictable RES generation makes it difficult to keep balance between demand and supply. Therefore, more frequency regulation reserves are required in the system for power output adjustment in real-time operation to compensate the RES generation. The effect of large RES penetration on frequency regulation reserves can be classified into two aspect: long-term fluctuation and short-term fluctuation as shown in Figure 2.7 [52].

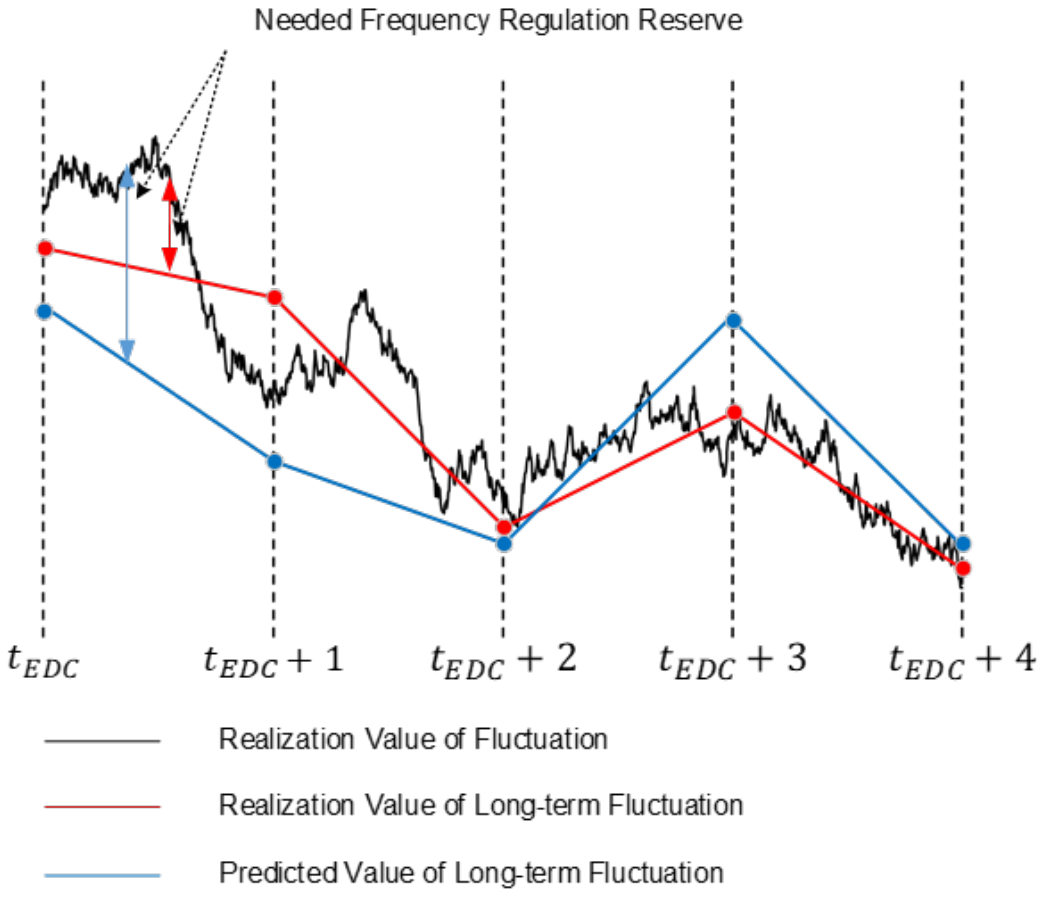

FIGURE 2.7: The effect of large RES penetration on frequency regulation reserves [52].

As discussed in Section 2.1, EDC and UC are responsible for the active power imbalance with a long time period. However, since the thermal generation units have operation constraints such as minimum on/off times, the real-time EDC might not have enough spinning reserves to adjust the

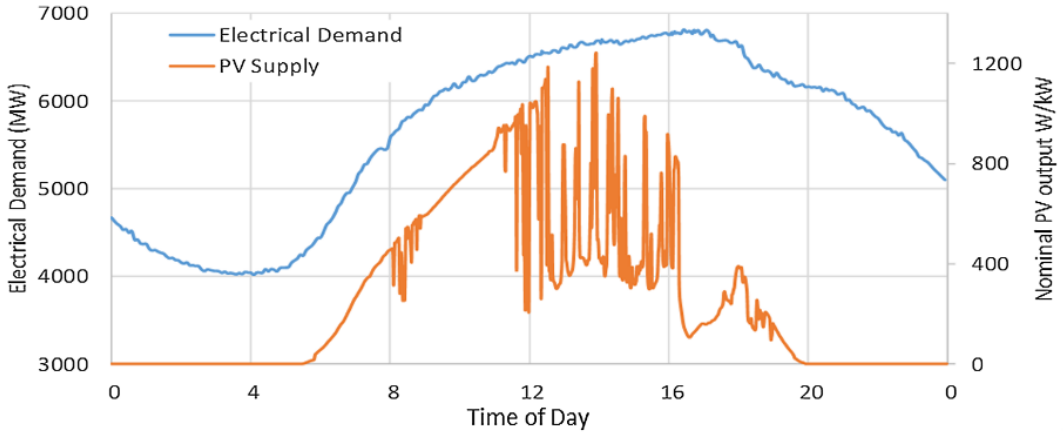

FIGURE 2.8: Intraday PV generation intermittency in the New York metro area compared to city-wide electrical load requirements. [57]

scheduled generation plan due to the large prediction error on long-term RES generation. Currently, for the safe operation of the system, most of the system operator has to schedule UC and EDC in a way that when the RES generation is lower than the prediction, there are enough spinning reserves in the system to increase power output to compensate the deficit of generation, and when the RES generation surpass the prediction too much, the spare RES generation is curtailed. Such a strategy will not be feasible if the system RES integration continues to increase, given that the capacity of spinning reserves decreases as the number of the operating generation unit decrease. Utilization of pumped-hydro and large battery energy storage system (BESS) is one potential strategy [53,54], and load shaping by dynamic electricity spot price is also proposed in many literature [55,56].

On the other hand, the short-term fluctuation of RES generation can be huge as well. Figure 2.8 shows a typical depiction of the intermittencies of PV generation in relation to typical electrical load demand on an intraday basis and points out the difficultly of matching the generation to the load clearly and qualitatively [57]. Besides, the long-term prediction error of RES generation will also result in more frequency regulation reserve requirement for short-term fluctuation [52]. Consequently, more frequency reserve with not only larger capacity but also faster response speed is required for LFC and PFC.

2.3 Performance-based Frequency Regulation Market

The electricity supply is a natural monopoly, usually in a form of a regional power company owning both generation, transmission, and distribution systems. However, with the development of the distributed generation and communication technology, it becomes possible for the participation of new power producers or suppliers, especially privately-owned ones, and form a competitive power market [58]. The liberalization or the deregulation of the power market has taken place for decades worldwide. In 1996, the Federal Energy Regulatory Commission (FERC) of the U.S. issued Order 888, spurring the creation of the Independent System Operator (ISO) which coordinates, controls, and monitors a power system. Independent power producers would have fair access to the transmission system and the marketplace, and the system is operated based on the power wholesale market [59]. Power systems in other countries like Japan and China have also begun the deregulation of the power market.

Ancillary services are the services needed to support and maintain the reliable system operation and the power quality [60]. The types of ancillary services can include:

- Frequency regulation
- Voltage control
- Spinning reserve
- Grid loss compensation
- Emergency control actions
- Black start capability
- ...

In a traditional power system, ancillary services are provided by the system operators with full access to all grid equipment. Contrarily, in a deregulation system, the system operator does not own the generation sources, hence ancillary services should be provided by utilities in the grid, and an unbundled market is required as well.

Concerning frequency regulation, most of the existing markets in the world are for LFC. Conventionally, the resources participating in the LFC regulation will offer the capacity with a certain price in every time slot in the ancillary service market. The market is cleared by selecting the resources from the one with the cheapest offer price to the more expensive ones until the system LFC regulation capacity requirement is met, as shown in Figure 2.9. Each block represents the bid submitted by a regulation resource, with the height is the offer price and the width is the offered capacity. The bids are ranked from the lowest price to the highest, and the blue block indicates that the bid is taken in the market clearing process. The resources receive their payment which is the product of their offered capacity and the market clearing price.

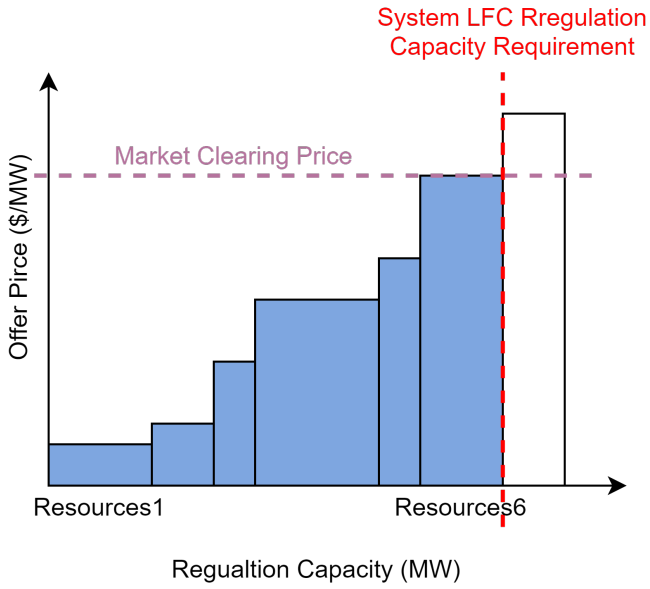

FIGURE 2.9: The market clearing process in conventional LFC regulation market.

As stated in Section 2.1.2, the LFC is a centralized control requesting all the participating resources to follow the dispatched LFC signal. However, the above market structure failed to provide enough incentive for the regulation resources to respond to the instructed LFC signal accurately since only capacity payment is considered during the clearing and settlement of the frequency regulation market. Thus, the system will require more regulation capacity in order to meet the stability and reliability criteria.

To solve this problem, on October 20, 2011, the FERC issued Order 755, requiring the ISOs to reward the LFC regulation resources based on the

actual performance of the provided service [61]. The payment to a regulation resource should include two parts:

- a capacity payment as in the previous market
- a performance payment that reflects the quantity of service when the LFC signal is closely followed by the resources

This performance-based market scheme encourages the investment on developing fast ramping technologies and incentivizes the participation of new regulation resources, especially energy storage devices with batteries. The resources with fast-ramping energy storage could be 17 times more effective compared to the conventional ramping-limited generation units [62].

To access the performance of the regulation resources, the concept of regulation mileage is proposed and widely accepted by the ISOs [63]. The mileage is calculated as the sum of the absolute movement of the response of the regulation resource in a given time period when providing regulation service. The mileage is an efficient index in evaluating the performance of service provided by the resource as it demonstrates the ramping capability and controllability of the resource in real-time operation. A resource with fast responsive characteristics like BESS will generally have a much larger mileage compared to the traditional thermal plants that suffer from ramping constraints. The mileage of two resources is demonstrated in Figure 2.10 [64]. Resource A is a BESS and resource B is a coal-fired generation unit. Despite the same provided regulation capacity of 10 MW, the response time of resource A is almost instant and moves more frequently and accurately compared to resource B, hence the mileage of resource A is higher. As a result, resource A will be paid more for its better performance in frequency regulation.

In some markets, like PJM, the concept of mileage is used for selecting the resources in the market clearing process. Apart from the capacity offer price, a resource is more likely to be selected if its historical performance is good. Mileage can also be used to generate a separate mileage payment to the resource. An approach for the implementation of the real-time operation of a performance-based market with a mileage payment is designed in [64, 65]. The optimization algorithm calculates the selected regulation capacity and mileage for each resource based on the offers in the market and clears the market. After the market clearing process, the payment to each resource is

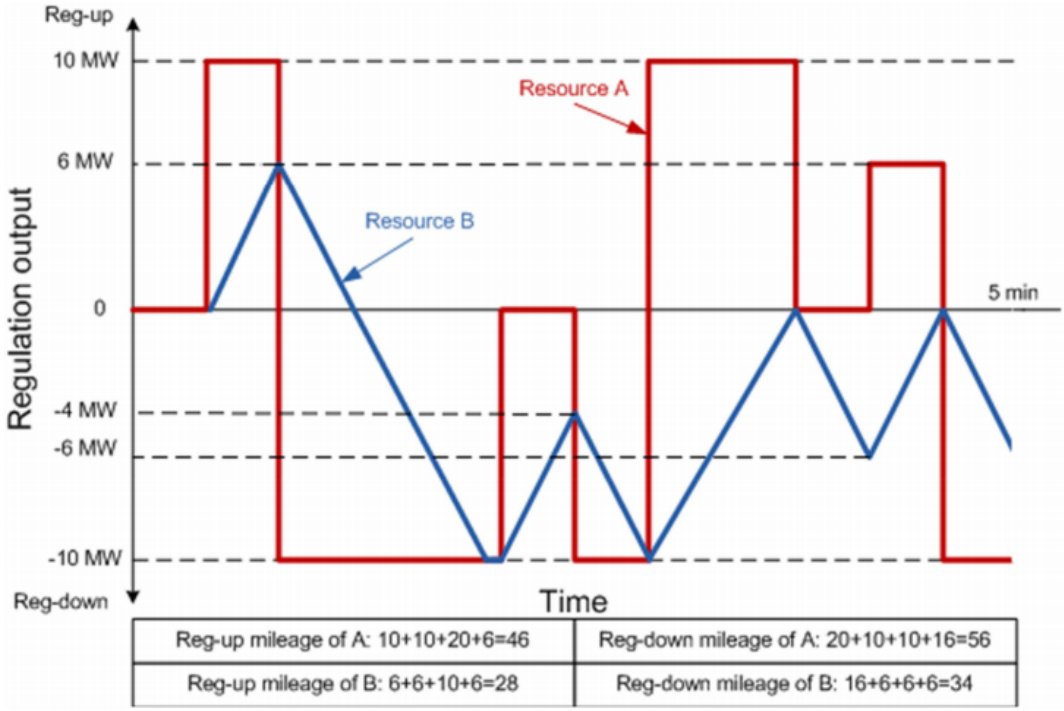

FIGURE 2.10: Illustration of mileage calculation [64].

calculated ex-post depending on not only the capacity but also the actual mileage provided. Currently, the mileage product is offered in the CAISO Expanded Region, NYISO (called Regulation Movement), and MISO [66].

2.4 Ancillary Service Market for Frequency Regulation

2.4.1 PJM

The Pennsylvania-Jersey-Maryland Interconnection (PJM) is an ISO operating power system in the eastern U.S. Prior to the issuance of FERC's Order 755, the PJM's frequency regulation market only provide a capacity payment for the participating resources [62]. Resources merely submitted a regulation capacity offer to the market. The regulation market clearing price (RMCP) was calculated as the sum of the highest regulation capacity offer price and the lost opportunity costs (LOC) among all the cleared regulation resources. Regardless the how accurately and quickly the resources followed the LFC signal, they were paid with RMCP which only related to the offered capacity.

PJM started to integrate the regulation performance market mechanism to compensate the well-performing resources in early 2021. In addition to the capacity offer, which is referred to as capability offer in PJM market manual, and a performance offer price can also be submitted to the market. The offers are submitted on an hourly basis. The resources should first submit the offer day-ahead for day-ahead co-optimization with other markets such as energy market. The resources must be able to provide at least 0.1 MW of regulation capability in order to enter the market. To reflect the resources' availability and capability accurately, the resources are allowed to alter the amount of offered capability 65-minute prior to the operation hour. Conversely, the offer price of capability and performance cannot be changed once submitted [67].

There are two types of LFC signal in PJM, namely RegA and RegD. RegA signal is the LFC signal passing through a low pass filter. It is received by traditional thermal generation units with limited ramping ability. The fast fluctuation in the LFC signal is extracted by a high pass filter (HPF) to generate the RegD signal. RegD signal is for resources with fast response time, such as batteries and flywheels. Thermal plants like Gas Turbine Combined Cycle (GTCC) plants with fast ramping ability could qualify for both RegA and RegD signal. The participating resources can submit the offer for one or both types of the LFC signal if qualified.

In the market clearing process, performance-related indices are applied to adjust the offers. Performance-related indices adopted in PJM include $Performance\ Score$, *Mileage Ratio*, and $Benefit\ Factor$. The offer price of each resource is adjusted with these indices and the market is cleared with the adjusted price rather than the original offer price. Thus, the performance of each resource is reflected in the adjusted price, and the resources with better performance will have better bidding chances and payment in the market.

Performance-related Indices

a) Performance Score

PJM collects the data of the LFC regulation signal and the response of the resources every 10 seconds. The performance score evaluates the accuracy of each resources following the dispatched LFC signal. The detailed calculation process is given in [68]. $Performance\ Score$ is a unitless scalar whose value

ranges from 0 to 1. It consists of three parts: *Correlation Score*, *Delay Score*, and *Precision Score*.

In PJM, the original LFC dispatch signal and the response signal of a regulation resource is compared by calculating the statistical correlation value of them. By shifting the time period of the signals from one time-step to 5 minutes, multiple correlation values are calculated. A signal's delay time δ is defined as the point in time of the maximum correlation value. The *Correlation Score* and *Delay Score* are calculated as:

$$\begin{aligned} \textit{Correlation Score} = & \textit{Corr}(\textit{LFC Signal}(t, t+1, .., t+5\text{min}), \\ & \textit{Response}(t+\delta, t+\delta+1, ..., t+\delta+5\text{min})) \end{aligned} \tag{2.3}$$

$$\textit{Delay Score} = |\frac{\delta - 5\text{min}}{5\text{min}}| \tag{2.4}$$

where *Corr* is the statistical correlation function of two datasets. Note that in (2.3), the response signal is shifted by the delay time δ. Therefore, the *Correlation Score* is actually the comparing the similarity of two signals' shapes without considering the effect of the delay. Furthermore, this also implies that if the response signal is a pure delay of the original LFC dispatch signal, the *Correlation Score* is 1.

The *Precision Score* describes the instantaneous error between the LFC signal and the response of the regulation resource:

$$\textit{Precision Score} = 1 - \textit{Average}(|\frac{\textit{Response} - \textit{LFC Signal}}{\textit{Hourly Average LFC Signal}}|) \tag{2.5}$$

Correlation Score, *Delay Score*, and *Precision Score* are all unitless scalars value range from 0 to 1. The final $Performance\ Score$ is an evenly weighted average of the three components:

$$Performance\ Score = \frac{1}{3}\textit{Correlation Score} + \frac{1}{3}\textit{Delay Score} + \frac{1}{3}\textit{Precision Score} \tag{2.6}$$

In the calculation of $Performance\ Score$, a 10-second latency is allowed in the response of the regulation signal for signal communication delay. The response signal can be shifted up to 10 seconds before being used for the $Performance\ Score$ calculation if necessary. For every regulation resource, the $Performance\ Score$ is calculated every hour and kept in the database. A *Historic* $Performance\ Score$, which is the average $Performance\ Score$ for the

previous 100 hours of operation, is used in the adjustment of the regulation offer.

b) Mileage Ratio

PJM keeps track of the historical mileage of each resource. The *Mileage Ratio* is the ratio between the mileage and the capability offer of a resource. It represents that averagely how much mileage can be provided by the resource per MW regulation offer. The *Historic Mileage Ratio* is calculated by PJM and used for the performance offer adjustment. Typically, the mileage of RegA resources is 3~6 while the mileage of RegD is 10~16 according to PJM's data, indicating a RegD resource generally moves almost three times as much as a RegA resource in one hour.

c) Benefits Factor

The *Benefit Factor* is an unitless factor introduced to convert the RegD capability to the RegA capability for market clearing. The *Benefit Factor* of RegA offers is set to 1 by default. The *Benefit Factor* of RegD offers is calculated according to a benefit factor curve with two or more segments. A typical benefit factor curve with two segments is shown in Figure 2.11 [69].

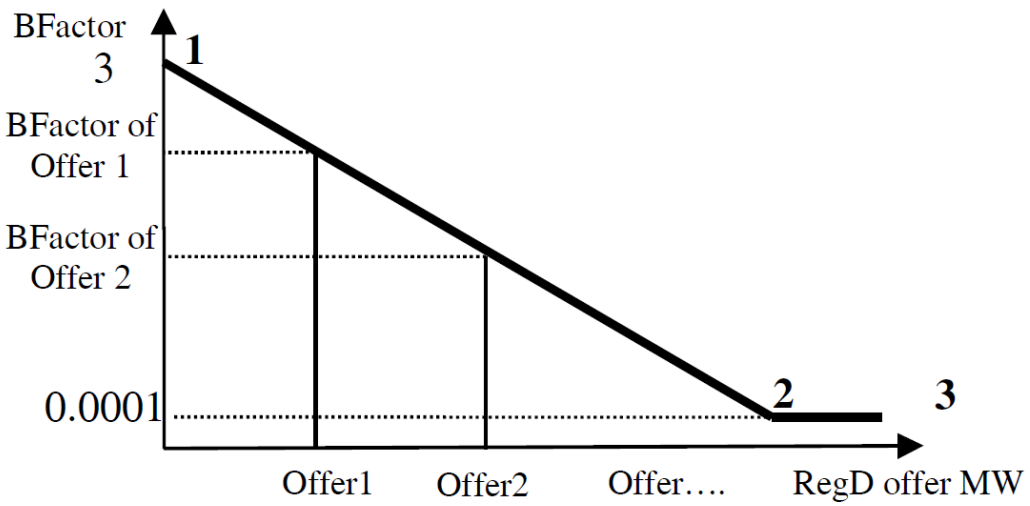

FIGURE 2.11: A two-segment benefit factor curve [69].

In the first segment between point 1 and point 2, the *Benefit Factor* is inversely related to the offered capability. The ranges of the *Benefit Factor*

is from 3 to 0.0001. In the second segment between point 2 and point 3, the $Benefit\ Factor$ is a constant value regardless of the offered capability. The calculation of the $Benefit\ Factor$ is determined by PJM according to system operation conditions. The performance of the regulation resources will not affect its $Benefit\ Factor$ directly.

Adjustment to Regulation Offer

In the frequency regulation market in PJM, a resource should submit its $Bid\ Capability$, $Capability\ Offer\ Price$, and $Performance\ Offer\ Price$ to the market.

The total offer price of each resource is calculated as:

$$\underset{Offer\ Price}{Adjusted\ Total} = \underset{Offer\ Price}{Adjusted\ Capability} + \underset{Offer\ Price}{Adjusted\ Performance} + \underset{Opportunity\ Price}{Adjusted\ Lost} \tag{2.7}$$

where

$$\underset{Offer\ Price}{Adjusted\ Capability} = \frac{Capability\ Offer\ Price}{Benefit\ Factor \times Historic\ Performance\ Score} \tag{2.8}$$

$$\underset{Offer\ Price}{Adjusted\ Performance} = \frac{Performance\ Offer\ Price \times Historic\ Mileage\ Ratio}{Benefit\ Factor \times Historic\ Performance\ Score} \tag{2.9}$$

$$\underset{Opportunity\ Price}{Adjusted\ Lost} = \frac{Estimated\ Lost\ Opportunity\ Price}{Benefit\ Factor \times Historic\ Performance\ Score} \tag{2.10}$$

The $Estimated\ Lost\ Opportunity\ Price$ and the $Adjusted\ Lost\ Opportunity\ Price$ is to compensate the generation units that could have used their capacity for power generation instead of providing regulation capacity. This item is only for energy resources that could provide generation to the system. Demand resources or energy resources that do not submit an energy offer to the system are not eligible and their $Adjusted\ Lost\ Opportunity\ Price$ will be zero.

The $Bid\ Capability$ is also adjust to an $Effective\ Capability$:

$$Effective\ Capability = \underset{Factor}{Benefit} \times \underset{Performance\ Score}{Historic} \times Bid\ Capability \tag{2.11}$$

A numerical example of regulation offer adjustment in PJM is given in [69] for clear understanding. The offer data submitted by a RegD resource and its performance indices are given in Table 2.2 and Table 2.3. The adjusted offer data calculated base on (2.112.8) is shown in Table 2.4.

TABLE 2.2: Offer data of a resource [69].

Bid Capability (MW)	*Capability Offer Price* ($/MW)	*Performance Offer Price* ($/Δ MW)
32	1	0.15

TABLE 2.3: Performance indices of a resource [69].

Historic Performance Score	*Historic Mileage Ratio*	*Benefit Factor*
0.954	16.001	2.536

TABLE 2.4: Adjusted offer data [69].

Effective Capability (MW)	*Adjusted Capability Offer Price* ($/MW)	*Adjusted Performance Offer Price* ($/MW)
77.4	0.41	0.99

Market Clearing

Every 5 minutes, the frequency regulation capacity requirement is determined according to the system operation condition, and PJM clears the market in a similar way as shown in Figure 2.9 with the *Adjusted Capability Offer Price* and *Effective Capability*. The highest-ranking price among all the cleared regulation resources sets the RMCP. The RMCP consists of two parts: a capability clearing price (CCP) and a performance clearing price (PCP). The PCP is determined as the highest *Performance Offer Price* among all the cleared regulation resources and the CCP is the difference between RMCP and PCP. The regulation resources receive the RMCP payment instead of the CCP and PCP payment separately, for the CCP and PCP are only for information.

Even though the market is cleared every 5 minutes, the offers of frequency regulation are submitted on an hourly basis. Therefore, the hourly RMCP can be viewed as the average RMCP in that hour for a regulation resource if all of its offers are cleared in that hour.

2.4.2 Electricity Demand & Supply Market in Japan

After the liberalization of the electricity retail market and the legal unbundling of the system operators in 2016, new ancillary markets have been established or will be established in Japan for further deregulation of the power system, including the Electricity Demand & Supply Market. Currently, the system operators in Japan collect frequency regulation capacity from the generation units in the local area. After the establishment of the Electricity Demand & Supply Market, all the resources will submit their offers by bidding in the Electricity Demand & Supply Market, and the system operator can utilize regulation resources not only locally but also nationwidely [70].

There are five products in the Electricity Demand & Supply Market for PFC, LFC and EDC [71]. The product information is summarized in Table 2.5.

TABLE 2.5: The products in the Electricity Demand & Supply Market.

Product Name	**Frequency Containment Reserve**	**Synchronized Frequency Restoration Reserve**	**Frequency Restoration Reserve**	**Replacement Reserve**	**Replacement Reserve for FIT**
Target	PFC	LFC	EDC	EDC	EDC
Signal	-	LFC Signal	EDC Signal	EDC Signal	-
Signal Time-step	-	0.5s~10s	several minutes	several minutes	30min
Minimum Response Time	10s	5min	5min	15min	45min
Minimum Capacity Offer	5MW	5MW	5MW	5MW or 1MW	5MW or 1MW
Offer Unit	1kW	1kW	1kW	1kW	1kW
Start Time	2024	2024	2023	2021	2021

The product for LFC regulation, Synchronized Frequency Restoration Reserve, is not in the market at present, thus the detailed market rules and mechanism have not been decided yet. Meanwhile, several LFC market designs for the Electricity Demand & Supply Market have been proposed in some studies [30, 72, 73]. [30] proposed an LFC market design with only capacity payment and analyzed the LFC regulation price under the

proposed market. The performance payment is included in the market designs proposed under the context of large RES penetration in [72, 73], and simulation on system frequency deviation is run to evaluate the performance of the proposed market.

2.4.3 Target Market

The target LFC market in this dissertation has basically the same bidding rules as PJM:

- The participants must be able to provide at least 0.1 MW to enter the market.
- The offer submitted by the participants should include the bid capacity, the capacity offer price, and the mileage offer price.
- The offer should be submitted on an hourly basis.
- The participants can change the amount of offered capacity 1 hour prior to the start of the operating hour.
- The participants can choose to receive a normal LFC signal or a fast LFC signal passing through a high-pass filter.

To clearly reflect the contribution of the participating resources in suppressing the system frequency deviation, the payment for LFC regulation is defined as:

$$LFC\ Payment = Performance\ Score \times (Capacity\ Payment + Mileage\ Payment) \tag{2.12}$$

where

$$Capacity\ Payment = Bid\ Capacity \times Capacity\ Clearing\ Price \tag{2.13}$$

$$Mileage\ Payment = Actual\ Mileage \times Mileage\ Clearing\ Price \tag{2.14}$$

The *Mileage Payment* and *Mileage Clearing Price* corresponds to the performance payment and PCP in PJM. In PJM, only historical mileage is used to assess the performance payment of the resource. In this dissertation,

the performance payment is determined by the actual mileage during the operating hour in the ex-post settlement, as proposed in [64, 65].

The *Performance Score* is calculated in the same way as PJM in (2.3-2.6). However, unlike the PJM's *Performance Score*, the allowance of a 10-second latency is abandoned to motivate the LFC regulation resources to further improve their performance and response time.

2.5 AGC30 Simulation Model

The power system model used in this dissertation for frequency dynamics simulation and control design verification is based on the AGC30 Model published by [74]. This model is widely accepted in the academic community in Japan for load balance and system frequency analysis. Precisely, the 2nd case study example of the AGC30 Model is adopted in this dissertation, where the system load is relatively light and renewable energy sources like PV and wind turbine are connected to the system. The AGC30 Model is built on MATLAB/Simulink environment. The simulation runs for 23 hours from 0:00 to 23:00, and the simulation time-step is 0.1 second.

2.5.1 Basic Information

The AGC30 Model is a two-area interconnected system. The block diagram of the AGC30 Model with an EV aggregator participating in the LFC regulation market is illustrated in Figure 2.12. Area A is the main target area with 30 generation units with detailed dynamics modeled. Area B is represented by a simplified model with only one single generator model.

The load profile and the PV generation of the Area A system is shown in Figure 2.13. The forecast of load basically coincides with the actual load. The amount of PV output matches the forecast, however the fluctuation is colossal. The system parameters is given in Table 2.6.

27 thermal generators and 3 hydro plants in Area A are modeled in detail. The 27 thermal generators include 7 oil-fired plants, 4 coal-fired plants, 6 LNG-fired plants, and 10 GTCC plants. The 3 hydro plants are 2 fixed-speed pumped hydro plants and 1 variable-speed pumped hydro plant. Another 1 hydro plant and 6 nuclear plants are the base load plants with constant

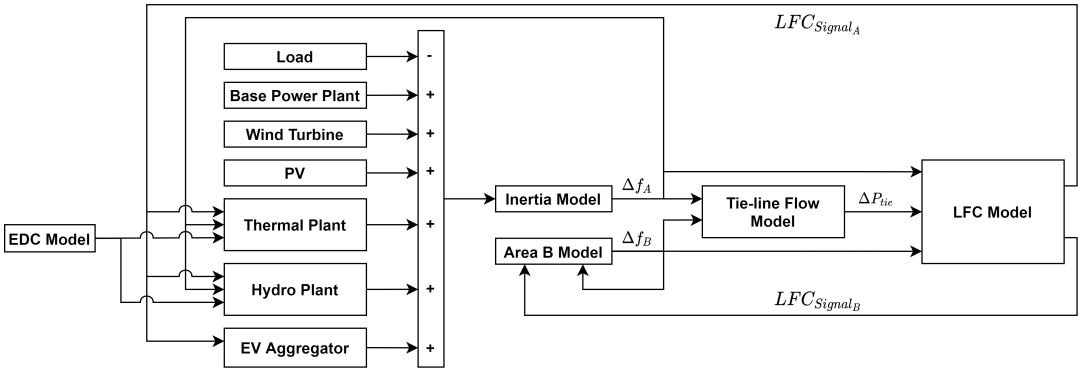

FIGURE 2.12: The block diagram of the AGC30 Model.

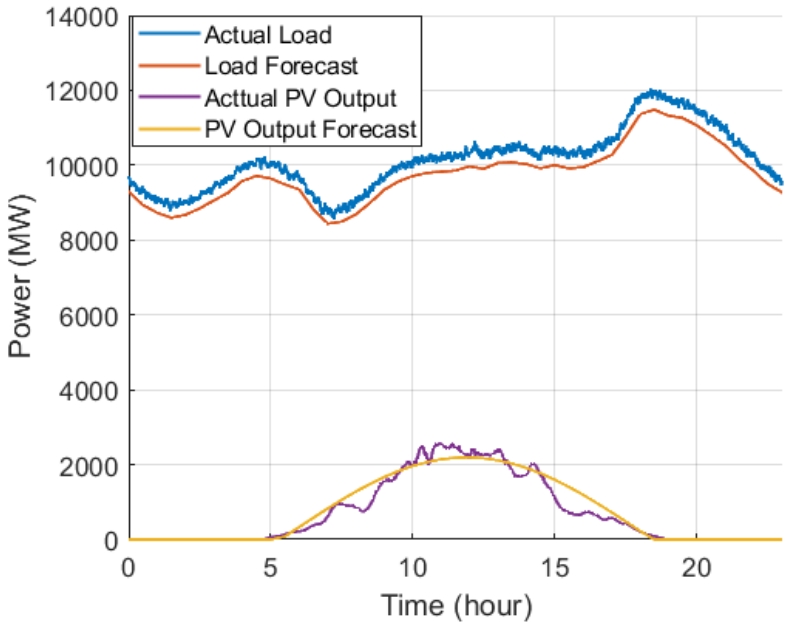

FIGURE 2.13: The load profile and the PV generation in Area A.

output. The base load plants and RES generation are treated as time-serial input data with no dynamics. Before the simulation, all generation units are scheduled with RES generation forecast and load forecast in order to supply the load demand and provide frequency regulation capacity. The information and the operation status of the generation units are specified in Table 2.7 and the UC schedule is depicted in Figure 2.14.

The large amount of PV generation in the system brings the requirement for extra LFC regulation capacity. According to [75], the requirement for the LFC regulation capacity is the sum of $\pm 2\%$ of the load demand forecast

TABLE 2.6: Power system parameters.

Parameters	Value
Nominal Frequency	50Hz
Nominal Tie Line Flow Bias	0MW
Rated Value of Thermal Capacity	12600MW
Rated Value of Hydro Capacity	900MW
Rated Value of Base Load Plant Capacity	7915MW
Peak Demand in Area A	10665MW
Peak Demand in Area B	10642MW
Peak PV Output	2575MW
Peak Wind Generation Output	77MW
System Inertia	9000MW·s
Load Damping Coefficient	2%MW/%Hz
PFC Capacity Requirement	±3%

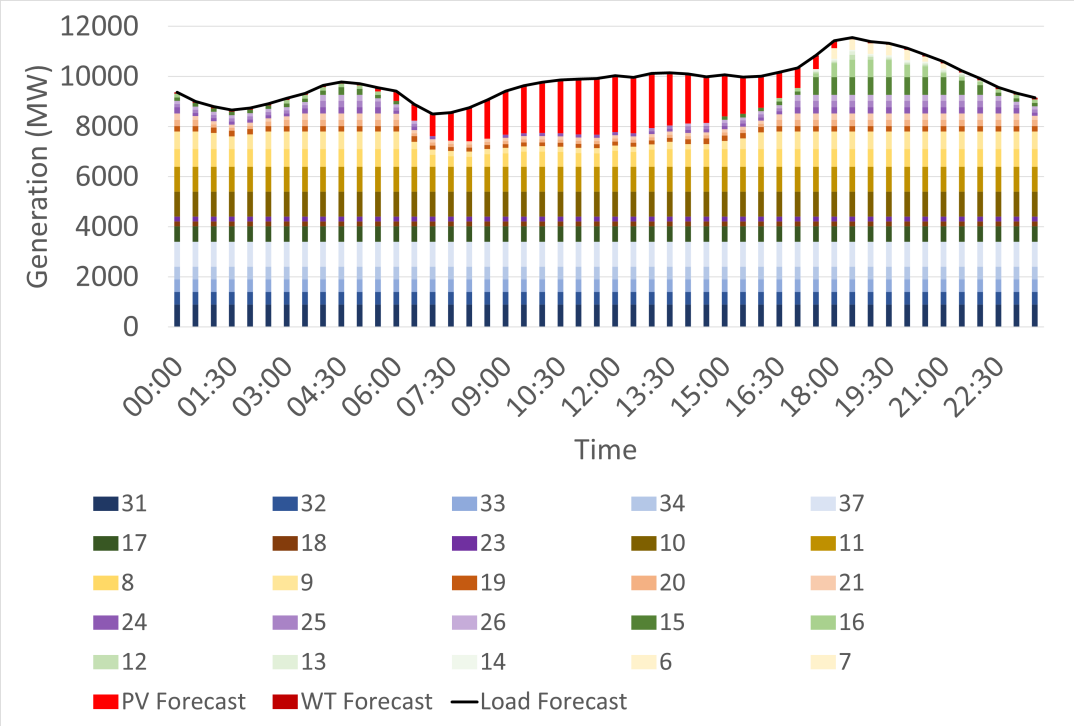

FIGURE 2.14: Scheduled UC.

and ±5% of the PV generation forecast. Figure 2.15 implies that due to the additional LFC requirement by PV generation, the regulation down LFC regulation capacity of the system is not enough in the afternoon.

TABLE 2.7: The information and the operation status of the generation units.

Model	No.	Type	Rated Power (MW)	On/Off	LFC	EDC	Ramp Rate (p.u./min)
Dynamics Model	1	Oil	250	-	-	-	0.03
	2		250	-	-	-	
	3		700	-	-	-	
	4		700	-	-	-	
	5		700	-	-	-	
	6		700	○	-	○	
	7		700	○	-	○	
	8	Coal	700	○	-	○	0.02
	9		700	○	-	○	
	10		1000	○	-	○	
	11		1000	○	-	○	
	12	LNG	200	○	-	○	0.03
	13		200	○	-	○	
	14		200	○	-	○	
	15		700	○	-	○	
	16		700	○	-	○	
	17		700	○	○	-	
	18	GTCC	250	○	○	-	0.05
	19		250	○	○	-	
	20		250	○	-	○	
	21		250	○	-	○	
	22		250	-	-	○	
	23		250	○	○	-	
	24		250	○	-	○	
	25		250	○	-	○	
	26		250	○	-	○	
	27		250	-	-	-	
	28	Fixed-speed Pumped Hydro	300	-	-	-	0.6
	29		300	-	-	-	
	30	Variable-speed Pumped Hydro	300	-	-	-	1
Time-series Data	31	Hydro	3415	○	-	-	-
	32	Nuclear	500	○	-	-	-
	33		500	○	-	-	
	34		500	○	-	-	
	35		1000	-	-	-	
	36		1000	-	-	-	
	37		1000	○	-	-	

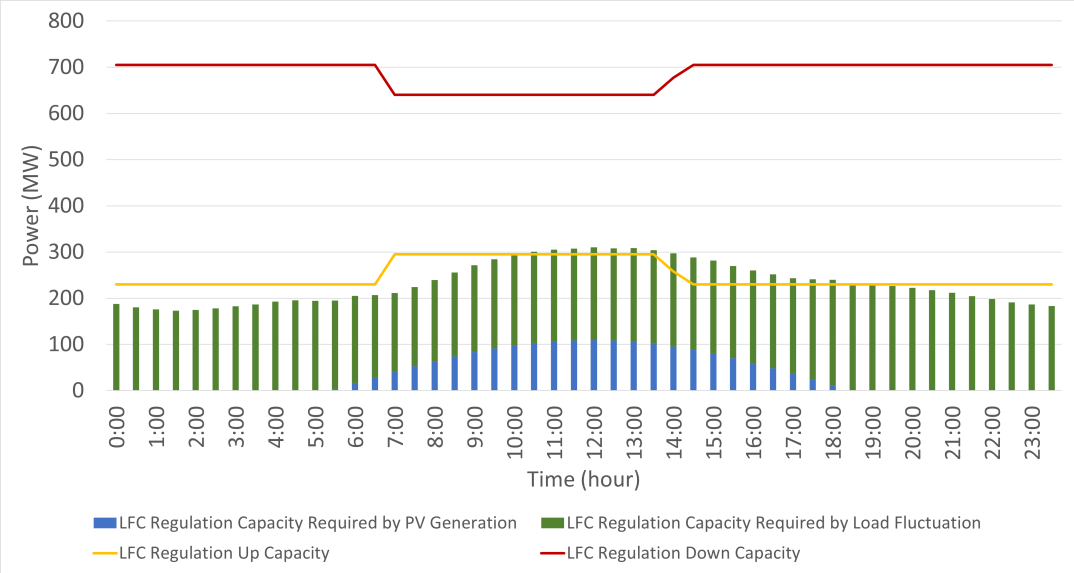

FIGURE 2.15: System LFC capacity requirement.

2.5.2 LFC Model

In the simulation, the LFC of Area A is in FFC mode and Area B is in TBC mode.

The block diagram of the LFC model in FFC mode is presented in Figure 2.16. In FFC, AR is calculated as the product of the system constant, area frequency deviation, and the real-time capacity in the whole system. A low pass filter (LPF) is applied to filter out the high-frequency components outside LFC's target range. A deadband is also implemented to prevent the occurrence of small but fast signal fluctuation, leading to the hunting in synchronous machines and possible system instability. A PI controller takes the filtered AR as the input error signal to generate the LFC signal for active power adjustments.

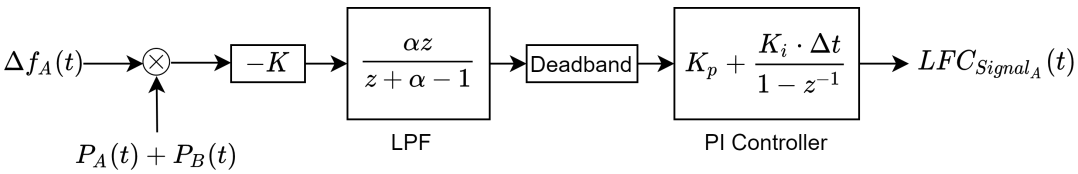

FIGURE 2.16: FFC-LFC model in Area A.

The structure of TBC is the same as that of FFC except that the AR is calculated in a different way. In TBC mode, tie-line flow bias is added to the

product of the system constant, area frequency deviation, and the real-time area capacity as shown in Figure 2.17.

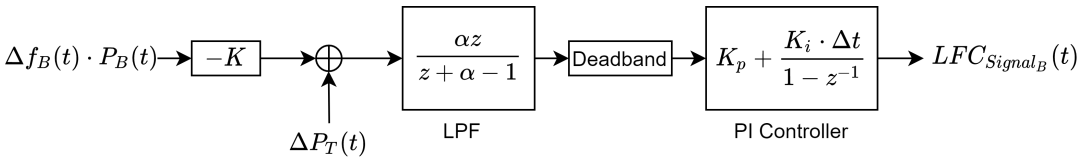

FIGURE 2.17: TBC-LFC model in Area B.

The power system in the simulation uses pro-rata dispatch introduced in Section 2.1.2 to assign the LFC signal to the regulation resources. For conventional thermal units, the LFC signal is directly dispatched by multiplying a participation factor based on their ramp rates:

$$p_i = \frac{ramp_i}{\sum_{j=1}^{n_{reg}} ramp_j} \tag{2.15}$$

A faster LFC signal is generated through an HPF for the regulation resource with faster response time, such as resources with a battery storage system. Such an approach can utilize the capacity of the fast resources more efficiently. This LFC signal corresponds to the fast LFC signal in the bidding rules stated in Section 2.4.3. The overall dispatching method of the LFC signal is illustrated in Figure 2.18.

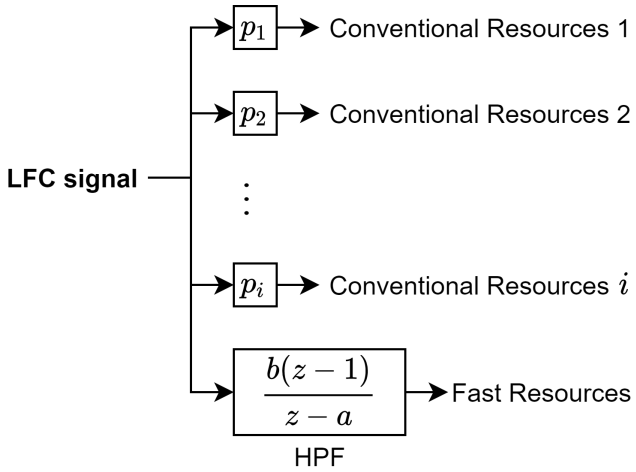

FIGURE 2.18: The dispatching of LFC signal in the simulation system.

The parameters of the LFC model are provided in Table 2.8. The design of the PI controller is not the focus of this dissertation, therefore the preset

values in the AGC30 model are adopted. The proportional gain is set to unity, given that AR already represents the requirement of active power change. The integral gain is set to 0.003 to avoid overshoot. The bandwidth of the LPF and HPF is 0.0115 Hz and 0.00348 Hz respectively, corresponding to a time span of 90 seconds and 5 minutes. The bode plots of the LPF and the HPF are given in Figure 2.19.

TABLE 2.8: LFC parameters.

Parameters	Symbol	Value
System constant	K	10%
LPF coefficient	α	0.07
Deadbnad bandwidth	-	$\pm$10MW
Propotional gain	K_p	1
Integral gain	K_i	0.003
HPF coefficients	a	0.9802
	b	0.952
LFC signal sampling time	Δt	1s

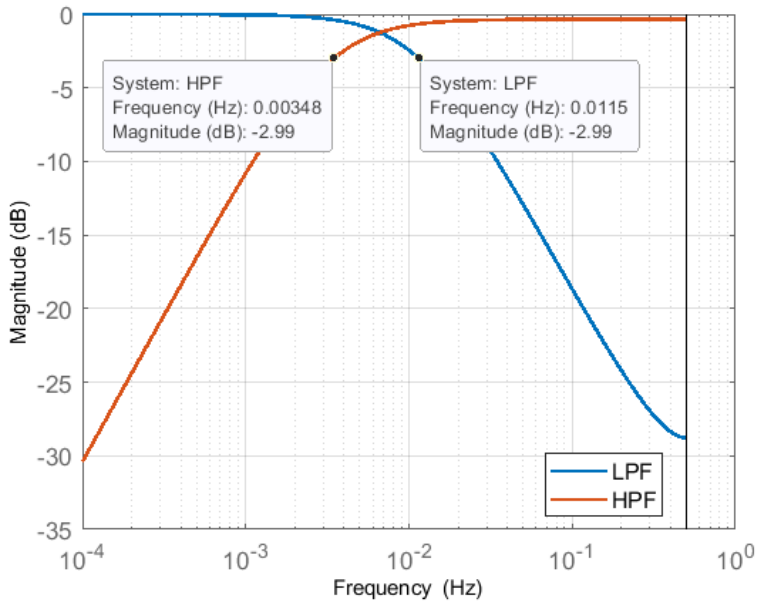

FIGURE 2.19: The bode plot of the filters in LFC.

To simulate the effect of the LFC signal transmission delay, a transmission delay of 3 seconds is included in the AGC30 model. The frequency fluctuation is depicted in Figure 2.20. The intermittent generation of PV brings more

active power fluctuation and urges more regulation capacity to be provided to the system. The maximum frequency deviation reaches 0.221 Hz and the root mean square (RMS) value is 0.0396 Hz. At around 10:40, a sudden rise in PV generation causes the peak frequency deviation, and the dip frequency deviation is due to the abrupt decrease at around 14:20.

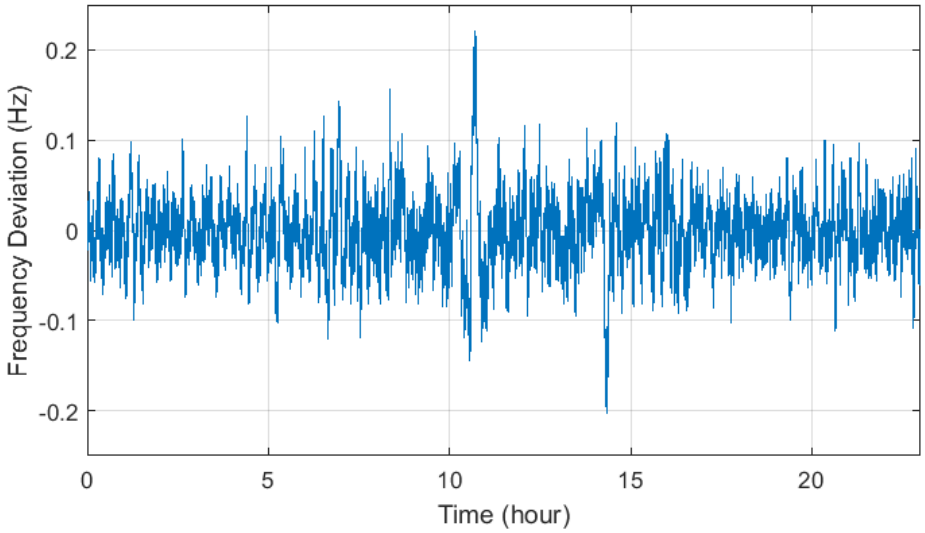

FIGURE 2.20: Frequency deviation in the power system.

Chapter 3

Electric Vehicles as Demand Response

3.1 Demand Response

Traditionally, most of the participants of LFC regulation, whether in a deregulated market or not, are the generation resources. Different types of resources have different ramping abilities and accuracy with which they can follow and responds to the assigned LFC dispatch signal. For example, the coal-fired plants have the slowest response speed and can barely respond to the LFC signal, hence they cannot provide frequency regulation service. The LNG-fired plant and the oil-fired plants are faster, while the GTCC plants have the best ramping ability. Some pumped hydro plants are also capable of providing LFC regulation capacity. In addition, the LFC regulation capacity a thermal plant can offer is the unloaded generation capacity that has been synchronized with the system and is ready to serve the additional load, namely how much power output it can reduce or increase. Thusly, the providable capacity is limited by the plant's operation state and its maximum and minimum output.

As the penetration of RES generation increases in the power system, the role of faster ramping sources becomes more critical. The volatility of RES generation renders the need for a larger capacity of fast-ramping resources even more pressing. One solution is to share the regulation reserves between areas through tie-lines. Especially, high voltage direct current (HVDC) systems can be used to share a large amount of regulation capacity between interconnected non-synchronous AC areas. By modifying the power control of the HVDC systems according to the frequency deviations among the interconnected areas, the adjacent systems can provide frequency support

even if it is not synchronized with the local area [76–78]. While obtaining the frequency deviations in multiple areas requires an extra communication link, other frequency regulation control schemes that need no information outside the local area are proposed to avoid the cost and effort for building communication links [79,80]. However, the investment and maintenance cost on HVDC is huge, and the re-planning of the existing power systems is also strenuous.

Another solution is to balance the active power within the area through energy storage systems. Of the diverse types of energy storage technology available, BESS has clear advantages. The response of batteries is fast, hence BESS has a wide scope of applications, not only frequency regulation capacity but also long-term energy management, uninterrupted power supply, reliability enhancement, and so on [81–84]. The standby power losses of batteries are usually very low, and the energy efficiency is comparatively high (60~95%) [85]. The superiority of BESS also lies in controllability and geographical independence [86]. However, the low energy density, small power capacity, and short life cycle result in the high investment and maintenance costs on BESS. The disposal of battery cells could also have a severe ecological impact [85]. Even though certain BESS technologies have been mature and technologically reliable [87], and the cost is expected to be further reduced [86], the economic concern is still the major barrier for the implementation of large-scale utility BESS. In this regard, the system operators need to optimize the BESS size economically to balance the trade-off between BESS cost and system performance. The optimization of BESS sizing in various systems has been discussed in [88–91]. With a limited size, provision of frequency regulation capacity by BESS alone is not cost-effective and preferable.

As the HVDC and BESS are measures taken by the system side, oppositely, the idea of providing frequency regulation capacity from the demand side has drawn tremendous attention in recent years. The power consumption on the demand side that can be controlled to better match the electric power supply is referred to as Demand Response (DR). There are many types of DR, such as EVs, air conditioners, refrigeration, water heaters, water distribution systems, and household battery systems [92–94]. DR can be equipment from commercial, residential, or industrial sectors [95].

Thanks to the development of Information and Communication Technology (ICT) and Internet of Things (IoT) technologies, the concept of DR

becomes feasible, and the labor and the cost of controlling DR according to the system requirement have been scaled down [96]. Since DR are devices from the demand side, there is no additional cost of implementation. The power level of DR is no match to the system side equipment like BESS and HVDC, but when aggregated, a considerable amount of capacity or energy can be gathered from DR [95]. With proper plans and control strategies, DR is a cost-effective solution and can contribute to reliable and safe system operation, comparable with system side approaches.

3.2 Vehicle-to-Grid

The advantages of EVs over other types of DR are apparent. EVs have battery systems for energy storage, which can respond almost immediately to the command of power adjustment. Compared to normal battery systems, EVs' battery systems are designed to withstand frequent power fluctuations, which is the nature of roadway driving. Meanwhile, according to [97], EVs are utilized only 4% of the time for transportation and remain idle for the rest of the time. The generally long immobility periods of EVs allow the provision of continuous service of secondary functions.

The unidirectional power interaction between EVs and the grid has been proposed in the literature [98–100]. During a period, the preferred operating point (POP) of EV charging is defined. POP can take any value ranging from zero to the maximum charging power. The EV's actual charging rate varies around POP during the period: by reducing or increasing the charging rate to deviate from POP, ancillary services such as up or down regulation can be provided.

However, the most valuable application of EVs is undoubtedly the ability to perform bi-directional power interaction with the grid compared to other kinds of DR. Controlling the two-way power flow during the EV ' s immobility period is the basic concept of vehicle-to-grid (V2G). In V2G, three elements are necessary for the EVs, namely [101]:

- connected to the grid for electrical energy flow
- a connection with the system operator for communication and/or control
- control and metering on the EV

Jurisdictions with any of the following characteristics might be well-suited to adopt V2G [102]:

- Improvement in power system reliability and stability is needed, but the construction of new system equipment such as new power plants or transmission lines is not preferable
- Be in areas with plenty EVs or relatively isolated power grids
- In great need of frequency regulation and spinning reserves
- Have competitive markets for ancillary services
- Have supporting policies for related industry, technology, or employment
- Transportation and electricity can be coordinated by the government.

To examine and verify the realistic implementations of V2G, many test projects have been carried out around the world. The feasibility of V2G concept in technical terms has been provide in [103]. The test EV is connected to the PJM SCADA (Supervisory Control And Data Acquisition) system through a communication protocol and a laptop. A bi-directional charger built by AC Propulsion enables the power exchange between the test EV and the grid, and the PJM system operator can dispatch the test EV as a regulation resource by a direct signal from the system control, just like traditional generators. The report also points out that V2G is more valuable in providing frequency regulation rather than spinning reserve. Two different control mechanisms are proposed for 15 EVs in the University of Delaware to provide frequency regulation service to PJM in [104]. A pilot project to evaluate both the technical challenge and the potential financial benefit of V2G participation is reported in [105]. A fleet with 40 EVs at the Los Angeles Air Force Base was enrolled in the CAISO's regulation up and regulation down markets. A remote server was setup to receive CAISO's dispatch instructions and forwarded the signals to individual EV. [106] demonstrate the results of an EV fleet participating in the Danish frequency regulation market through a commercial V2G hub. In the project, an aggregator gathers information from the EVs by telecommunication and submits bids to the market. In Japan, a demonstration experiment was carried out to access the performance of EVs providing imbalance compensation [107].

3.3 EV Aggregator

The power level of a single EV is small, generally from 3 kW to 10 kW. Even with the fast charging technique, the charging power can reach only around 50 kW. Since most of the ancillary markets have a lower power limit for entrance, the EVs must be aggregated [108]. The main function of an EV aggregator is to act as an intermediary between the system and individual EV. The EV aggregator is responsible for submitting bids to the market, and perform centralized control of the EVs to fulfill the requirement instructed by the system operator. As presented in [104], a centralized control scheme considering the condition of all participating EVs outperforms the decentralized control scheme where each EV decides its offer independently. Financially, the EV aggregator receives the market payment on behalf of the participating EVs from the system operator and then shares the benefits with the participants.

When aggregated, various options of ancillary services exist for the EVs. The EV charging infrastructure includes power electronics, whose reactive power can be controlled and managed for voltage regulation [109]. Another common service is to provide spinning reserve or imbalance compensation by scheduling the EVs' charging and discharging periods. However, this requires the full charging or discharging of EV batteries for a relatively long period, usually 30 minutes or 1 hour. The state-of-charge (SOC) of EV batteries moves drastically and could damage the battery critically, resulting in battery degradation such as decreased capacity and short life cycle.

By contrast, the most promising and widely studied application of EV aggregators is certainly frequency regulation. Unlike spinning reserve and imbalance compensation, frequency regulation requires inconstant but shallow charging/discharging of EV batteries. The damage on the batteries is low compared to deep charging/discharging, and the fast response characteristics of EV batteries can be fully utilized. Specifically, aggregated EVs not only increase the system frequency regulation capacity but also provide fast response capacity, which is essential in a power system with the integration of a large amount of RES generation. Moreover, in a performance-based market, the EV aggregator will have more advantages over traditional generation units due to the fast response characteristics of the battery. Therefore, for the EV aggregators and the participating EVs, the provision of frequency regulation is also the most beneficial and attractive

choice compared to other services.

3.4 Potential Problems for EV Aggregators in the LFC Regulation Market

As described in the previous sections, in LFC, the EV aggregator is responsible for submitting the offer to the market and dispatching the received LFC signal to each participating EV. The LFC scheme with the participation of an EV aggregator is shown in Figure 3.1. Regarding the control of EVs, there are two potential problems for the EV aggregators. First, there could be a communication delay in the LFC signal. The communication delay can be categorized into two parts: the transmission delay and the processing delay. With a delayed signal, the EVs cannot follow the original LFC signal closely, leading to poor performance assessment in a performance-based market. Second, the EV aggregator needs to figure out how to dispatch the received LFC signal to individual EVs. The dispatching of the LFC signal must not violate the EV users' convenience since the priority of the EV is transport usage. Meanwhile, with an optimized dispatching schedule, the EV aggregator can earn more profits from the LFC market.

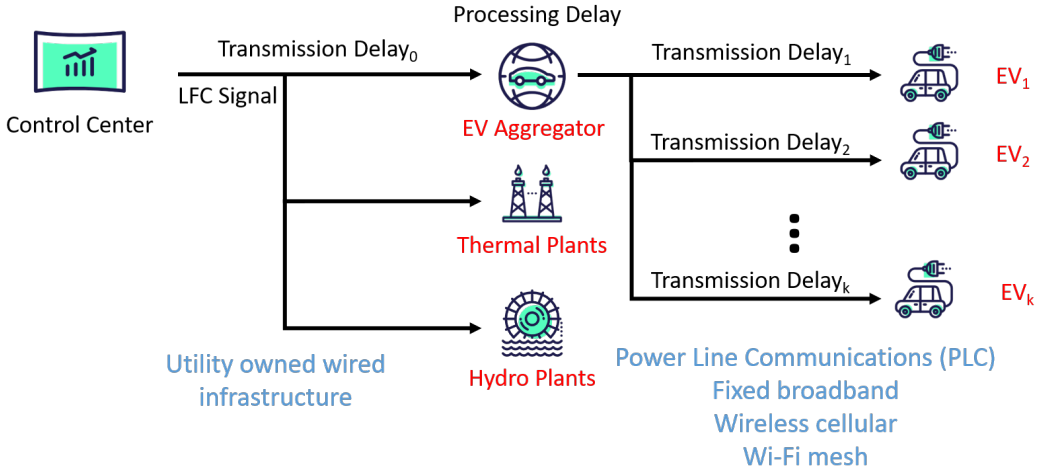

FIGURE 3.1: LFC scheme with an EV aggregator.

3.4.1 Communication Delay

Transmission Delay

The transmission delay is the time that the signal travels from one end to another. As portrayed in Figure 3.1, the transmission delay can happen from the control center to the EV aggregator, and from the EV aggregator to each EV.

Normally, the control center sends the LFC signal via a utility-owned wire infrastructure to the resources [110]. The delay is generally assumed to be within a few seconds [111]. In the AGC30 model, this transmission delay is modeled as a constant delay of 3 seconds.

When dispatching the LFC signal to individual EVs, in order to keep the implementation costs low, the EV aggregator might prefer to choose an open communication infrastructure like power line communications, fixed broadband, wireless cellular or Wi-Fi mesh [112]. This is likely to produce another transmission delay longer than the one from the control center to the EV aggregator. The participating EVs are not necessarily parking in the same location, therefore the length of this transmission delay can differ from EV to EV.

Processing Delay

Processing delay refers to the time it takes when the EV aggregator's server or computer is reading or writing on the database during dispatching.

Compared to other relay facilities in the LFC signal transmission network, the EV aggregator is likely to have a greater processing delay. Normal relay facilities like routers are just routing the signal without any modification, therefore the processing delay is disregardable and independent of the size of the EV aggregator. On the other hand, the EV aggregator needs to derive dispatched control signals for every participating EVs, hence the more EVs are aggregated, the more severe the processing can possibly be [113, 114].

Another factor that affects the processing delay is the storage technology of the server or computer of the EV aggregator [114]. Obviously, SSD (Solid State Drive) can support reading and writing speed considerably faster than

that of HDD (Hard Disk Drive). Although SSD is more suitable for the rapid control of EVs, the current cost of SSD is much higher than that of HDD.

3.4.2 Dispatching of LFC Signal

Users' Convenience

It would be putting the cart before the horse if the provision of ancillary services with EV inconveniences the daily travel of the EV owners. There should be enough energy in the EV battery for travel at the EV owner's departure. Mostly, the constraint on users' convenience is described as that the user pre-define his departure time and required SOC level for the next trip. There are two simple charging strategies commonly used for EVs participating in LFC regulation to ensure that the SOC reaches the required level at the departure time.

The first method puts a priority on EV battery charging, and the EV provides LFC regulation capacity only when its SOC level is higher than the required level [115, 116]. Since providing LFC regulation capacity usually does not deviate from the SOC level too much, the SOC level could probably still meet the requirement even if the EV users plug out in advance.

The second method allows an EV to provide LFC regulation capacity soon after plugging in. After a certain time, the EV starts to charge at full power so that its SOC level can reach the required level right at the departure time [104, 117]. This method is generally accompanied by a schedule of POP when providing LFC regulation capacity, namely only charging at a certain power and use the rest of the charging power to provide LFC regulation capacity, hence its SOC will increase at a rate slower than that of full charging. The SOC fluctuation caused by the provision of LFC regulation is taken into consideration in this method.

These two methods are both simple and straightforward. However, the fixed charging schedule makes them ill-suited in a market mechanism. As long as the total amount of the charging power is enough, the EV users' convenience will not be violated. Therefore, if assuming the probability of the sudden departure is small, the charging period can be arranged at any time during the EV's parking flexibly, especially the time that the market clearing price is low.

The Efficiency of EV Utilization

When an EV is not being charged or discharged at full power, the rest of the power could be used for LFC regulation. To submit the bid so that the revenue from the LFC regulation market could be maximized, the EV aggregator has to schedule the dispatching of the LFC signal. The optimization of the dispatching control will decide for each EV that in each time-step how much power should be used for charging or discharging the battery and how much power should be used for providing regulation capacity. After the dispatching is optimized, the EV aggregator could submit the bid for each time-step to the LFC regulation market and dispatch the LFC signal in real-time operation according to the optimization result.

In the previous studies, the time-step of the dispatching is considered to be the same as the time-step for market bidding [98, 118]. In this way, the optimization problem can be formulated as a linear programming problem and be solved easily. However, such optimization will assume that an EV could provide regulation capacity only when it plugs in for the whole time-step. For example, as shown in Figure 3.2, EV_1 plugs in at 14:30 and EV_2 plugs out at 14:45, and EV_3 is connected from 13:00 to 16:00. From 13:00 to 14:00 and 15:00 to 16:00, there are two EVs that could provide LFC regulation capacity. However, from 14:00 to 15:00, only EV_3 could provide regulation capacity since a regulation resource should assure the capacity for all time if the bid is submitted to and taken by the market.

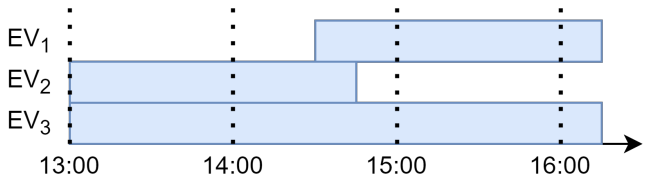

FIGURE 3.2: An example of EV travel profile.

Therefore, a dispatching control with a time-step equal to or longer than the market bidding time-step could not fully utilize the EVs' LFC regulation capability. Contrarily, if the dispatching control could be optimized in a faster time-step, for example, 15min, the EV aggregator could dispatch the regulation power to EV_2 from 14:00 to 14:45 and then to EV_1 from 14:45 to 15:00 and provide more regulation capacity. With a faster dispatching time-step, not only could the EV aggregator utilize the plug-in EVs more efficiently, but also there will be more flexibility in scheduling the dispatch.

3.5 Business Scheme of the Target EV Aggregator

Many types of EV aggregators have been discussed in the literature. Especially in the early stage of V2G concept around a decade ago, during which time the number of commercial EVs is relatively small, the EV aggregator is assumed to be controlling the EV fleet owned by a certain facility, such as university, military base, or government department [104–106]. It is easy to gather the EVs without extra effort since the aggregator is usually the facility itself. In some cases, the facility can even adjust the usage of the EV fleet in order to cooperate with the provision of ancillary services. However, the number of EVs in the fleet is too small, normally around a dozen. It is very unlikely that a facility can own and deploy over a hundred EVs. Therefore, the total providable regulation capacity is also small, and might not be eligible for entering the actual market.

With the growth of the EV market share, more and more research works begin to focus on the business scheme to aggregate the household EVs. A third-party company will be the EV aggregator and share the profits from the ancillary service market with the participating EVs. By providing V2G charging equipment or requesting access to control V2G charging equipment, the EV aggregator can utilize the EVs during either the night parking at home or the day parking in the workplace [98, 117–121].

Theoretically, the control scheme proposed in this dissertation can be applied by any type of EV aggregator to increase the performance and the payment from the LFC regulation market, regardless of its business scheme. To present the analysis clearly and quantify the simulation results reasonably, this dissertation will focus on the EV aggregator described below.

The target EV aggregator in this dissertation is a third-party company that owns several parking lots in the central city area. EVs are gathered from the EV owners who park their EVs in the parking lots when arriving at work. The participating EV users plug out their EVs when leaving work. Compared to the business aggregating EVs from home at night, the daytime aggregation is more profitable and preferable since the PV generation induces more severe frequency fluctuation during the daytime. The target EV aggregator choose to receive the fast LFC signal to earn more mileage payment.

The participating EV owners will inform the EV aggregator of their arrival time, departure time, and requirement of departure SOC in advance. It is

assumed that the EV owners will not change their travel profiles afterward. During the parking time, the EV aggregator provides the EV owners with charging equipment in its parking lots and controls their EVs to provide LFC regulation services to the system. In return, the EV owners can enjoy a lower parking fee.

In many previous research works, the EV aggregator participates in not only frequency regulation services but also other markets, such as the energy market. The scheduling and control of the EVs are derived by co-optimizing the bidding strategies in multiple markets [98, 118, 119, 121]. Since the main topic of this dissertation is the control scheme design of LFC, the target EV aggregator will participate merely in the LFC regulation market. The energy fee for charging the EV battery will be directly paid to the system operator by the EV owner.

A flow chart is illustrated in Figure 3.3 to depict the business scheme plainly.

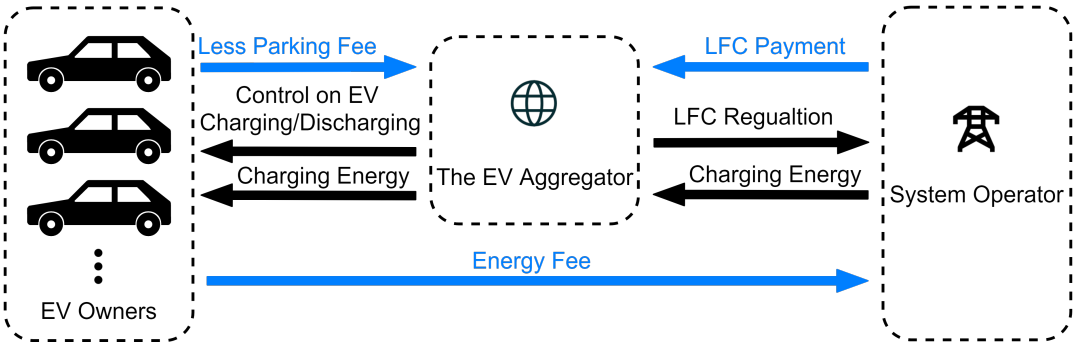

FIGURE 3.3: The business scheme of the target EV aggregator.

Chapter 4

Delay Compensation Control

4.1 Overview

The communication delay of the LFC signal has been one of the main topics in power system stability analysis [111, 122–124]. These researches focus on deriving the robust design of the PI controller in LFC. The proportional gain and the integral gain are tuned based on H_2/H_∞ control theory using the Linear Matrix Inequality approach with the state-space model of the power system. The robust PI controllers guarantee the power system with a larger delay margin, thus the system can operate normally even with the LFC communication delay.

Another technique that is commonly mentioned when dealing with the communication delay in a system is the Smith predictor [125]. The block diagram is shown in Figure 4.1. $R(s)$ is the reference signal, $U(s)$ is the control signal, $C(s)$ is the controller, and $G(s)$ is the target plant. The feedback of the output signal $Y(s)$ is delayed by time τ. $G'(s)$ and τ' are the estimation of the target plant and the delay time respectively. If the estimation $G'(s)$ and τ' match the actual $G(s)$ and τ perfectly enough, the feedback signal $Y'(s)$ can be expressed as:

$$\frac{Y'(s)}{U(s)} = G(s)\dot{e}^{-\tau s} + G'(s)\dot{(}1 - e^{-\tau' s}) \approx G(s) \tag{4.1}$$

The communication delay in the feedback loop is compensated with the Smith predictor.

In a performance-based market, the bidding chance and the payment of the resources are affected by their actual performance. The resources need to follow the LFC regulation signal closely in order to obtain a high performance score. Figure 4.2 compares the response of two regulation

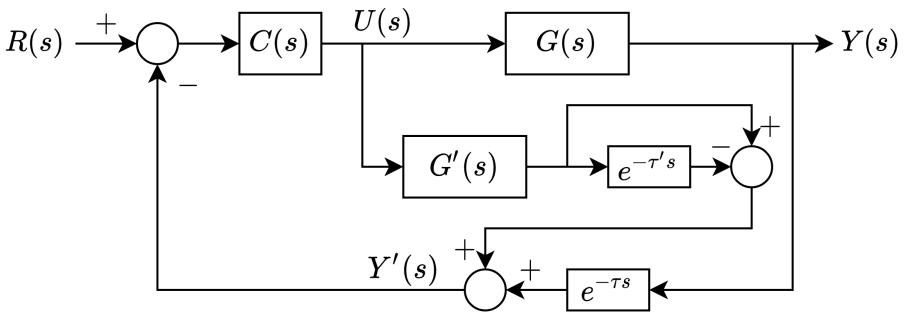

FIGURE 4.1: The block diagram of the smith predictor.

resources to the RegD signal in PJM [126]. The first resource is a utility-owned battery and the second one is a hydro plant. The performance score of the battery is 0.977, thanks to its close tracking of the LFC signal. In contrast, the hydro plant cannot track the LFC signal accurately, and its performance score is only 0.747.

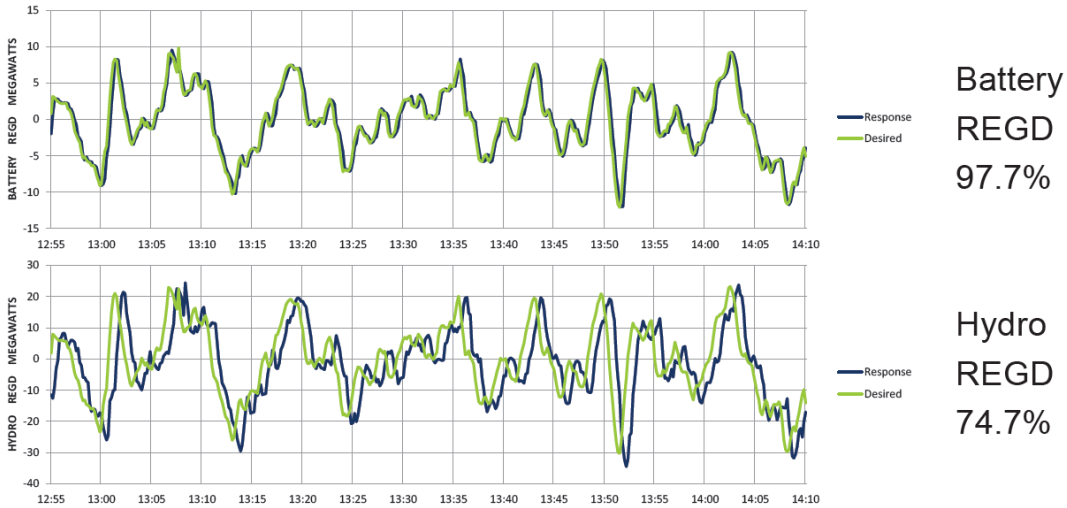

FIGURE 4.2: The response of two regulation resources to the RegD signal in PJM [126].

Provided that the communication structure of an EV aggregator is far more complicated than conventional regulation resources, it is likely to suffer from a more severe communication delay. Moreover, the communication delay will deteriorate the EV aggregator's performance more seriously because of the fast-response characteristic of EV batteries. According to (2.3-2.6), a pure delay in LFC signal will cause a gap between the LFC signal and the EV aggregator's power output, leading to a drop in *Delay Score* and *Precision Score*.

The HIL (hardware-in-the-loop) experiment in [127, 128] also shows the effect on suppressing the frequency fluctuation caused by the LFC signal delay. The RMS value of the system frequency deviation is calculated under two cases: a HIL experiment and a non-hardware simulation. Despite that in both cases the system frequency deviation drastically decreased compared to the case without EV, the result of the HIL experiment is slightly worse than the result of the non-hardware simulation. The reason is that in the HIL experiment, the LFC signal sending to the EV via an Ethernet cable has a 0.8-second delay.

The main objective of the control strategies proposed in previous researches is to improve the overall system performance and robustness in the presence of delay, therefore the system will not lose stability even with delay existing in the communication network of the control loop. Hence, the tracking ability of the participants is not improved. Besides, these strategies are applied on the system operator side, modifying the LFC controller tuning and structure. The mechanism of the performance-based market urges the participating resources to improve their tracking ability by themselves. The resources are not supposed to rely on the system operator to address their own problems on communication delay in a competitive market.

In this chapter, an adaptive controller to compensate for the communication delay from the resource side is proposed. To the best of the author's knowledge, this kind of controller design has not been discussed in previous studies. The proposed controller is aimed at power systems under FFC mode. The structure of the proposed controller is very simple, and it is expected to be able to be equipped in the individual charging pile of each EV. The controller adjusts its parameters based on the received LFC signal data and measured frequency deviation data from the system. Under this operation, a control signal that is close to the original LFC signal without the communication delay can be estimated and reconstructed. The communication delay can be compensated by controlling the EVs with the reconstructed signal.

4.2 Controller Design

In an FFC system, the LFC signal is calculated only based on the current frequency deviation in the system and the system capacity, as introduced in

Section 2.1.2. Even though more complex control logic might be included by system operators in practice, it is reasonable to assume that the dynamics can be modeled as a linear system with a PI controller approximately, as shown in Figure 2.16.

Under steady-state operation, the system capacity P_A and P_B only fluctuate within a small range during a relatively short time period, thus can be considered as a nearly constant gain. The dispatching of the LFC signal only includes linear components such as constant gain or HPF as well. Therefore, the system frequency deviation, Δf, and the LFC signal dispatched to the k^{th} EV, LFC_k, can be regarded as the input and the output of a single-input-single-output (SISO) system with a certain delay. This system is basically linear time-invariant (LTI), given that the control strategy of the system control center is unlikely to change drastically under normal conditions and the effects of the nonlinear components like deadband are small. To conclude, this LTI system can be described in the discrete-time domain as

$$LFC_k(t) = z^{-d_k} G_k(z)[\Delta f](t), t \in \{t_0, t_0 + 1, \dots\} \tag{4.2}$$

The notation of (4.2) is used to denote the output of an LTI system with an input signal. This simple notation combines both the time domain and the frequency domain signal operation and is widely adopted in adaptive control systems presentation [129]. z^{-d_k} represents a delay of d_k samples during the whole communication from the control center to the k^{th} EV. Here it is assumed that the communication network imposes an identical delay on each message.

For stable operation of the power system, all the parameters of the LFC have to be carefully tuned, and then $G_k(z)$ can be regarded as a proper, minimum, and stable discrete transfer function in Z-domain:

$$G_k(z) = \frac{a_m z^m + a_{m-1} z^{m-1} + \dots + a_1 z + a_0}{z^n + b_{n-1} z^{n-1} + \dots + b_1 z + b_0} \tag{4.3}$$

where a_i, $i = 0, 1, \dots, m$ and b_i, $i = 0, 1, \dots, n-1$, with $n \geq m$, are the parameters of the system. $G_k(z)$ is unknown to the EV aggregator.

Since the frequency is identical in the whole system, if $G_k(z)$ can be estimated as $G'_k(z)$ and the frequency can be measured at the EV side, then

the LFC signal dispatched to each EV can be reconstructed at the EV side as

$$LFC'_k(t) = G'_k(z)[\Delta f](t), t \in \{t_0, t_0 + 1, \dots\} \tag{4.4}$$

With this the estimated signal $LFC'_k(t)$, the communication delay can be compensated if $G'_k(z)$ is equal or close enough to $G_k(z)$. The block diagram of the proposed delay compensation controller is given in Figure 4.3. θ is the parameter vector of the estimated parameters of $G'_k(z)$.

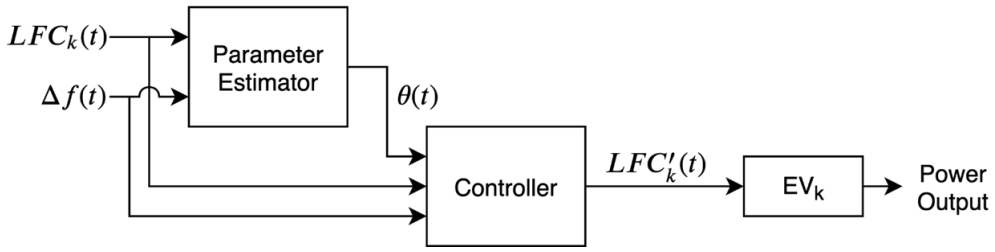

FIGURE 4.3: The block diagram of the proposed delay compensation controller.

4.3 Estimation Algorithm

Theoretically, a SISO system can be estimated with its input and output signal. Given that the received signal $LFC_k(t)$, which is the output signal for estimation, is already delayed by d_k-sample, the measured frequency deviation Δf is delayed intentionally by d'_k-sample as the input signal for estimation. The system to be estimated become:

$$LFC_k(t) = z^{-(d_k - d'_k)} G_k(z)[\Delta f'](t) \tag{4.5}$$

where

$$\Delta f'(t) = z^{-d'_k}[\Delta f](t) \tag{4.6}$$

And the system estimation $G'_k(z)$ will be

$$G'_k(z) = z^{-(d_k - d'_k)} G_k(z) \tag{4.7}$$

If the EV aggregator is aware of the actual delay time d_k, then d'_k can be chosen to be equal to d_k, making $G'_k(z) = G_k(z)$. If d_k is unknown to the EV aggregator, d'_k can be found by doing offline analysis: derive $LFC'_k(t)$ with

some historical data starting with $d'_k = 0$ or the smallest guess of d'_k and then gradually increase d'_k. The dynamics of $LFC'_k(t)$ will not change much except that the time frame is moving advance as d'_k increase if only $d'_k \leq d_k$. When $d'_k > d_k$, the dynamics of $LFC'_k(t)$ will change because additional zeros of $z = 0$ are included to $G'_k(z)$, causing the estimated system becomes unstable.

Define $G'_k(z)$, the estimated parameter vector θ, and the regressor vector $\phi(t)$ to be

$$G'_k(z) = \frac{a'_{m'} z^{m'} + a'_{m'-1} z^{m'-1} + \ldots + a'_1 z + a'_0}{z^{n'} + b'_{n'-1} z^{n'-1} + \ldots + b'_1 z + b'_0} \tag{4.8}$$

$$\theta = [a'_0, a'_1, \ldots, a'_{m'}, -b'_0, -b'_1, \ldots, -b'_{n'-1}]^T \tag{4.9}$$

$$\begin{aligned} \phi(t) = [&z^{-n'}[\Delta f'](t), z^{-n'+1}[\Delta f'](t), \ldots, z^{-n'+m-1}[\Delta f'](t), \\ &z^{-n'+m}[\Delta f'](t), z^{-n'}[LFC_k](t), z^{-n'+1}[LFC_k](t), \ldots, z^{-1}[LFC_k](t)]^T \end{aligned} \tag{4.10}$$

where $n' \geq m'$. n' and m' are the degrees of the numerator and the denominator of the estimated plant $G'_k(z)$, which can be chosen by the EV aggregator. $\theta \in \mathbb{R}^{n'+m'+1}$ is the unknown parameter vector to be estimated. $\phi(t) \in \mathbb{R}^{n'+m'+1}$ is the regressor signal vector generated by the input signal $\Delta f'(t)$ and the output signal $LFC_k(t)$. Two algorithms that can be used to estimate a'_i, $i = 0, 1, \ldots, m'$ and b'_i, $i = 0, 1, \ldots, n' - 1$ are introduced in this section.

4.3.1 Linear Regression

Equations (4.5), (4.7), and (4.8) can be rewritten as

$$LFC_k(t) = \phi(t)^T \theta \tag{4.11}$$

Since the control parameters and structure in LFC are unlikely to change drastically in relatively short time, the parameter vector θ can be obtained by solving the linear regression problem using the least-squares model with

l sets of input and output data:

$$\begin{bmatrix} LFC_k(t) \\ z^{-1}[LFC_k](t) \\ \vdots \\ z^{-l}[LFC_k](t) \end{bmatrix} = \begin{bmatrix} \phi(t)^T \\ z^{-1}\phi(t)^T \\ \vdots \\ z^{-l}\phi(t)^T \end{bmatrix} \theta \tag{4.12}$$

where $l > m' + n' + 1$.

However, the actual LFC system contains nonlinear components such as deadbands and measurement disturbance, which will lead to incorrect result of solving (4.12). Besides, the system capacity and the PI gains could be time variant in the long term. The estimation result might lose accuracy after some time. Therefore, the algorithm must be able to distinguish and avoid the incorrect estimation and repeat itself in a certain time period to keep the accuracy.

Figure 4.4 shows the overall structure of the algorithm. At time t_0, a new round of estimation is to be run. The recorded l sets of data in ΔT_{-1} is used for estimation. Equation (4.13) is used for a self-evaluation process for the controller.

$$u = \sum^{\Delta T_p} |LFC'_k(t) - LFC_k(t)| - \sum^{\Delta T_p} |z^{-d'_k}[LFC_k](t) - LFC_k(t)| \tag{4.13}$$

If u is negative, then the estimated LFC signal by the controller is closer to the original one than the delayed one during the estimation period ΔT_p. In this case, the estimation result is accurate and trust worthy. If the result is positive, then the estimated signal is not better than the delayed one and should be considered inaccurate.

Meanwhile, when the system dynamics remain the same, the poles and zeros of $G'_k(z)$ will not alter too much. The poles and zeros can be obtained through the estimated parameters a'_i and b'_i. If the poles of $G'_k(z)$ are outside of the unit circle of z-plane, the estimated $G'_k(z)$ is not stable, and the result is certainly incorrect and should not be used. Instead, the result of the previous estimation from the data in ΔT_{-2} is taken as the result of this estimation to replace the incorrect one. Additionally, if the poles and zeros are too far away from those in the previous estimation, the result is also treated as incorrect and the previous result should be adopted. Equation (4.14) gives the criteria for determining whether the estimation is correct by calculating the total

distance of the corresponding zeros and poles of $G'_k(z)$:

$$\begin{cases} \text{incorrect}, & \text{if } \sum_i^{m'} |zero_i - \tilde{zero}_i| > \sigma_z \text{ or } \sum_i^{n'} |pole_i - \tilde{pole}_i| > \sigma_p \\ \text{correct}, & \text{if } \sum_i^{m'} |zero_i - \tilde{zero}_i| \leq \sigma_z \text{ and } \sum_i^{n'} |pole_i - \tilde{pole}_i| \leq \sigma_p \end{cases} \tag{4.14}$$

where $zero_i$, $pole_i$ and $\tilde{zero}_i$, $\tilde{pole}_i$ are the zeros and poles of $G'_k(z)$ in ΔT_{-1} and ΔT_{-2} respectively. σ_z and σ_p are adjustable variables.

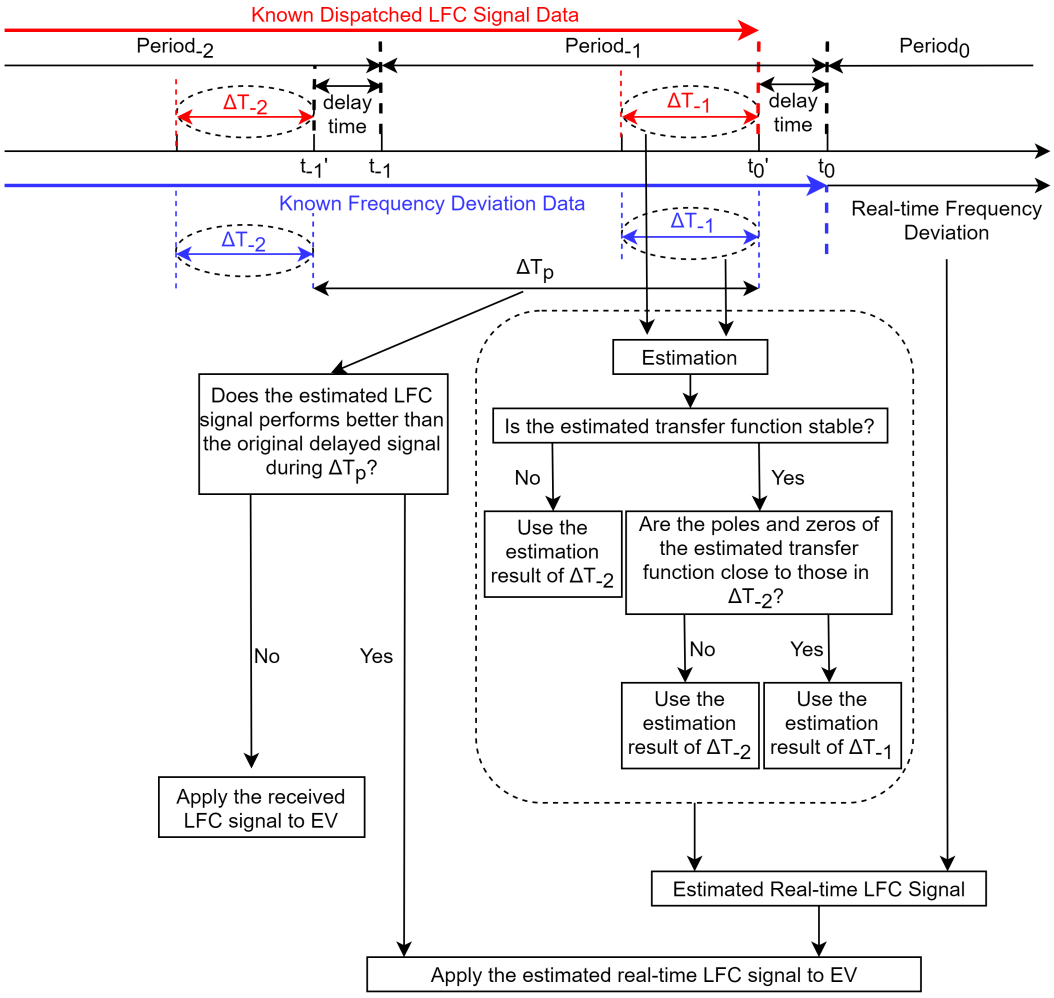

FIGURE 4.4: The flow diagram of the estimation by linear regression.

4.3.2 Adaptive Parameter Estimation

The linear regression algorithm presented in Section 4.3.1 is straightforward but suffers from a few drawbacks. $G_k(z)$ must be approximated by $G'_k(z)$ with low order (small n' and m'), losing some of the dynamics of the original

system. This is due to the fact that the calculation of (4.12) requires matrix inversion, which will increase computational cost exponentially if the order is set to be too high. Besides, obtaining the zeros of poles for 4.14 becomes difficult with higher order. Secondly, the nonlinearity in the actual system, even though quite small, has significantly negative effects on the estimation process. Other disturbances such as measurement error of $\Delta f(t)$ could deteriorate the estimation even more.

Subsequently, adaptive parameter estimation is applied in this section for deriving $G'_k(z)$. There are several algorithms for adaptive parameter estimation. Note that in this application, the actual parameter values of $G'_k(z)$ are required to reconstruct $LFC'_k(t)$, so the normalized least-squares algorithm is chosen as the estimation algorithm. The discrete-time version of the normalized least-squares algorithm is clearly introduced in [130].

In adaptive parameter estimation, the parameter vector θ is updated every time-step. The normalized least-squares algorithm searches for the $\theta(t) \in \mathbb{R}^{n'+m'+1}$ for time-step t to minimize the following cost function:

$$J(\theta) = \frac{1}{2}\sum_{\tau=t_0}^{t-1}\frac{1}{\kappa}(\theta^T(t)\phi(\tau) - LFC_k(\tau))^2 + \frac{1}{2}(\theta(t)-\theta_0)^T P_0^{-1}(\theta(t)-\theta_0) \quad (4.15)$$

where $P_0 \in \mathbb{R}^{(n'+m'+1)\times(n'+m'+1)}$ is a symmetric positive definite matrix and κ is a positive real number. $\theta_0 \in \mathbb{R}^{n'+m'+1}$ is the initial estimation. Note that:

$$\phi^T(t)\theta(t) = G'_k(z)[\Delta f'](t) = G'_k(z)\cdot z^{-d'_k}[\Delta f](t) = LFC'_k(t-d'_k) \quad (4.16)$$

Therefore, the first part of the cost function $J(\theta)$ at time-step t is to minimize the accumulative square error between the reconstructed LFC signal with a manual delay $LFC'_k(t-d'_k)$ and the received LFC with the communication delay $LFC_k(t)$ from the start time t_0 to $t-1$. The second part is a penalty on the initial estimation θ_0.

The minimum value of $J(\theta)$ is reached when its derivative equals zero:

$$\frac{\partial J(\theta)}{\partial \theta} = \sum_{\tau=t_0}^{t-1}\frac{1}{\kappa}(\theta^T(t)\phi(\tau) - LFC_k(\tau))\phi(\tau) + P_0^{-1}(\theta(t)-\theta_0) = 0 \quad (4.17)$$

One might question the necessity of the second part in (4.16) since penalizing the error of $\theta(t)$ deviating from the initial value θ_0 seems irrational. However, without this part, provided that $\phi(\tau)$ and κ are nonzero, (4.17)

becomes:

$$\theta^T(t)\sum_{\tau=t_0}^{t-1}\phi(\tau)=\sum_{\tau=t_0}^{t-1}LFC_k(\tau) \tag{4.18}$$

Obviously, (4.18) has infinite solutions. Hence, to make (4.17) numerically solvable with a unique solution, the second part in (4.16) must be added. As the error of $\theta(t)-\theta_0$ should be less penalized, one can choose a sufficiently large P_0 so that P_0^{-1} is small and the effect of the second part can be numerically ignored.

The solution of (4.17) can be derived as:

$$\theta(t)=\left(P_0^{-1}+\sum_{\tau=t_0}^{t-1}\frac{1}{\kappa}\phi(\tau)\phi^T(\tau)\right)^{-1}\left(P_0^{-1}\theta_0+\sum_{\tau=t_0}^{t-1}\frac{1}{\kappa}LFC_k(\tau)\phi(\tau)\right) \tag{4.19}$$

Calculating $\theta(t)$ directly from (4.19) at each time-step is too complex with matrix inversion. To simplify the calculating process, define:

$$P(t-1)=\left(P_0^{-1}+\sum_{\tau=t_0}^{t-1}\frac{1}{\kappa}\phi(\tau)\phi^T(\tau)\right)^{-1} \tag{4.20}$$

Rewrite (4.20) into:

$$P^{-1}(t-1)=P_0^{-1}+\sum_{\tau=t_0}^{t-1}\frac{1}{\kappa}\phi(\tau)\phi^T(\tau)=P^{-1}(t-2)+\frac{1}{\kappa}\phi(t-1)\phi^T(t-1) \tag{4.21}$$

This equation shows that $P^{-1}(t)$ is nondecreasing and symmetric positive definite as well. That is, for any t, $P^{-1}(t)=(P^{-1}(t))^T\leq P^{-1}(t_0)>0$. In other words, we have $P(t)=P^{-1}(t)>0$, and $P(t)$ is bounded.

Reform (4.21) to avoid the matrix inversion on $P(t)$:

$$P(t-1)=P(t-2)-\frac{P(t-2)\phi(t-1)\phi^T(t-1)P(t-2)}{\kappa+\phi^T(t-1)P(t-2)\phi(t-1)} \tag{4.22}$$

Combine (4.19-4.22), $\theta(t)$ can be obtained as:

$$\begin{aligned}
\theta(t+1) =& P(t)\left(P_0^{-1}\theta_0 + \sum_{\tau=t_0}^{t}\frac{1}{\kappa}LFC_k(\tau)\phi(\tau)\right)\\
=& P(t)\left(P^{-1}(t-1)\theta(t) + \frac{1}{\kappa}LFC_k(t)\phi(t)\right)\\
=& P(t)\left((P^{-1}(t) - \frac{1}{\kappa}\phi(t)\phi^T(t))\theta(t) + \frac{1}{\kappa}LFC_k(t)\phi(t)\right)\\
=& \theta(t) - \frac{1}{\kappa}P(t)\phi(t)(\phi^T(t)\theta(t) - LFC_k(t))\\
=& \theta(t) - \frac{1}{\kappa}\left(P(t-1) - \frac{P(t-1)\phi(t)\phi^T(t)P(t-1)}{\kappa + \phi^T(t)P(t-1)\phi(t)}\right)\cdot\\
& \phi(t)(\phi^T(t)\theta(t) - LFC_k(t))\\
=& \theta(t) - \frac{1}{\kappa}\left(P(t-1)\phi(t) - \frac{P(t-1)\phi(t)\phi^T(t)P(t-1)\phi(t)}{\kappa + \phi^T(t)P(t-1)\phi(t)}\right)\cdot\\
& (\phi^T(t)\theta(t) - LFC_k(t))\\
=& \theta(t) - \frac{1}{\kappa}\left(\frac{\kappa P(t-1)\phi(t)}{\kappa + \phi^T(t)P(t-1)\phi(t)}\right)(\phi^T(t)\theta(t) - LFC_k(t))\\
=& \theta(t) - \frac{P(t-1)\phi(t)}{\kappa + \phi^T(t)P(t-1)\phi(t)}(\phi^T(t)\theta(t) - LFC_k(t))
\end{aligned} \tag{4.23}$$

Compared to (4.19), $\theta(t+1)$ can be calculated directly based on the result in the last time-step $\theta(t)$ and there is no need to perform matrix inversion anymore.

To summarize, at time-step t, the estimated parameter vector for the next time step $\theta(t+1)$ is updated by the following adaptive law:

$$\theta(t+1) = \theta(t) - \frac{P(t-1)\phi(t)\epsilon(t)}{m^2(t)},\ \theta(t_0) = \theta_0 \tag{4.24}$$

$$P(t) = P(t-1) - \frac{P(t-1)\phi(t)\phi^T(t)P(t-1)}{m^2(t)},\ P(t_0-1) = P_0 = P_0^T > 0 \tag{4.25}$$

$$m(t) = \sqrt{\kappa + \phi^T(t)P(t-1)\phi(t)} \tag{4.26}$$

$$\epsilon(t) = \theta^T(t)\phi(t) - LFC_k(t) \tag{4.27}$$

where $t \in \{t_0, t_0+1, \dots\}$. P_0 is the initial value of the gain matrix $P(t) \in \mathbb{R}^{(n'+m'+1)\times(n'+m'+1)}$ at $t = t_0 - 1$. $\kappa > 0$ is a design parameter.

The system frequency is constantly fluctuating randomly, hence $\phi(t)$ can be regarded as persistently exciting, ensuring that:

- $\forall t \in \{t_0, t_0+1, \dots\}$, $P(t) = P^T(t) > 0$ is bounded
- $\forall t \in \{t_0, t_0+1, \dots\}$, $\theta(t)$ and $\epsilon(t)/\sqrt{1+\phi^T(t)\phi(t)}$ is bounded
- As $t \to \infty$, $P(t)$ and will converge to a constant matrix
- As $t \to \infty$, $\theta(t)$ will converge to the actual parameter vector

To ensure that all the dynamics of $G_k(z)$ can be captured, the order of $G'_k(z)$ should be greater than $G_k(z)$, which means $m' \geq m$, $n' \geq n + d_k - d'_k$, and $n' - m' \leq n + d - d' - m$ should be satisfied according to (4.7). Especially, the last condition can be easily procured by letting $m' = n'$. Although the actual order of $G_k(z)$ is unknown to the EV aggregator, m' and n' can be chosen to be as large as possible to avoid problems.

As an example, the block diagram of the proposed delay compensation controller adopting adaptive parameter estimation with $m' = n' = 2$ is illustrated in Figure 4.5.

Both linear regression and adaptive parameter estimation are looking for θ that minimizes the least square error between the reconstructed LFC signal and the original LFC signal over a certain time period. Figure 4.6 depicts the difference between these two algorithm. For linear regression algorithm, every period ΔT_p, a new θ is calculated independently to minimize the least square error within that period. For adaptive parameter estimation algorithm, $\theta(t)$ minimizes the least square error from the starting time to the current time. Therefore, the adaptive parameter estimation algorithm should be more accurate and stable. Moreover, the θ at the current time-step is updated from the θ at the last time-step, which can drastically reduce the computational burden.

4.4 Simulation Results

Simulations are run to test the performance of the proposed controller. Firstly, case studies are examined with different communication delays and

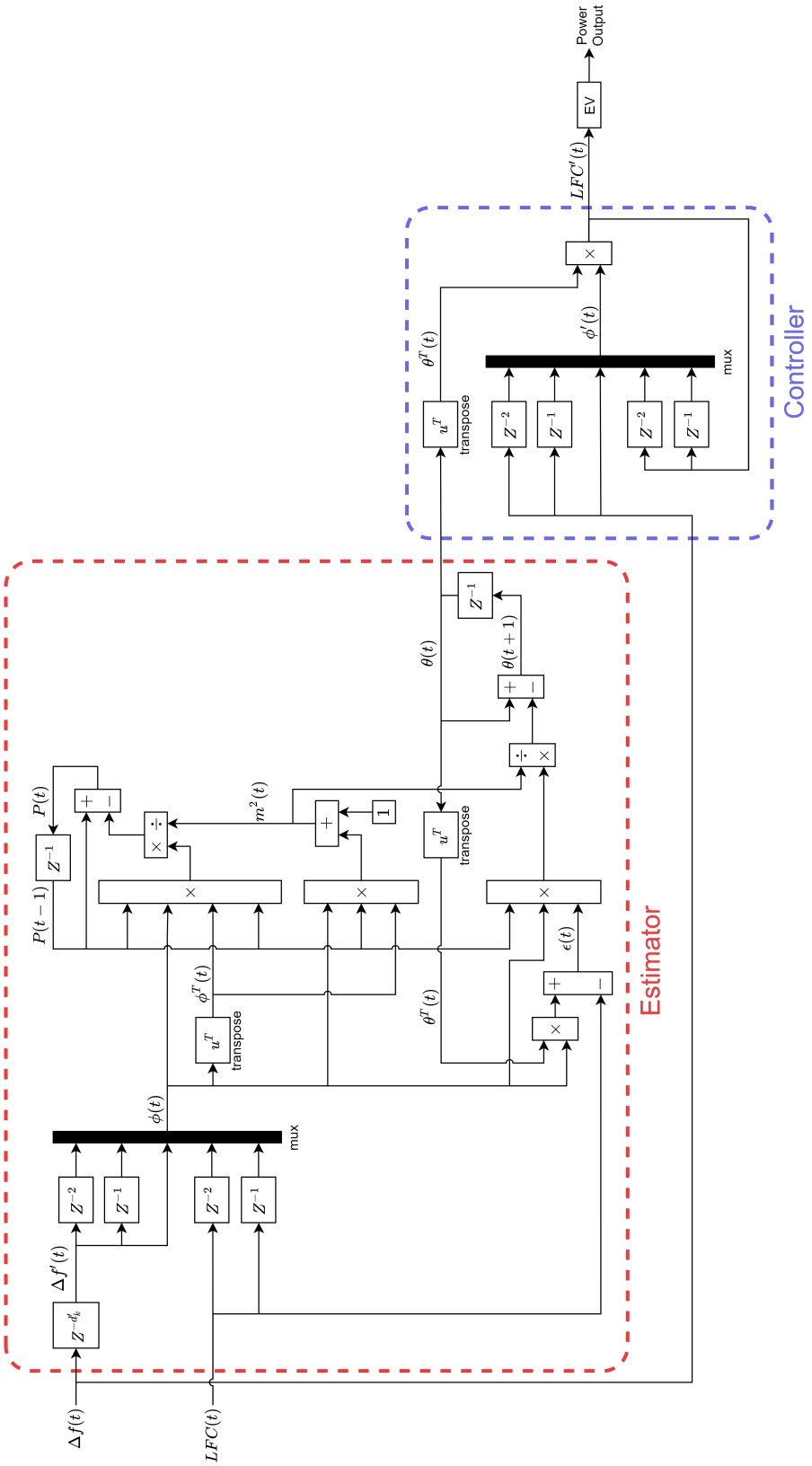

FIGURE 4.5: The block diagram of the proposed delay compensation controller adopting adaptive parameter estimation with $m' = n' = 2$.

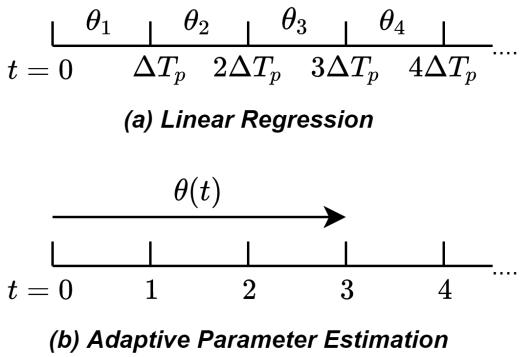

FIGURE 4.6: Difference between linear regression and adaptive parameter estimation.

different levels of measurement noise in the system frequency deviation on the EV side. Then, a system simulation is run to see the effects of the proposed controller on suppressing system frequency deviation. To focus on the communication delay, the simulations in this section do not consider the detailed travel profile of individual EVs. It is assumed that the EV aggregator provides a constant amount of LFC regulation capacity with the aggregated EVs during the simulation.

4.4.1 Case Study

In the case study, the EV aggregator responds to a given LFC signal. 5000 EVs are aggregated during the simulation, and the maximum charging power of each EV P^{max} is 7 kW. The system LFC signal is given in Figure 4.7, which is the fast LFC signal passing through an HPF from the 2nd example case of the AGC30 Model [74]. The system LFC signal is dispatched to the EV aggregator by a partial factor p, which is the ratio of LFC regulation capacity offered by the EV aggregator to the system's fast LFC capacity requirement. The maximum value of the LFC signal is around 125 MW, therefor p is set to be 0.28. The inherent charging and discharging dynamic of the EV's battery is modeled as a first-order transfer function with the time constant set to be 1. The simulation runs for 3 hours.

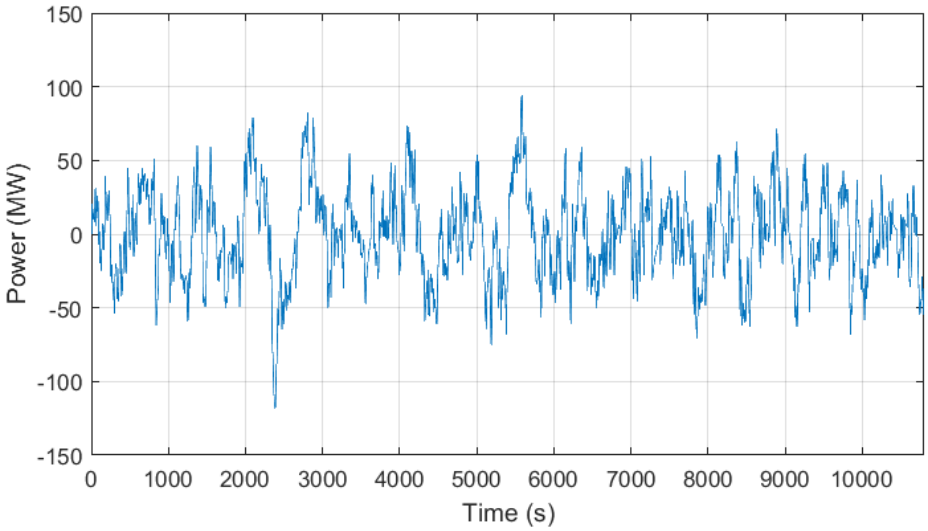

FIGURE 4.7: The system LFC signal in the case study.

Delay Time Identification

The implementation of the proposed delay compensation controller requires the prior knowledge of the delay time on the LFC signal to tune d'_k for the controller. If the LFC signal sent from the system control center is tagged with a timestamp, the EV aggregator can easily find out the delay time by comparing the sending time and receiving time of the signal. If the system operator does not provide the information of the sending time to the regulation resources, the EV aggregator can identify the delay time with the proposed delay compensation controller.

The basic concept and procedure for delay time identification are already explained in Section 4.3. A segment of historical data of the received LFC signal and the frequency deviation is needed. As an example for delay time identification, assume that the actual total communication delay time is 5s. The sampling time of the LFC signal in the simulation is 1s, hence the signal is delayed by $d_k = 5$ samples.

5min of the historical data (300 samples) is used for delay time identification. The reconstructed LFC signals using linear regression algorithm and adaptive parameter estimation with different value of d'_k are shown in Figure 4.8 and Figure 4.9 respectively with d'_k tuned to be 4, 5, and 6. Other tuning parameters for the controllers are given in Table 4.1. I is the identity matrix.

Regardless of the choice of the algorithm, the reconstructed LFC signals

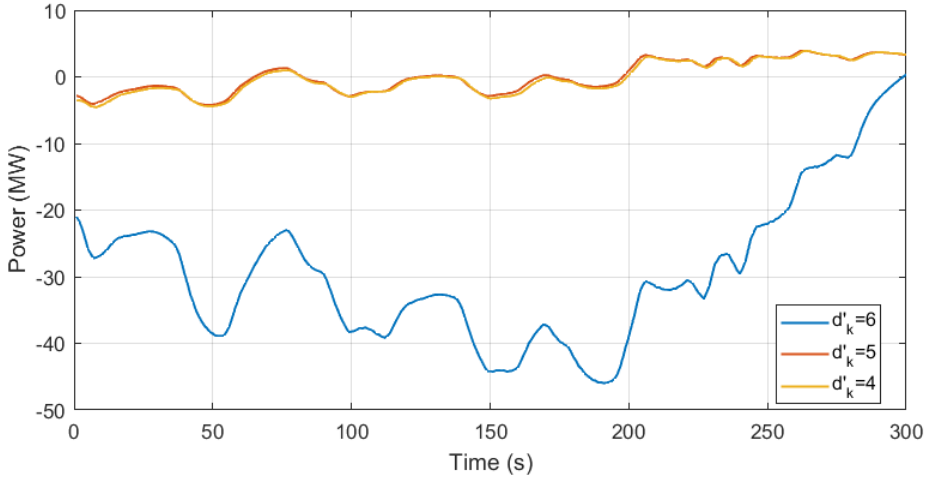

FIGURE 4.8: Delay time identification using linear regression algorithm.

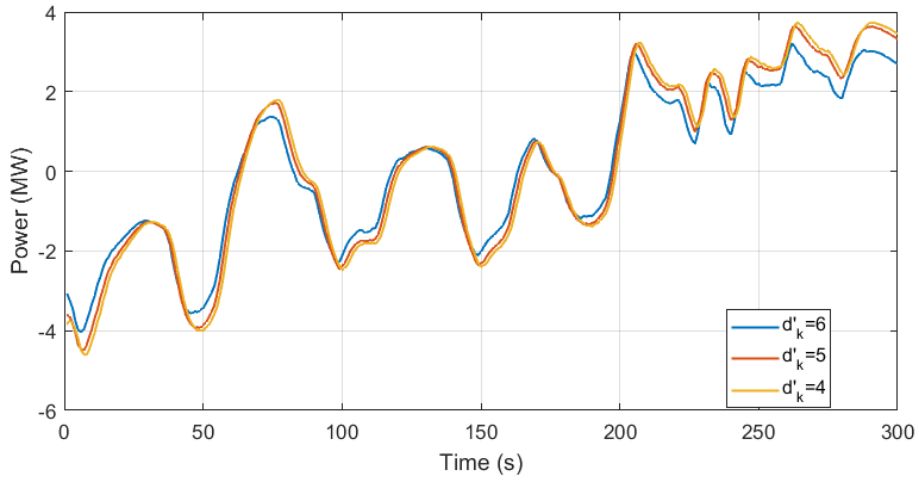

FIGURE 4.9: Delay time identification using adaptive parameter algorithm.

with $d'_k = 5$ and $d'_k = 4$ have the same shape. However, the $d'_k = 4$ signal is lagged by 1 sample. The signal's dynamics is completely different when $d'_k = 6$ since an additional zero is included to $G'_k(z)$. The change of dynamics is more obvious when using linear regression algorithm, given that it is more unstable compared to adaptive parameter estimation algorithm. As a result, the communication delay can be identified as 5 samples, and d'_k should be tuned to 5.

TABLE 4.1: Delay compensation controller parameters.

Algorithm	Parameter	Value
Linear Regression	ΔT_p	3min
	m'	3
	n'	3
Adaptive Parameter Estimation	κ	1
	P_0	$5 \times 10^5 I$
	m'	10
	n'	10

Effects of Communication Delay

In the AGC30 Model, the built-in transmission delay from the system control center to each regulation resource is 3s. The processing delay of the EV aggregator is assumed to be 2s. Four cases of the transmission delay from the EV aggregator to individual EVs are considered: 0s, 3s, 6s, and 8s. Therefore, the total communication delay is 5s, 8s, 11s, and 13s. The performance scores of the EV aggregator are calculated with the assumed delays. Besides, the performance score of the EV aggregator without any communication delay is also calculated for comparison. Different ISOs have different approaches to assess the performances of the participating resources. For example, in New York Independent System Operator (NYISO), the performance index of a regulation resources will be affected if the real-time output is out of the boundary of the maximum and minimum values of the LFC signal in every 30-second interval [131]. However, the above requirement of NYISO's performance index is loose and not suitable for EVs with a fast-response characteristics [132]. Therefore, the target market in this dissertation will adopt PJM's performance score in (2.3-2.6) for performance evaluation, as mentioned in Section 2.4.3. The result is shown in Table 4.2.

Clearly, according to (2.3-2.6), a perfect delay occurring in the LFC signal communication will only have effects on the *Delay Score* and the *Precision Score* theoretically. The *Correlation Score* does not consider the delay effects and simply compares the shapes between the LFC signal and the resource's output. Moreover, for a delay time below 20s, the effects on the *Delay Score* are very small, since the delay time is small compared to the 5-minute base in *Delay Score* computation. The main reason for the low performance score induced by delay is the *Precision Score*. The

TABLE 4.2: The EV aggregator's performance score with different communication delays.

Delay Time (s)	*Correlation Score*	*Delay Score*	*Precision Score*	*Performance Score*
0	0.999	0.993	0.898	0.964
5	0.999	0.976	0.621	0.866
8	0.999	0.967	0.498	0.821
11	0.999	0.957	0.401	0.785
13	0.999	0.950	0.346	0.765

Performance Score in the case with no communication delay at all is the theoretically highest value but dose not reach 1 due to the inherent charging and discharging dynamics of the EV battery.

Effects of Frequency Measurement Noise

An EV aggregator can control the EVs in several different parking lots that have different communication delays. In this simulation, it is assumed that those individual EVs can be combined into 3 groups with transmission delays of 3s, 6s, and 8s separately. Thus, the total communication delays are $d_1 = 8$, $d_2 = 11$, and $d_3 = 13$. All the delays are pre-identified by the EV aggregator. In the simulation, the delay time varies randomly from 80% to 120% of its setup value to simulate the practical situation. For simplicity, it is assumed that the EV aggregator dispatched the LFC signal evenly to every controllable EV, so the 3 groups of EVs all received one-third of the LFC signal.

To keep the implementation cost economical, the frequency measurement devices of EVA might not have high accuracy. In the simulation, it is assumed that the measurement noise $df \in \mathbb{N}(0, (0.02x/3)^2)$, namely, 99.7% of the noise stays within $0.02x$Hz. Three cases of the simulation are run with $x = 0$, $x = 0.5$, and $x = 1$. For each case, the performance of EV aggregator adopting the proposed controller with different estimation algorithms and without any delay compensations is evaluated. The tuning parameters for the controllers are the same as in Table 4.1. The result is shown in Table 4.3.

Since the *Correlation Score* does not consider the effect of delay but only the similarity of the "shape" of the signals, the case without any

TABLE 4.3: The EV aggregator's performance score with different noise level.

Controller Algorithm	x	*Correlation Score*	*Delay Score*	*Precision Score*	*Performance Score*
Linear Regression	0	0.976	0.987	0.763	0.909
	0.5	0.938	0.960	0.463	0.787
	1	0.942	0.960	0.447	0.783
Adapitve Parameter Estimation ($m' = n' = 10$)	0	0.989	0.993	0.816	0.932
	0.5	0.987	0.993	0.781	0.920
	1	0.979	0.990	0.635	0.868
Adapitve Parameter Estimation ($m' = n' = 20$)	0	0.997	0.990	0.880	0.956
	0.5	0.997	0.990	0.864	0.950
	1	0.994	0.990	0.813	0.932
No Compensation	-	0.998	0.957	0.425	0.793

controller should have the highest *Correlation Score*. The improvement in *Delay Score* by the proposed delay compensation controller is relatively small. The primary contribution of the proposed delay compensation controller lays on the precision score. The gap area caused by delay decreases the *Precision Score* value. When there is no measurement noise ($x = 0$), both linear regression and adaptive parameter estimation performs quite well. The *Correlation Score* value is kept high and the *Precision Score* value is greatly improved than the case without compensation. As the noise level increase, linear regression failed in the estimation, leading to a drop on *Precision Score*. Oppositely, adaptive parameter estimation algorithm shows better noise resistance. Precisely, more dynamics of $G'_k(z)$ can be captured with larger m' and n'. When the noise is large ($x = 1$), the *Correlation Score* and the *Precision Score* are higher with larger m' and n'. The overall *Performance Score* stays above 0.9 using adaptive parameter estimation algorithm with $m' = n' = 20$.

A fraction of the EV aggregator's output power during the simulation of $x = 1$ is shown in Figure 4.10. The EV aggregator's power output with the proposed delay compensation controller using adaptive parameter estimation algorithm (blue and blue dashed) tracks the original LFC signal closely. The linear regression algorithm (green) fails in the estimation due to the high noise level. At some point, the EV aggregator's power output without delay compensation (red) is moving in the opposite direction of the

original LFC signal (black), i.e. from 6770s to 6800s due to the delay. Such behavior might easily trigger a large frequency deviation of a sudden because the output becomes the reverse of the actual requirement.

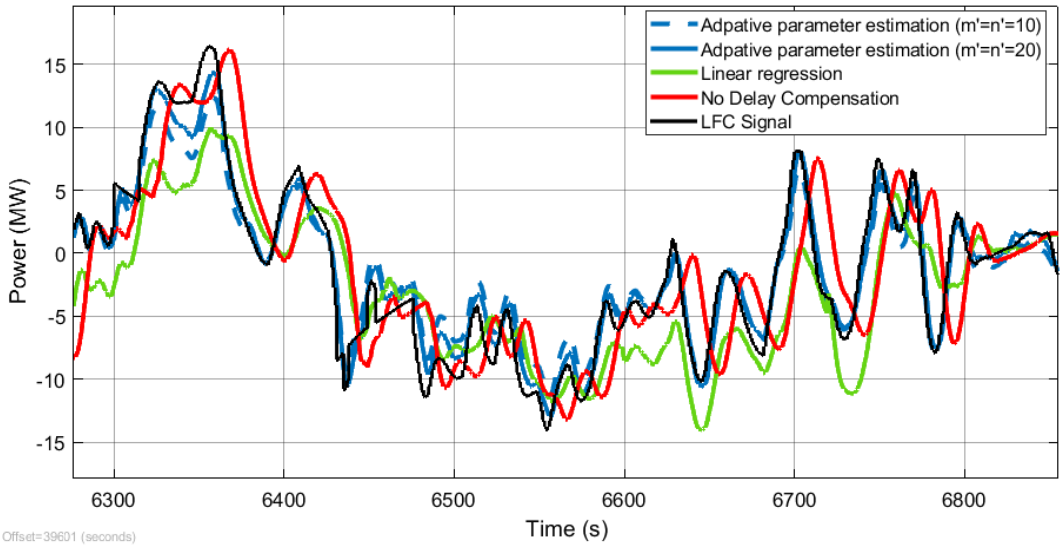

FIGURE 4.10: The EV aggregator's power output under high measurement noise level.

Figure 4.11 depicts the EV aggregator's power output with the proposed delay compensation controller using adaptive parameter estimation algorithm with $m' = n' = 10$ under different measurement noise level. When the measurement noise is large, the power output becomes smoother and less "aggressive". This shows that strong noise will reduce the frequency suppressing effect of the EV aggregator since the LFC signal is not tracked accurately.

A simple hardware experiment is conducted to evaluate the noise level in practical frequency measurement. The system frequency in Tokyo is measured by a household multimeter and a power Quality Analyzer from 11:00 to 16:30 on May 5, 2021. The household multimeter is a HIOKI DT4281 and the selling price is around ¥50,000 JPY. The household multimeter measures system frequency directly from a power strip. The power quality analyzer is a HIOKI PQ3100, which can provide measurement with high precision for industrial applications. The price of the power quality analyzer is ¥280,000 JPY. The system frequency is measured from the power distribution board. Figure 4.12 and Figure 4.13 demonstrate the setup of system frequency measurement by the household multimeter and the power quality analyzer respectively.

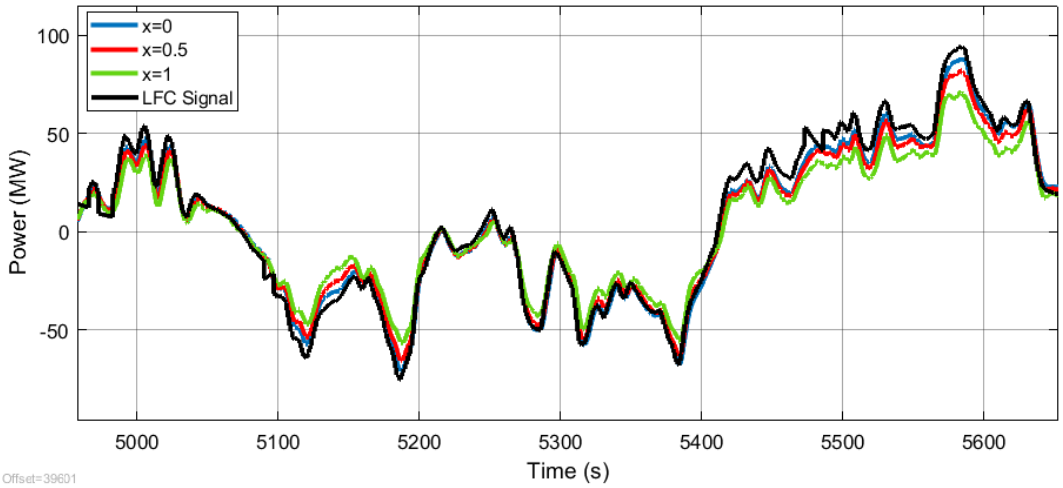

FIGURE 4.11: The EV aggregator's power output under different measurement noise level.

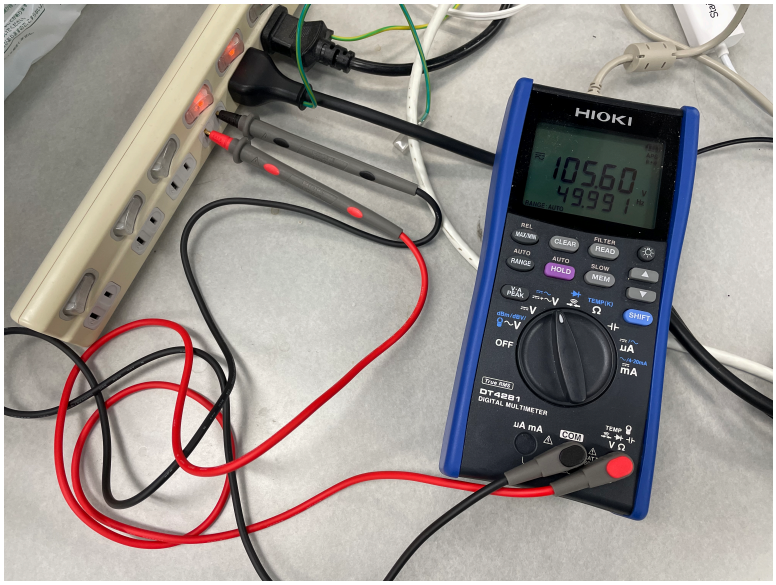

FIGURE 4.12: Measuring system frequency with a household multimeter.

The measured frequency is presented in Figure 4.14 and the distribution of the measurement noise is plotted in Figure 4.15. The maximum noise is smaller than 0.01Hz and most of the noise stay within 0.005Hz. Hence, even with a common household multimeter, the frequency measurement can still achieve enough accuracy, and the noise level is unlikely to exceed $x = 0.5$ in reality.

FIGURE 4.13: Measuring system frequency with a power quality analyzer.

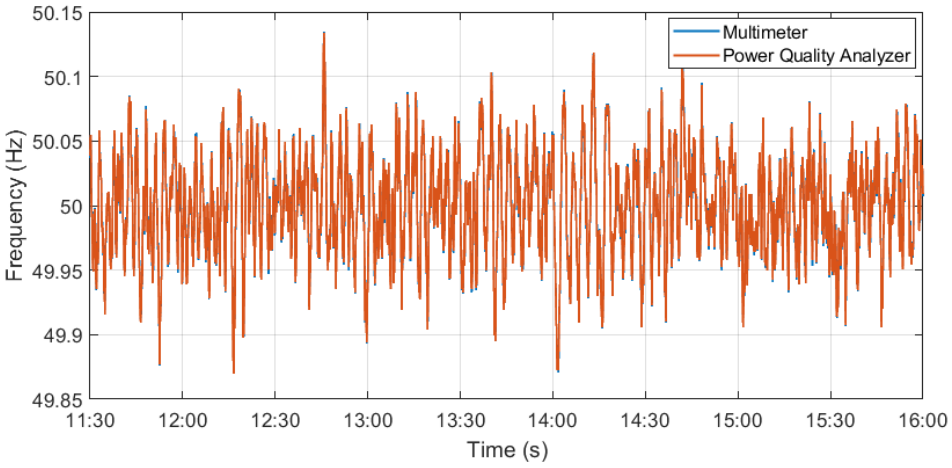

FIGURE 4.14: System frequency measurement with actual hardware.

4.4.2 System Simulation

The simulation is performed to examine the effect on suppressing system frequency deviation. Provided that one single EV aggregator can not have a significant influence on system frequency deviation, it is assumed that all the EVs participating in the LFC regulation adopt the proposed delay compensation controller. There are 15000 EVs in the system providing 105MW regulation capacity. The system model is the AGC30 Model introduced in

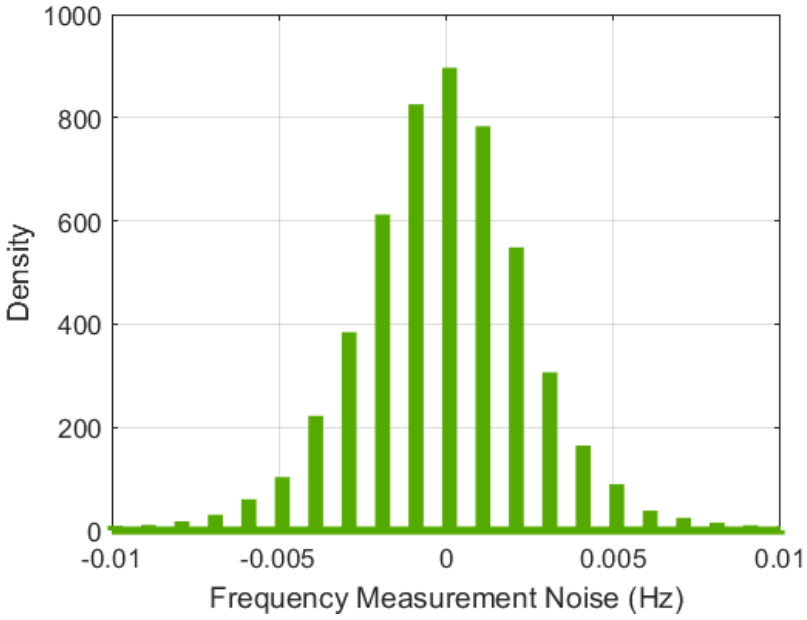

FIGURE 4.15: The distribution of the measurement noise.

Section 2.5. The simulation runs for 5 hours from 10:00 to 15:00 when the PV output is large and causes the frequency to fluctuate drastically.

The system simulation is run under four scenarios:

Scenario 1 There is no EVs participating in LFC regulation

Scenario 2 There is no communication delay in the EV aggregator (an ideal situation)

Scenario 3 There is a communication delay in the EV aggregator but the delay is not compensated

Scenario 4 There is a communication delay in the EV aggregator and the delay is compensated by the proposed delay compensation controller

The controller uses adaptive parameter estimation with $m' = n' = 20$. The maximum and the RMS values of frequency deviation are listed in Table 4.4. The frequency deviation is suppressed with EVs participating in LFC regulation. When there is no measurement noise, the maximum value and the RMS value of the frequency deviation are significantly suppressed to the level of the ideal situation (Scenario 2). As the noise level increases, the suppressing effect on frequency deviation becomes worse because the noise makes the controller output less "aggressive" than the original LFC

signal. When the noise level is extremely high, the benefit of the proposed delay compensation controller on frequency regulation can hardly be seen. However, as pointed out in Section 4.4.1, the noise level is unlikely to surpass $x = 0.5$ in reality. Thus, it is fair to say that with a proper frequency measurement device, the proposed delay compensation controller can help to suppress the frequency deviation.

TABLE 4.4: System simulation results on frequency deviation.

Scenario		**Frequency Deviation (Hz)**	
		Max	**RMS**
1		0.221	0.0539
2		0.145	0.0389
3		0.153	0.0399
4	$x = 0$	0.147	0.0392
	$x = 0.5$	0.150	0.0395
	$x = 1$	0.154	0.0402

Chapter 5

Optimal Dispatching Control

5.1 Overview

LFC is a centralized control where every regulation resources receive a control signal from the system operator. When the EV aggregator receives the LFC signal, it needs to dispatch the signal into every single EV. Meanwhile, the users' travel convenience must be assured by the dispatching control. Different methods of the dispatching control for the EV aggregator have been presented in many researches and generally can be classified into two categories:

(i) dispatch each sample of the LFC signal by specifically designed rules

(ii) dispatch the LFC signal on a pro-rata basis by participation factors

In the first kind of dispatching control, specific rules are determined regarding individual EVs' states and information, such as SOC level and departure time. Every time a sample of the regulation signal is received, the EV aggregator calculates the amount of power output for each EV according to the predefined rules. In [115, 116], when the received LFC signal requires EVs to charge, the EV aggregator assigns the charging amount to EV's with low SOC in priority, and vise versa when the received LFC signal requires EVs to discharge. The SOCs of all the EVs synchronize with this dispatching control. The authors of [133, 134] model the aggregated EVs by state-space representation, and the controller matrix is formed by each EV's charging and discharging state. [135, 136] propose dispatching strategies to minimize the tracking error of the frequency regulation signal.

Despite the advantage of more degrees of freedom in EV charging and discharging control, this kind of dispatching methods suffers from several crucial drawbacks:

- Intricate control structures or logic are involved for determining the dispatch of every signal sample. The sampling rate of the frequency regulation signal cannot be too fast since the calculation of the dispatching at every time-step takes time. The intervals of the frequency regulation signal are 15min and 5min in [133] and [135] respectively, which cannot utilize the fast response characteristic of the EV battery.

- The LFC signal might not be distributed completely. Minimizing the tracking error is usually one of the control objectives in these controllers [133, 135, 136].

- The SOC of EVs will be affected severely due to the provision of LFC regulation capacity. Especially in a market that only allows symmetric bidding, since the mean of the LFC signal is close to zero, charging EVs with LFC signal will be accompanied by deep discharge of EV batteries inevitably, which is not favorable.

- Detailed information on EVs' states is required frequently every time a sample of the LFC signal is received.

In contrast, dispatching the LFC signal on a pro-rata basis by participation factors is much simpler in both concept and application. In pro-rata dispatching, the EV's charging capacity is divided into two parts: a part for scheduled charging (mostly referred to as POP) and the rest part for provision of the ancillary services. The participation factor of an EV is calculated as the ratio of the LFC regulation capacity it provides to the total LFC regulation capacity of the EV aggregator. In this way, perfect tracking of the received LFC signal can be assured as the sum of all the participation factors equals to 1. The authors of [137] propose a dispatching method based on the real-time SOC and the expected SOC of individual EVs. The method is improved in [138] by including a real-time correction of the scheduled V2G power. Smart Charging control for LFC is proposed in [117, 139]. However, the above methods do not consider the regulation market price of LFC regulation and do not control the dispatching to maximize the EV aggregator's revenue. A dispatching method considering market prices for EVs entering both LFC market and energy market is designed in [98,118,119].

In this chapter, a novel LFC signal dispatching control is proposed for EV aggregators. In previous studies, the time-step of the dispatching control is the same as the market, usually one hour [98, 118, 119]. As

explained in Section 3.4.2, a dispatching control with a time-step equal to or longer than the market bidding time-step could not fully utilize the LFC regulation capability of the aggregated EVs. To utilize the EVs more efficiently, the proposed optimal dispatching control operates at a faster time-step. To the author's best knowledge, such a dispatching control has not been considered in the existing literature. With this optimal dispatching control, EV aggregators can arrange the charging schedule of EVs so that they could provide more LFC regulation capacity and earn more revenue, and meanwhile ensuring that the SOC of individual EVs will meet the users' demand before departure. A genetic algorithm (GA) is also designed for searching for the optimal solution of the dispatching. The optimal dispatching control proposed in this chapter is in a form of day-ahead scheduling.

5.2 Problem Formulation

For simplicity and clear analysis, this dissertation only considers the symmetry bidding for EV aggregators. The EV aggregator will provide the same amount of capacity for regulation up and regulation down. It is also assumed that the EV's maximum charging power and the discharge power are the same. Three states are defined for each plug-in EV at each time-step as shown in Figure 5.1. In state (a), the EV is providing full-power of LFC regulation capacity and does not charge its battery. In state (b), the EV is providing LFC regulation capacity at half power and charges its battery at half power. In state (c), the EV is providing no LFC regulation capacity and charges its battery at full power.

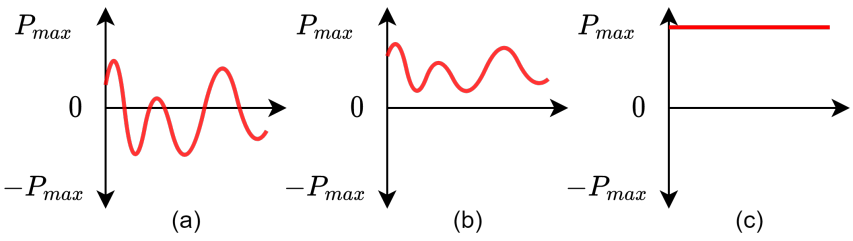

FIGURE 5.1: Power output of EVs in different states.

5.2.1 Fitness Function

Denote the LFC market bidding time-step and the dispatching control time-step as Δt_m and Δt_c respectively. Δt_c should be chosen as a factor of Δt_m. The fitness function is defined as

$$\max_{Cap_k^{EV}(t_c)} Fitness = \sum_{t_m} Price(t_m) Cap_{bid}(t_m) \tag{5.1}$$

where

$$\begin{aligned} Cap_{bid}(t_m) = \min\{Cap(t_c), t_c = \frac{\Delta t_m}{\Delta t_c}(t_m - 1) + 1, \\ \frac{\Delta t_m}{\Delta t_c}(t_m - 1) + 2, \cdots, \frac{\Delta t_m}{\Delta t_c} t_m\} \end{aligned} \tag{5.2}$$

$Price(t_m)$ is the capacity price of LFC regulation market. It could be a prediction of the actual market CCP. $Cap_{bid}(t_m)$ is the LFC regulation capacity that the EV aggregator bids in the market, and $Cap(t_c)$ is the LFC regulation capacity that could be provided in every dispatching time-step. t_m and t_c are the time index of market and dispatching. This fitness function describes the capacity payment of the EV aggregator from the LFC regulation market.

When the regulation capacity is bid, the EV aggregator has the responsibility to ensure that during the bidding time t_m the bid capacity could always be met. This requirement is secured by (5.2). $\frac{\Delta t_m}{\Delta t_c}(t_m - 1) + 1, \frac{\Delta t_m}{\Delta t_c}(t_m - 1) + 2, \cdots, \frac{\Delta t_m}{\Delta t_c} t_m$ are the indices of the dispatching time-step within t_m. An example of the relationship between the dispatching time-step indices t_c and the market time-step indices t_m when $\Delta t_m = 1$hr and Δt_c=15min is depicted in Figure 5.2. Precisely, at $t_m = 1$, the EV aggregator should submit the bid as the minimum of the regulation capacity that can be provided in $t_c = 1, 2, 3, 4$, and so forth.

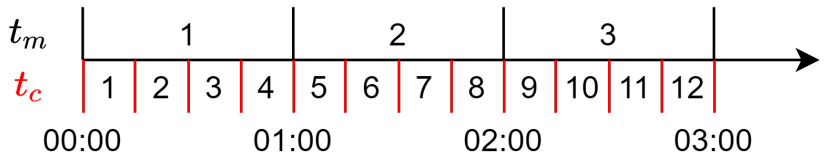

FIGURE 5.2: An example of the relationship between the dispatching time-step indices t_c and the market time-step indices t_m.

In each dispatching time-step t_c, the provided regulation capacity is the sum of the regulation capacity provided by each EV:

$$Cap(t_c) = \sum_{k=1}^{n_{EV}(t_c)} Cap_k^{EV}(t_c) \tag{5.3}$$

where

$$Cap_k^{EV}(t_c) \in \{P_k^{max}, 0.5P_k^{max}, 0\} \tag{5.4}$$

$Cap_k^{EV}(t_c)$ is the LFC regulation capacity offered by the k^{th} EV at t_c. P_k^{max} is its maximum power output. $n_{EV}(t_c)$ is the total number of EVs in the EV aggregator at t_c. Equation (5.4) corresponds to the three states (a), (b) and (c) in Figure 5.1. The objective of the optimization on dispatching control is to decide the state of each EV in each dispatching time-step so that the value of the fitness function (5.1) could be maximized.

One might argue that a continuous state of $Cap_k^{EV}(t_c)$ will be better than the discrete state in (5.4). However, given that the capacity of a single EV is small, the improvement that a continuous state could bring is also small. Furthermore, since the fitness function is a nonlinear and nonconvex function, applying a continuous state will drastically increase the amount of calculation in optimization. Therefore, in this dissertation, the author will apply the discrete state in (5.4).

5.2.2 Constraint

The main constraint for EV aggregators is the charging requirement of EV batteries. Assume that the k^{th} EV with initial SOC, SOC_k^{ini}, plugs in at t_k^{arrive} and requires the battery to be charged to the SOC requirement, SOC_k^{req}, when it plugs out at t_k^{leave}. The energy capacity of the EV battery is E_k. The constraint becomes:

$$SOC_k^{ini} + \frac{\Delta E_k^{charge} + \Delta E_k^{reg}}{E_k} >= SOC_k^{req} \tag{5.5}$$

ΔE_k^{charge} and ΔE_k^{reg} is the energy changes in the battery due to scheduled charging and frequency regulation. In steady-state operation, the mean of system frequency deviation for a relatively long period is close to zero, therefore the mean of the LFC regulation signal is also close to zero. As

a result, it is reasonable to assume that the change in EV's SOC due to frequency regulation is neglectable when applying symmetry bidding on LFC regulation capacity, especially in the day-ahead scheduling. The EV aggregator could also compensate for the effect of frequency regulation on SOC by slightly increasing the SOC requirement SOC_k^{req} or using a Model Predictive Control (MPC) scheme to update the SOC information during real-time operation. The implementation of MPC will be presented in Section 6.1 later. Hence, it is assumed that $\Delta E_k^{reg} = 0$ when scheduling the dispatching control. The constraint is finally modified into:

$$SOC_k^{ini} + \frac{\Delta E_k^{charge}}{E_k} >= SOC_k^{req} \tag{5.6}$$

where

$$\Delta E_k^{charge} = \sum_{t_c=t_k^{arrive}}^{t_k^{leave}-1} [P_k^{max} - Cap_k^{EV}(t_c)] \cdot \Delta t_c \tag{5.7}$$

Usually, besides the constraint on satisfying users' transport requirement, a constraint on SOC level will be set for problems regarding EV charging control. For example, the SOC should stay always within 20% to 95%. However, (5.1) maximizes the profit of providing LFC regulation service, which is contrary to the charging energy as expressed in (5.7). The more capacity is used for charging the less regulation service can be provided. Therefore, the charging energy will be limited to the minimum but sufficient required amount, and the batteries will not be overcharged. EV batteries only discharge according to the LFC signal, hence the SOC will not drop below the minimum level either. Therefore, the constraint on SOC level is reasonable but not necessary for the optimal scheduling in the proposed optimal dispatching control.

Note that if the initial SOC of an EV is too low and it parks only for a short period, then the constraint (5.6) might not be satisfied even if the EV is charging at full power for the whole parking time. As a result, the optimization will certainly fail since no possible solution can be found. However, EVs with this kind of travel profile cannot provide any regulation capacity from the first place. Hence, they are not considered to be aggregated for the provision of LFC regulation capacity. The EV aggregator can just remove this kind of EVs from the optimization and simply control them to charge at full power during parking to raise their SOC as high as possible.

By doing so, the possible failure of the optimization can be avoided.

5.2.3 Dispatching Control

The LFC regulation signal $LFC_{Signal_{EV}}(t)$ assigned to the EV aggregator is dispatched by a participation factor $p_k(t_c)$ for the k^{th} EV at t_c. $p_k(t_c)$ is calculated as:

$$p_k(t_c) = \frac{Cap_k^{EV}(t_c)}{Cap(t_c)} \tag{5.8}$$

According to (5.3), the sum of p_k always equals to 1, guaranteeing the perfect tracking of $LFC_{Signal_{EV}}(t)$. During time t_c, the regulation power output and the charging power output for the k^{th} EV are:

$$P_k^{reg}(t) = p_k(t_c) LFC_{Signal_{EV}}(t) \tag{5.9}$$

$$P_k^{charge}(t) = P_k^{max} - Cap_k^{EV}(t_c) \tag{5.10}$$

And the total power output is:

$$P_k^{tot}(t) = P_k^{reg}(t) + P_k^{charge}(t) \tag{5.11}$$

The system operator will not request a regulation resource to output more power than the regulation capacity it bid:

$$|LFC_{Signal_{EV}}(t)| <= Cap_{bid}(t_m) <= Cap(t_c) \tag{5.12}$$

Hence, the total power output will never exceed the limits of P_k^{max}:

$$P_k^{tot}(t) <= P_k^{max} \tag{5.13}$$

5.3 Optimization by Genetic Algorithm

5.3.1 Algorithm Design

As noted in the last subsection, the optimization of (5.1) is nonlinear and nonconvex. As a stochastic global optimization method, GA is capable

of searching for the global optimal solution in complex multidimensional search spaces [140]. GA does not require auxiliary information such as derivatives and uses probabilistic transition rules to guide the search toward the region with likely improvement [141]. The three states defined in (5.4) for EVs make it suitable to apply GA to the optimization. In this section, a simple genetic algorithm is designed.

In this optimization problem, the variables are the states of EVs in each dispatching time-step. Unlike conventional GA where only 1s and 0s are used to express the variables, an EV's states are converted into a string of 1, 0.5, and 0: state (a) is converted to 1; state (b) is converted to 0.5; and state (c) is converted to 0. The states of an EV form one chromosome, and one solution contents n_{EV} chromosomes. Figure 5.3 shows an example of a solution when $n_{EV} = 5$. Each block represents the state of EVs in each dispatching time-step. The empty space without blocks indicates that the EV is plug-out at that time-step.

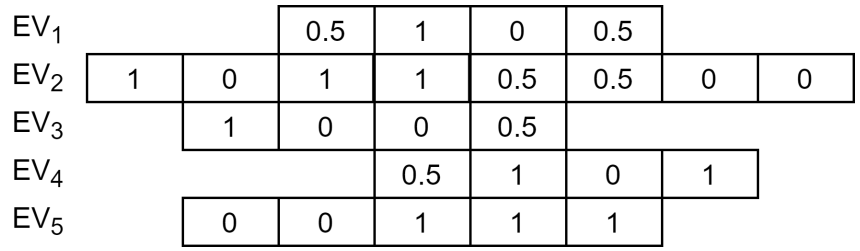

FIGURE 5.3: An example of a GA solution.

Crossover

The first generation of solutions that do not violate the constraint of (5.6) is generated randomly. When reproducing the next generation, two parents are randomly picked from the last generation to produce two offspring. The crossover is defined as the random exchange of some of the chromosomes, namely the dispatching control of individual EVs, between parents. An example of crossover is shown in Figure 5.4. The crossover may or may not happen during the reproduction. If the crossover does not happen, the two offspring will be exactly the same chromosomes as their parents.

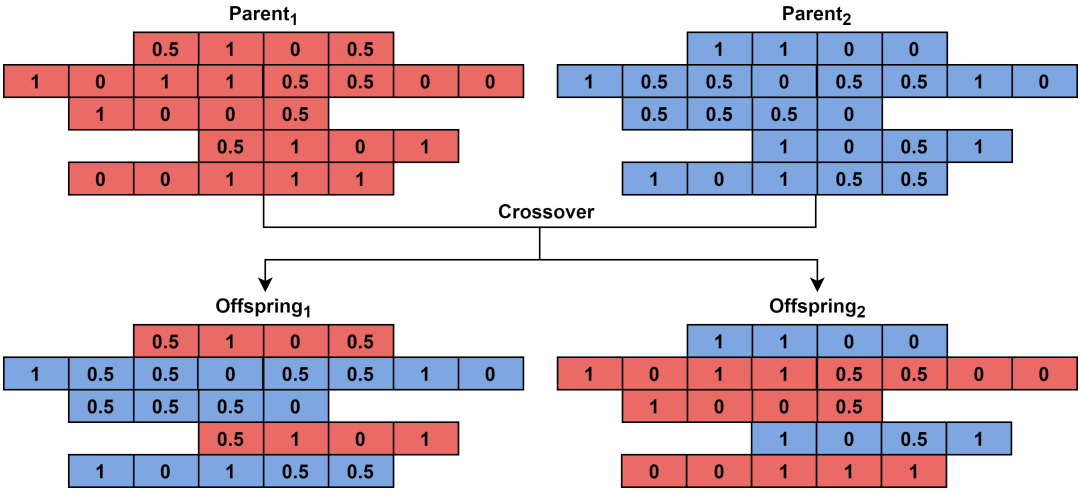

FIGURE 5.4: An example of the crossover.

Mutation

After the crossover process, whether happened or not, the mutation could happen randomly in the offspring's chromosome. Two types of mutation are defined for a single chromosome. *Mutation*1 is that a random pair of 1 and 0 in the chromosome mutates into a pair of two 0.5s, or vice versa. *Mutation*2 is that the chromosome breaks at a random point, and then the front part and the back part exchange their positions. *Mutation*1 and *Mutation*2 will not happen at the same time on the same offspring, and it is obvious that the constraint (5.6) will not be violated after the mutation. There are also possibilities that the mutation might not happen at all. Figure 5.5 illustrates an example of *Mutation*1 and *Mutation*2.

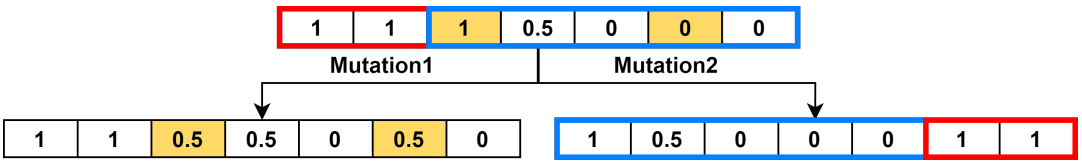

FIGURE 5.5: An example of the mutation.

Reproduction Process

The overall reproduction process is summarized as the following steps:

Step 1: Select two parents from the previous generation.

Step 2: Determine whether crossover will happen based on the preset probability of crossover and reproduce two offspring.

Step 3: For each offspring, determine whether mutation will happen and the kind of mutation based on the preset probability of mutation. Randomly choose a chromosome from the offspring and perform the determined mutation on it.

Step 4: Repeat from the first step until the number of offspring is equal to the population of the previous generation.

Step 5: Form the new generation from the offspring and the last generation with the highest value of the fitness function (5.1). The population of the new generation is equal to that of the previous generation.

5.3.2 First Generation Setup

Although GA conducts a random search in the whole solution space, it is possible that it converges to a local optimal solution rather than the global optimal solution. Generally, the GA should have a large population and allow more mutations and crossovers to explore more solution space and avoid convergence on a local optimal solution, which will exceedingly increase the computational burden.

In the case of the proposed optimal dispatching control, when $\Delta t_c = \Delta t_m$, the optimization is linear and can be easily solved by Mixed Integer Linear Programming (MILP). Faster Δt_c enables more precise control and can utilize the EVs more efficiently, but the optimal schedule should be similar to the solution given by MILP. Therefore, the MILP solution can be used as an initial start point for the search of the global optimal solution with a faster Δt_c.

The result solved by MILP is first converted to the target dispatching time-step Δt_c. Provided that the dispatching control with a faster Δt_c is more precise, some of the time-steps involving scheduled charging (denoted by 0 and 0.5) might not be necessary anymore. An example is depicted in Figure 5.6 for a clear explanation. Δt_m is 1hr and Δt_c is 15min. An EV plugs in at 13:30 with $SOC^{ini} = 60\%$ and plugs out at 17:15, requiring the EV battery to be charged to $SOC^{req} = 80\%$. With the battery energy capacity $E = 40$kWh and the maximum charging power $P^{max} = 7$kW, the EV needs to charge for at least $1.5\Delta t_m$. After the conversion, 3 additional time-steps appear since more

precise t_{arrive} and t_{leave} can be taken into consideration, and the number of the charging time-steps becomes $6\Delta t_c$. The additional time-steps are set to 1 for providing full LFC regulation capacity. The minimum number of charging time-step can be easily calculated as $5\Delta t_c$, indicating that 1 charging time-step is redundant. Hence, random changes are applied to the EV's states so that the charging time-step is reduced to $5\Delta t_c$.

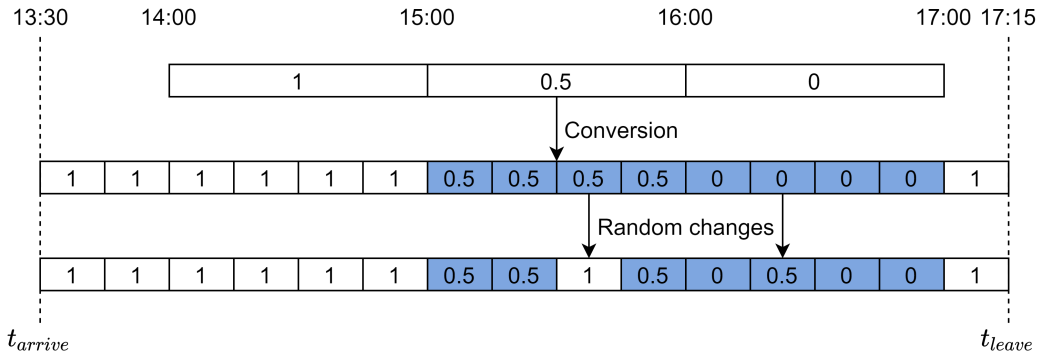

FIGURE 5.6: An example of the setup of the first generation.

The above procedure is conducted for every chromosome in every MILP solution. Compared to a first generation that is generated completely randomly, the first generation generated based on the result of MILP allows GA to reach the optimal solution faster. The other advantage of this process is that the direct implementation of the constraints is avoided, which is very difficult in GA optimization. Together with the proposed crossover and mutation rules, the constraint (5.6) will never be violated during the searching of GA. To rephrase, the proposed GA will only search in the feasible solution space.

5.3.3 Selection Method

After the first generation is generated, parents are randomly selected to reproduce the offspring. The selection method is essential to guide the GA to the acceptable and satisfactory optimal solution [142]. Without the selection method, GA is nothing but a simple random method that gives different optimization values each time [143]. An appropriate selection method should balance the exploitation and exploration of the search. A strong selection pressure might limit the search space and cause GA to

converge to a local optimum. Oppositely, a low selection pressure might cause the GA to merely produce random results that do not converge [144].

Many selection methods for GA have been designed with different properties, such as the roulette wheel selection, rank selection, tournament selection, etc. [145]. Given that the fitness value in the proposed dispatching control optimization is always a positive real number, the proposed GA designed in this dissertation will apply the roulette wheel selection. The probability that a solution i is selected as a parent in the reproduction process is the ratio of its fitness value to the sum of all fitness values in the generation:

$$pro_i = \frac{Fitness_i}{\sum_{j=1}^{n_{pop}} Fitness_j} \tag{5.14}$$

Apparently, the solution with a larger fitness value has a larger probability to reproduce offspring. Besides, the selection will repeat again if the same individual is selected to be both of the parents accidentally. The major drawback of this technique is "the risk of premature convergence of the GA to a local optimum, due to the possible presence of a dominant individual that always wins the competition and is selected as a parent" [145]. This problem is handled by the special setup of the first generation presented above.

5.4 Simulation Results

5.4.1 EVs' Travel Profile

The EV aggregator for the simulation in this section is introduced in Section 3.5 with 4900 EVs gathered. 245 travel profiles of EVs are made from the Fundamental Survey of Social Life in 2016 [146]. The survey shows the percentage of people arriving at work or leaving from work every 15 minutes along the day, from which the plug-in and plug-out time are derived: the EV users plug in their EVs when arriving at work and plug out when leaving. The exact plug-in and plug-out time is randomly assigned within the 15-minute period. The distribution of the plug-in and plug-out time and the number of plug-in EVs during the day are shown in Figure 5.7 and Figure 5.8. For the simplicity of the calculation, it is assumed that each travel profile contains a group of 20 EVs with the same travel pattern.

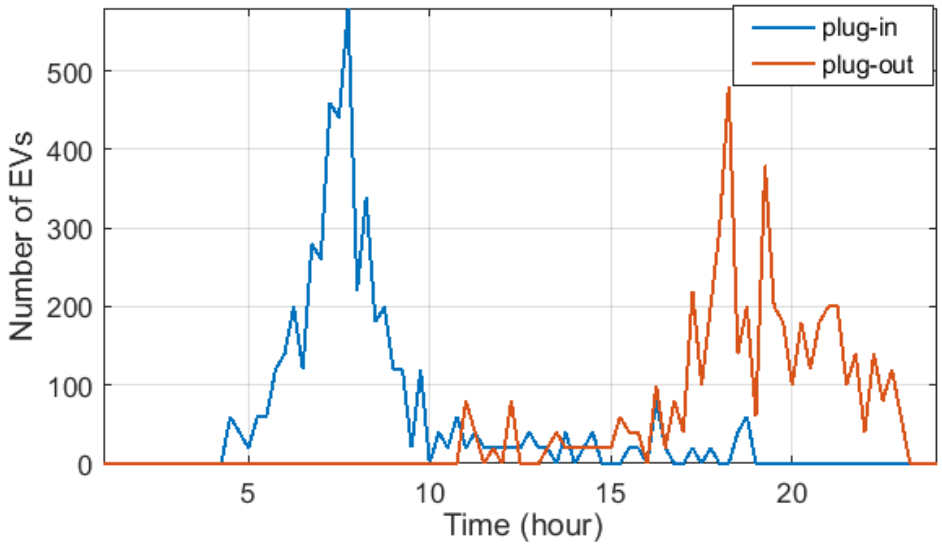

FIGURE 5.7: The distribution of plug-in and plug-out time.

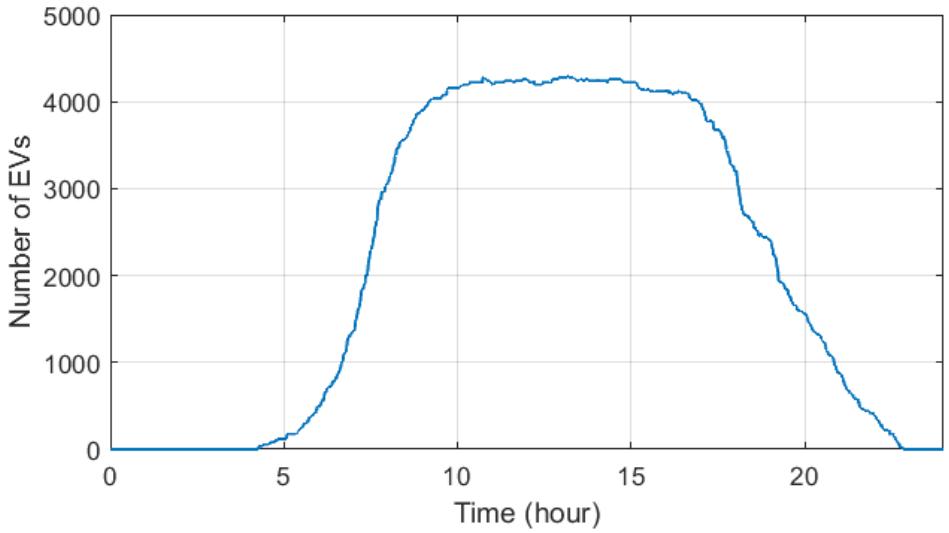

FIGURE 5.8: The number of plug-in EVs during the day.

The arrival SOC for each group of EVs is randomly assigned from 20% to 50%. All the EVs users would expect the SOC to be charged to around 80% at the plug-out time. All the EVs have the same maximum charging power at 7kW and battery capacity at 40kWh. The EV aggregator is requested to submit the bid to the LFC regulation market on an hourly basis. The parameters are summarized in Table 5.1.

TABLE 5.1: The parameters of the EV aggregator.

Parameters		Value
The EV aggregator	Total number	4900
	Initial SOC	20%~50%
	Required departure SOC	80%
	Maximum power	7 kW
	Battery capacity	40 kWh
Market biding time-step		1 hr

5.4.2 Optimization Results

In real market operation, the LFC regulation price can only be known after the market is cleared. To focus on the proposed dispatching control itself, in this section, it is assumed that the EV aggregator could predict the price perfectly according to their studies on the market and schedule the dispatching control based on the predicted price for the 245 groups of EVs. The prediction of the LFC regulation price will be discussed in Section 6.1. The LFC regulation price is from ISO New England's Regulation Clearing Prices on February 5, 2021 [147] and is shown in Figure 5.9.

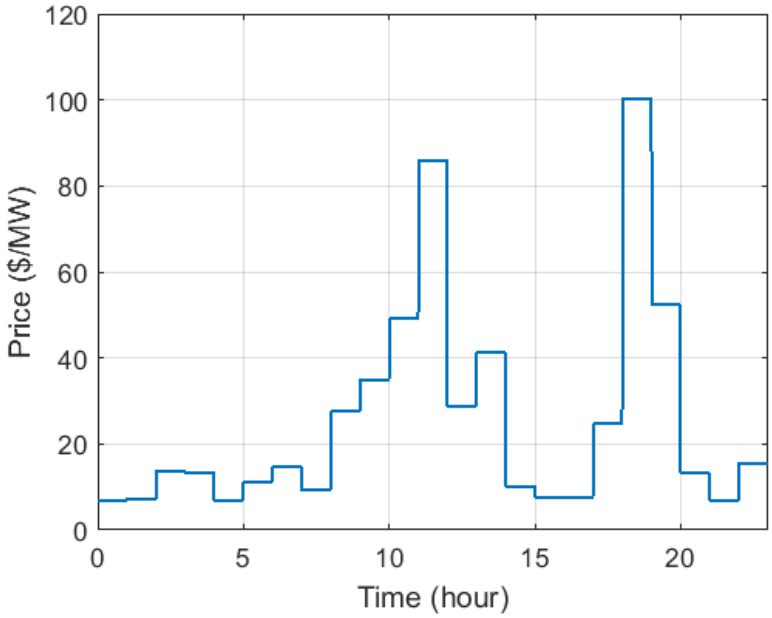

FIGURE 5.9: Hourly LFC regulation price.

The tuning of the GA is given in Table 5.2. The probability of mutation is set to 0.7, which is much higher than the usual case of GA. The reason is that

in this case, one solution contains 245 chromosomes for the 245 groups of EVs. Mutation on a single chromosomes will not bring too much difference, therefore more mutations are encouraged to expand the searching space. The probability of *Mutation*1 and *Mutation*2 indicates that if a mutation happens, the chance of being *Mutation*1 is the same as that of *Mutation*2.

TABLE 5.2: The parameters of GA.

Parmeters	Value
Number of Generation	1000
Number of Population in Each Generation	1000
Probability of Crossover	0.9
Probability of Mutation	0.7
Probability of *Mutation*1	0.5
Probability of *Mutation*2	0.5

The simulation period is from 0:00 to 23:00. The LFC regulation capacity that the EV aggregator could submit to the market with different Δt_c is shown in Figure 5.10. The black dashed line indicates the regulation capacity that could be provided when $\Delta t_c = \Delta t_m$ =1hr, calculated by MILP. With a faster Δt_c, a significant improvement in the provided regulation capacity can be observed from 7:00 to 9:00 and from 14:00 to 17:00 thanks to the more efficient utilization of the EVs. From 10:00 to 13:00 and from 18:00 to 20:00, even though the LFC regulation price is relatively high, the improvement in the regulation capacity is less obvious. The main reason is that at those time the regulation capacity is limited by the number of plug-in EVs. Nearly all the plug-in EVs are already providing LFC regulation capacity due to the high regulation price, therefore even with high efficiency, there is little regulation capacity that could be increased in those time periods.

The best fitness value of (5.1) in each generation is shown in Figure 5.11. The GA designed in Section 5.3 is functioning properly as the fitness values converge after 1000 generations. The final optimal fitness value is given in Table 5.3. The capacity payment is improved by 6% when Δt_c = 15min. However, further decreasing the dispatching time-step does not bring too much further improvement. Besides, a faster time-step of dispatching control requires the EV aggregator to obtain more detailed information of the plug-in and plug-out time of each EV, and the amount of calculation of GA also increases with a faster time-step. For EV aggregators such as a rental car company that knows the exact arrival and departure time of EVs according

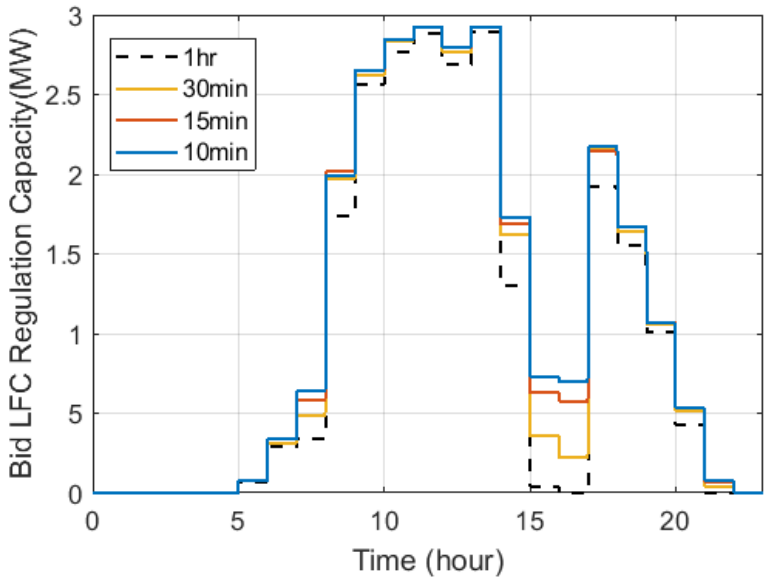

FIGURE 5.10: LFC regulation capacity provided by the EV aggregator with different Δt_c.

to the booking information in advance, a control time-step faster than 10min can be implemented to boost the revenue. Otherwise, a time-step of 15min is good enough for normal EV aggregators who can only assume EVs' plug-in or plug-out time within a certain period of time according to the above simulation results.

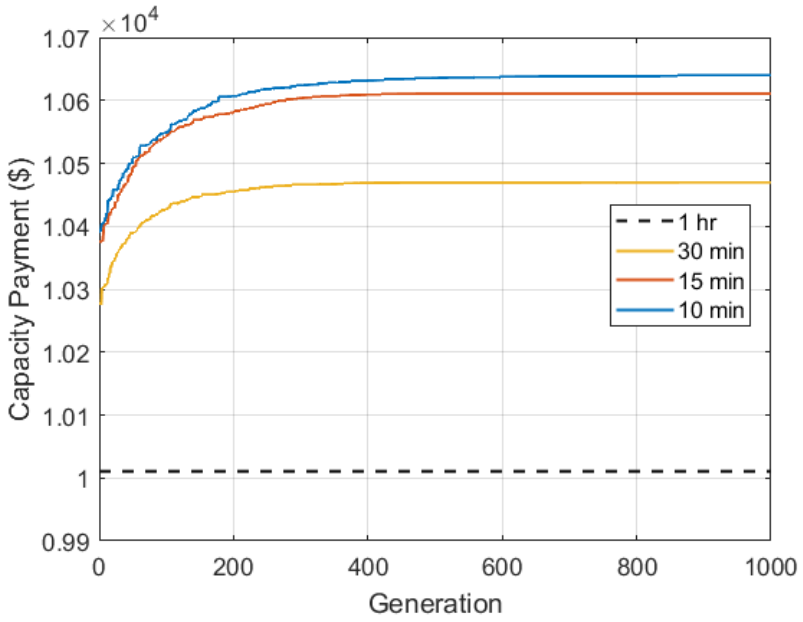

FIGURE 5.11: The performance of the proposed GA.

TABLE 5.3: The capacity payment of the EV aggregator with different Δt_c.

Δt_c	1hr	30min	15min	10min
Capacity Payment ($)	10010.46	10469.96	10610.68	10639.72
Improvement (%)	-	4.59	6.00	6.28

The detailed optimization results with different Δt_cmin are shown in Figure 5.12-5.15 for reference. The plots consist of $245 \times 23(\Delta t_m / \Delta t_c)$ tiny colored blocks. Each row of the blocks is the dispatching control strategy for a group of EVs from 0:00 to 23:00. A purple block indicates that the EV does not provide any LFC regulation capacity in that time-step due to plug-out or charging at full power. Yellow blocks and green blocks corresponds to the (a) and (b) state in Figure 5.1.

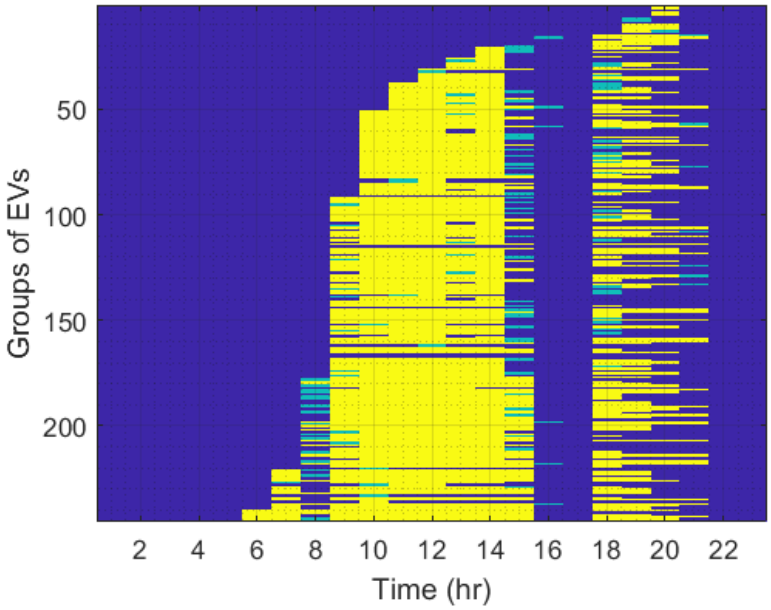

FIGURE 5.12: The optimal dispatching control when Δt_c = 60min.

5.4.3 EV's SOC

A system simulation is performed with the AGC30 Model introduced in Section 2.5. The EV aggregator dispatches the fast LFC signal to individual EVs and the detailed operation of the proposed optimal dispatching control is examined.

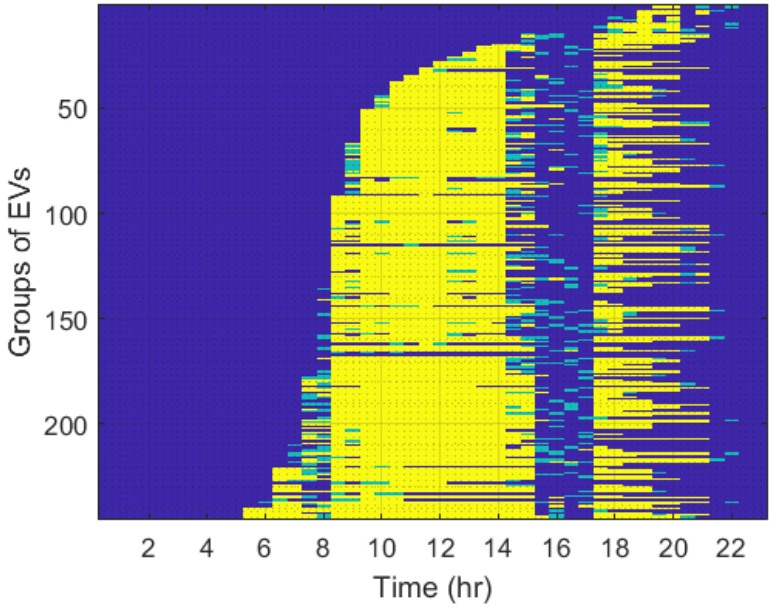

FIGURE 5.13: The optimal dispatching control when Δt_c = 30min.

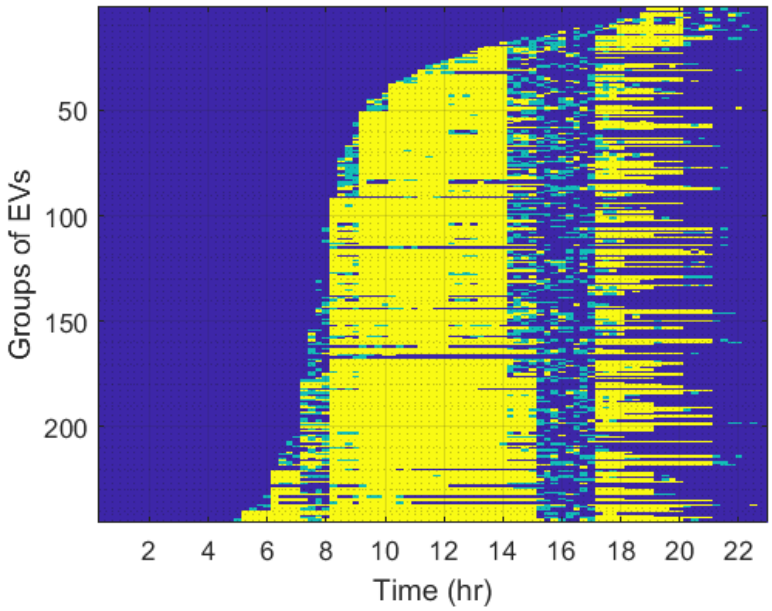

FIGURE 5.14: The optimal dispatching control when Δt_c = 15min.

The EV battery is modeled as in [148]:

$$SOC_k(t) = SOC_k^{ini} + \frac{1}{E_k} \int P_k^{tot}(t) dt \tag{5.15}$$

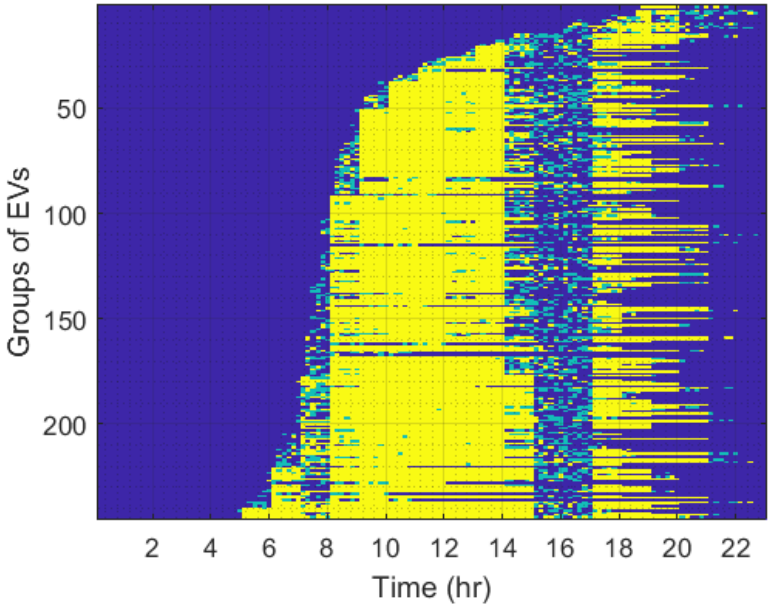

FIGURE 5.15: The optimal dispatching control when Δt_c = 10min.

Assume that all the submitted bids of the LFC regulation capacity of the EV aggregator are taken by the market. The LFC signal assigned to the EV aggregator during t_m is:

$$LFC_{Signal_{EV}}(t) = \frac{Cap_{bid}(t_m)}{LFC_{req}(t_m)} LFC_{Signal_{Fast}}(t) \tag{5.16}$$

where $LFC_{Signal_{Fast}}(t)$ is the overall system fast LFC control signal. $LFC_{req}(t_m)$ is the total system fast regulation capacity requirement at t_m. $LFC_{req}(t_m)$ is defined as the maximum absolute value of $LFC_{Signal_{Fast}}(t)$ during t_m:

$$LFC_{req}(t_m) = \max\{|LFC_{Signal_{Fast}}(t)|, t \in t_m\} \tag{5.17}$$

$LFC_{Signal_{EV}}$ is dispatched by the participation factors calculated in (5.8) according to (5.9). The SOC level of a certain EV in the EV aggregator is shown in Figure 5.16. The EV plugs in at 10:09. When Δt_c = 1hr, the EV starts to provide regulation capacity only after 11:00. When Δt_c = 30min, the EV starts to provide LFC regulation capacity after 11:30. Some other EVs will be controlled to provide LFC regulation capacity from 11:00 to 11:30 to make sure that the LFC regulation capacity can be met anytime within the hour. When Δt_c = 15min, the EV starts charging from 11:15 to 11:30, and

then starts to provide LFC regulation capacity.

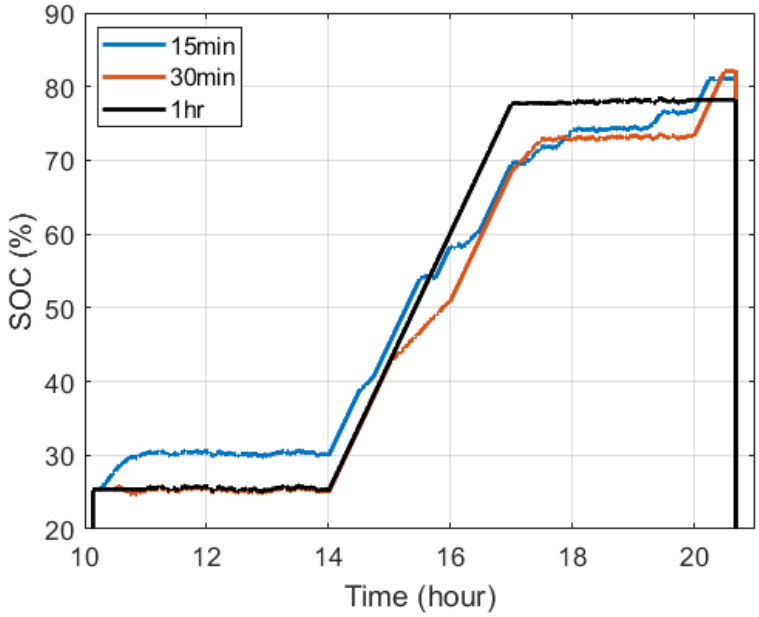

FIGURE 5.16: The SOC level of a certain EV under the proposed optimal dispatching control.

The departure SOC of the 245 groups of EVs with different Δt_c is illustrated in Figure 5.17. The EVs request the SOC to be around 80% before departure. The request is denoted by the black dashed line. A faster Δt_c can suppress the SOC deviation from the users' request because a long Δt_c asks EVs to provide LFC regulation capacity for a long continuous time, therefore the effect of ΔE_k^{reg} on SOC is more severe.

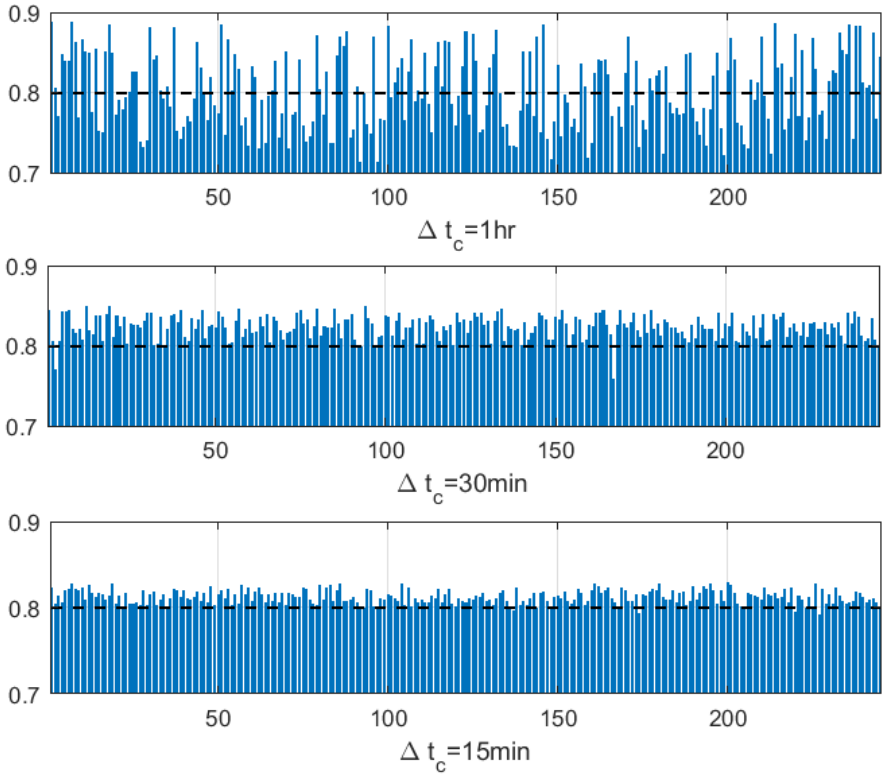

FIGURE 5.17: The departure SOC of the EVs with the proposed optimal dispatching control.

Chapter 6

Overall Control Structure

6.1 Model Predictive Control Scheme

MPC is an optimization-based control method that adjusts the control strategies in every time-step according to the current information and the prediction on future information [149]. It is preferable for EV control and scheduling to adopt an MPC scheme since the states of EVs such as real-time SOC and availability suffers from random changes.

In this section, the optimal dispatching control proposed in Chapter 5 is implemented in an MPC scheme. Moreover, the application of a seasonal-autoregressive-integral-moving-average (SARIMA) model to predict the LFC market clearing price is proposed. While the forecast of the electricity spot price with time-series analysis or sophisticated artificial neural networks has been introduced in many studies [150–152], the prediction on frequency regulation market price is rarely discussed. [118,119] apply the MPC scheme with a prediction on the frequency regulation market price. However, [118] predicts the prices by simply assuming that today's price will be exactly the same as yesterday's. The prediction method is not discussed in [119] and it is assumed that perfect prediction can be obtained somehow, which is not practical in reality. In this section, the SARIMA model is implemented for forecasting the LFC market clearing price, and its performance is compared with the simple prediction with yesterday's price used in [118] in the simulation. The SARIMA model is implemented in a way that cooperates with the MPC scheme. To the best of the author's knowledge, an MPC scheme for EV aggregator with SARIMA prediction on the frequency regulation market price has not yet been discussed in any existing literature.

6.1.1 Overall MPC Scheme

The market clearing mechanism of the LFC regulation market indicates that the market clearing price in (5.1) cannot be known before the market clearing is finished. Therefore, it is necessary to forecast the CCP (Capacity Clearing Price) for scheduling the optimal dispatching.

The overall MPC scheme is illustrated in Figure 6.1. At the current operation market time-step t_m, the EV aggregator is allowed to change its bid capacity at the next time-step $(t_m + 1)$, as introduced in Section 2.4.3. Meanwhile, only the CCP up to the last time-step $(t_m - 1)$ is determined. The predictive horizon of the proposed MPC scheme is from t to the end of the day t_m^{end}. The CCP during this period are obtained from the prediction. The EV scheduling from the next time-step $(t_m + 1)$ to t_m^{end} is optimized with the predictive prices and the real-time information of EVs at time-step t. The control horizon is the next time-step $(t_m + 1)$: the capacity offer at the next time-step $Cap_{bid}(t_m + 1)$ is updated to the LFC regulation market and the participation factors for regulation signal dispatching are re-calculated according to the optimization result.

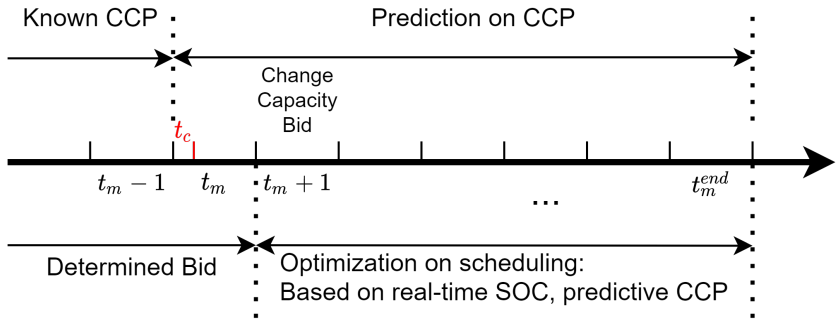

FIGURE 6.1: The Proposed MPC scheme.

The optimization problem is basically the same as formulated in Section 5.2. Note that if an EV is currently plug-in at t_c ($t_c > t_k^{arrive}$), the constraint in (5.6) should be modified into:

$$SOC_k(t_c) + \frac{\Delta E_k^{charge}}{E_k} >= SOC_k^{req} \tag{6.1}$$

where

$$\Delta E_k^{charge} = \sum_{\tau t = t_c}^{t_k^{leave}-1} [P_k^{max} - Cap_k^{EV}(\tau)] \cdot \Delta t_c \tag{6.2}$$

$SOC_k(t_c)$ is the real-time SOC of the EV.

6.1.2 Prediction on the CCP

Obviously, how high the final capacity payment for the EV aggregator can be is related to the accuracy of the predictive CCP. Compared to the electricity spot price, the CCP is more difficult to forecast since the system requirement of LFC regulation capacity is very irregular and the market mechanism is not exactly the same. One way to obtain a fair prediction is simply to assume that today's CCP will be exactly the same as yesterday's, as in [118].

ARIMA model and SARIMA model are commonly used for time series analysis and forecasting future values based on the historical values without extra information input. Therefore, it is very suitable to apply SARIMA prediction on CCP in MPC scheme. In this subsection, the period of the seasonal part of the SARIMA model is set to be 1 day.

The implementation of the SARIMA prediction is as follow:

Step 1: At the beginning of a day, derive a new SARIMA model based on historical data of CCP up till today

Step 2: At market time-step t_m, use the historical CCP data up till $t_m - 1$ as input to predict the price from t_m to t_m^{end}

Step 3: If any of the predicted prices is lower than 0, the predicted price is certainly incorrect and is replaced by the price of yesterday at the same time-step

Step 4: Optimize the EV dispatching scheduling (5.1) from $(t_m + 1)$ to the end of the day (t_m^{end}) and update the capacity offer at $(t_m + 1)$

Step 5: Repeat from Step 2 until t_m^{end}

Step 6: Repeat from Step 1 in the next day

6.1.3 Simulation Results

Simulation based on actual frequency regulation market price is conducted to examine the performance of the proposed MPC scheme with SARIMA Prediction on CCP. The EV aggregator is the same as the one in Section

5.4.1 and the parameters are summarized in Table 5.1. The control time-step Δt_c is set to equal to the market time-step Δt_m and the optimization of the dispatching control is calculated by MILP in order to speed up the calculation so that the performance can be evaluated in a long time span.

SARIMA Prediction

The CCP used in this simulation is the actual CCP in PJM from March 1, 2020 to March 1, 2021 [153].

In time-series analysis, the present datum can be affected by a historical datum in two ways: directly or indirectly, as depicted in Figure 6.2. The indirect influence means that a historical datum affects its following datum and gradually affects the present datum. The direct influence is the influence that a historical datum has on the present datum directly, not through the data between the historical datum and the present datum. The direct influence and the indirect influence are evaluated by partial autocorrelation function (PACF) and autocorrelation function (ACF) respectively. For a set of time-series data D, the ACF value with lag k is calculated as the correlation between the original data and the lagged data:

$$ACF(k) = corr(D, L^k D) \tag{6.3}$$

where L is the lag operator and L^k indicates the data is lagged by k samples. To calculate the PACF with lag k, the indirect influence of the historical data must be removed first. A multivariate linear model D' with order $k-1$ is derived first to represent the indirect influence. The residue D_R is calculated as the difference between the original data D and the linear model D', containing only direct influence of the data lagged by k. The PACF value with lag k is calculated as the correlation between the residue and the lagged residue:

$$PACF(k) = corr(D_R, L^k D_R) \tag{6.4}$$

The PACF and ACF plots of the CCP are shown in Figure 6.3 and Figure 6.4. Generally, PACF and ACF are used to determine the order of the autoregressive part and the moving average part in SARIMA models separately [154]. The red lines at each lag indicate the influence of the lagged data on the present data. The larger the value is, the larger the influence the lagged data has. The blue lines are the confidence bound of

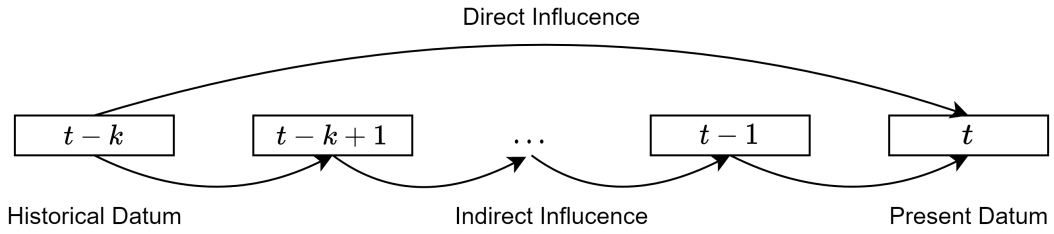

FIGURE 6.2: The influence of a historical datum.

2 standard deviations. The lagged data whose value is within the blue lines are regarded as having almost no influence on the present data. The plots of PACF and ACF indicate relatively significant relationships between the present data and the data lagged by 1, 24, and 48 samples, and the data lagged by 72 samples has a weaker relationship. Accordingly, the non-seasonal autocorrelation order and moving average order are chosen to be 1, corresponding to data lagged by 1 sample. With the seasonal period set to be 24, the seasonal autocorrelation order and moving average order are chosen to be 3, corresponding to data lagged by 24, 48, and 72 samples. The degree of integration is set to be 0 since the data seems stationary.

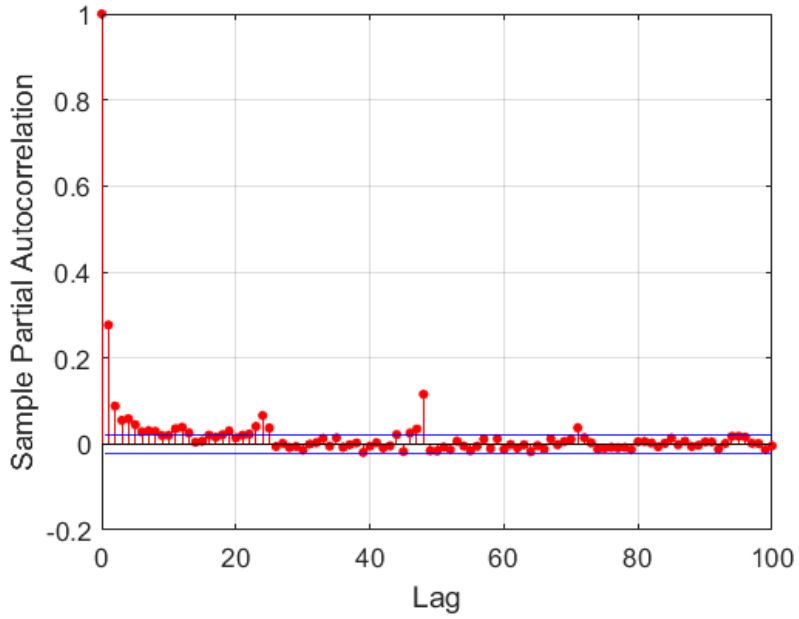

FIGURE 6.3: The PACF plot.

In the simulation, every day a new SARIMA model of $(1,0,1)(3,0,3)_{24}$ is derived based on the historical data of the past 120 days using the

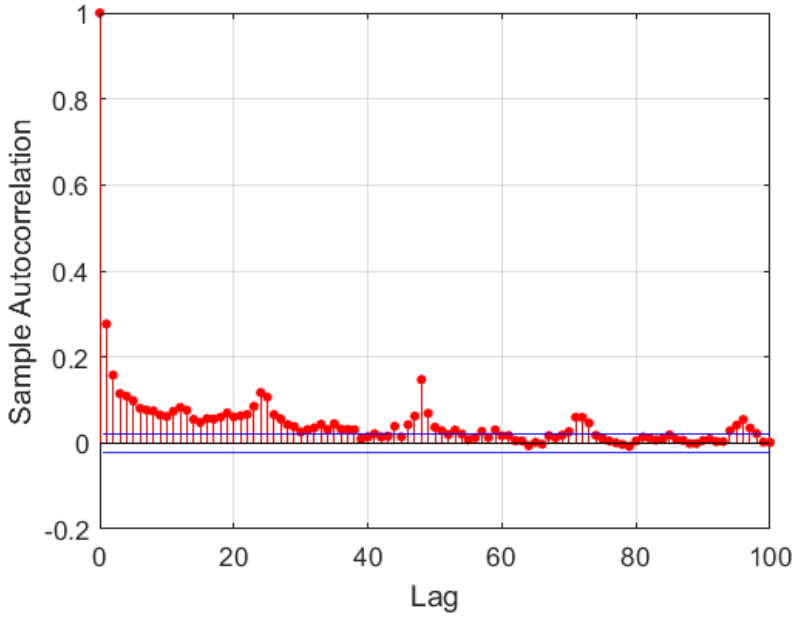

FIGURE 6.4: The ACF plot.

Econometrics Toolbox in MATLAB. Hence, the above setting of the non-seasonal order and the seasonal order of SARIMA model might not be the optimal option for every single day. Surely, one can try to pursue a better prediction results by comparing SARIMA models with different orders everyday and select the best one with lowest Akaike information criterion (AIC) value or Bayesian information criterion (BIC) value. However, such an approach is extremely laborious, while the performance of fixing the SARIMA orders for every day is adequate. Figure 6.5 shows the final result of the predicted CCP in relation to the actual price. The prediction residue is shown in Figure 6.6. The RMS value of the prediction error is 19.79$.

Payment with the Proposed MPC Scheme

The capacity payment of the EV aggregator from the frequency regulation market adopting the proposed MPC scheme is simulated in three cases:

- SARIMA: the EV aggregator predicts today's market CCP with the SARIMA prediction
- YESTERDAY: the EV aggregator predicts today's market CCP by simply assuming today's price will be exactly the same as yesterday's price.

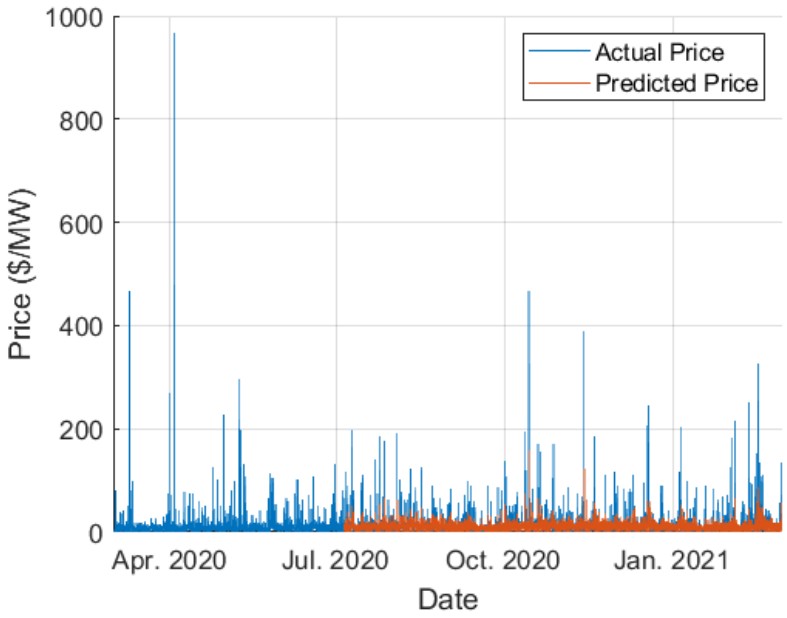

FIGURE 6.5: The CCP from July 4, 2020 to March 1, 2021.

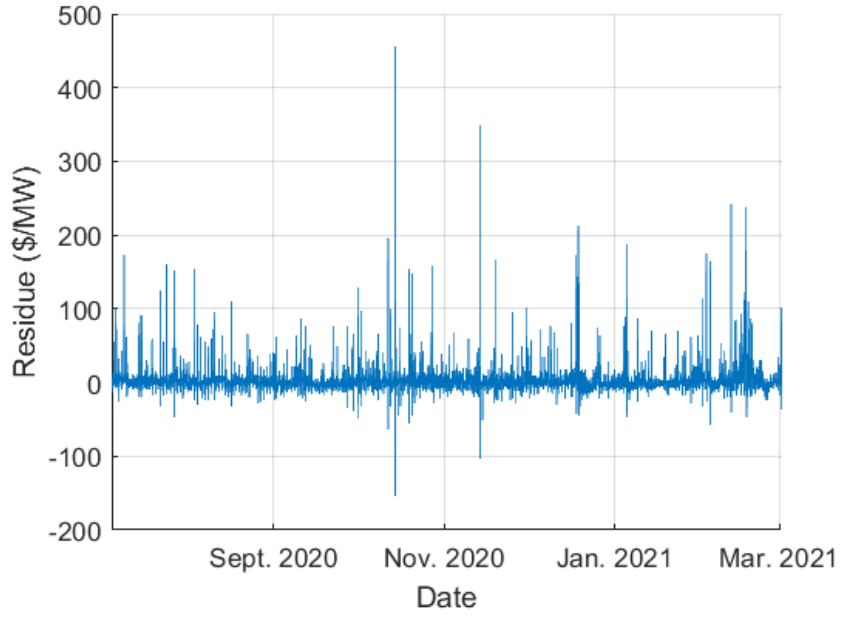

FIGURE 6.6: The prediction residue of the CCP from July 4, 2020 to March 1, 2021.

- ORACLE: the EV aggregator predicts today's market CCP accurately.

In the YESTERDAY case, the MPC scheme adopts the commonly used simple prediction method on frequency regulation prices that can be found in [118]. The capacity payment of the ORACLE case represents the theoretically best

payment the EV aggregator could possibly get from the LFC regulation market since it has the perfect prediction results. The result of the proposed SARIMA prediction is compared to the results of these two cases in this subsection.

The simulation is run for 240 days from July 4, 2020 to March 1, 2021. During this period, the EV aggregator scheduled the aggregated EVs to participate in the LFC regulation market. To focus on the effect of the prediction methods, it is assumed that the traveling profile of the aggregated EVs are the same every day within the simulation period. The total capacity payment of the three cases is shown in Table 6.1.

TABLE 6.1: The total capacity payment in 240 days.

SARIMA	YESTERDAY	ORACLE
9.10×10^5 \$	8.65×10^5 \$	10.30×10^5 \$

In the YESTERDAY case, the capacity payment reaches 84.0% of the ORACLE case, meaning 84.0% of the theoretically best payment can be acquired by the EV aggregator by simply using yesterday's price as the prediction on today's price. As shown in the previous analysis, the price one day before (24 lags) has some influence on the current hour, therefore the performance of simply applying yesterday's price is decent. In the SARIMA case, the capacity payment is further boosted to 88.3% of the ORACLE case since more effects of the previous prices are considered, despite that the RMS value of the SARIMA is not so small. The daily payment ratio of the SARIMA case and the YESTERDAY case to the ORACLE case is illustrated respectively in Figure 6.7. During the simulation period, the daily payment ratio of the SARIMA case is generally slightly better than that of the YESTERDAY case.

The detailed simulation results on December 10, 2020 and February 4, 2021 are given in Table 6.2 to examine the performance of the proposed MPC scheme. The CCP prediction result on December 10, 2020 is shown in Figure 6.8. It can be seen that on this day, even though the SARIMA model does not predict the value of the price pick at 7:00 as accurate as yesterday's price, the overall trend of the SARIMA prediction is closer to the trend of the actual price. The capacity that the EV aggregator can provide to the LFC regulation market is restricted by the number of plug-in EVs in that hour. Therefore, it is more important to predict the overall trend of the price during the day and schedule the EVs to charge rather than capacity provision at the lowest price. The capacity offer submitted to the LFC regulation market is shown in

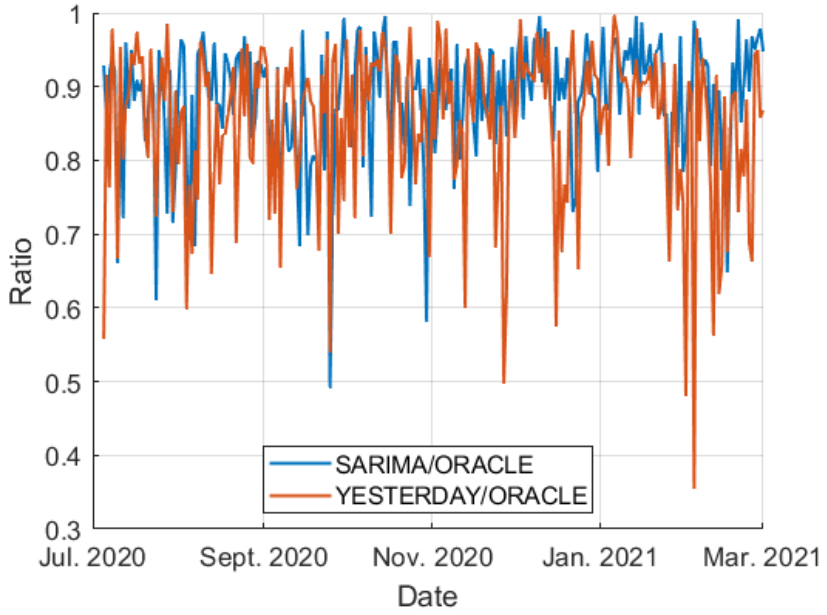

FIGURE 6.7: The daily payment ratio from July 4, 2020 to March 1, 2021.

Figure 6.9. The SARIMA prediction found the lowest price to be around 15:00 and 16:00 correctly and avoided providing capacity at that time. Meanwhile, yesterday's price indicated the lowest price would come at 10:00 and 11:00 and provided regulation capacity at 15:00 and 16:00, leading to profit loss. The same situation can also be observed on February 4, 2021, during which the trend of the actual price is very different from that of yesterday's price, as shown in Figure 6.10. Figure 6.11 reveals that the offered capacity in the YESTERDAY case deviated from the theoretically best solution in the ORACLE case, hence the payment reduced drastically.

TABLE 6.2: The detailed simulation results on December 10, 2020 and February 4, 2021.

Date	**2020/12/10**	**2021/02/04**
SARIMA	2,770.05$	7,216.35$
YESTERDAY	2,554.24$	2,588.31$
ORACLE	2,781.15$	7,295.01$
SARIMA/ORACLE	99.6%	98.9%
YESTERDAY/ORACLE	91.8%	35.5%

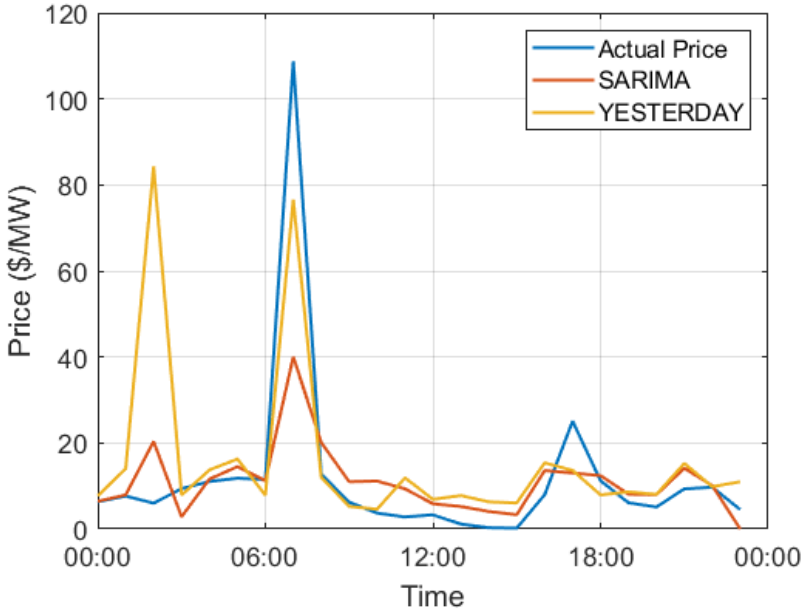

FIGURE 6.8: The predicted CCP on December 10, 2020.

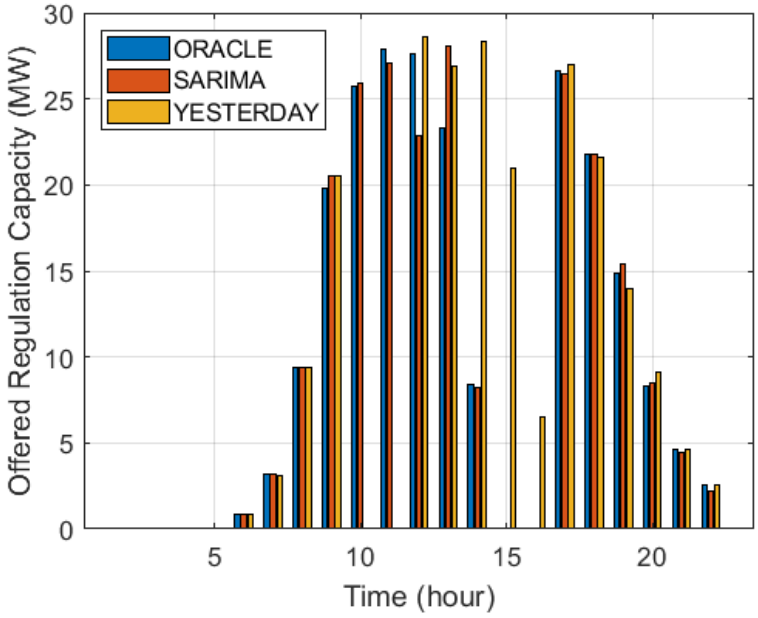

FIGURE 6.9: The offered capacity on December 10, 2020.

Departure SOC

The distribution of the departure SOC with the proposed MPC scheme and SARIMA prediction on CCP during the simulation period in Figure 6.12. Most of the departure SOCs stay above 80%, which satisfies the

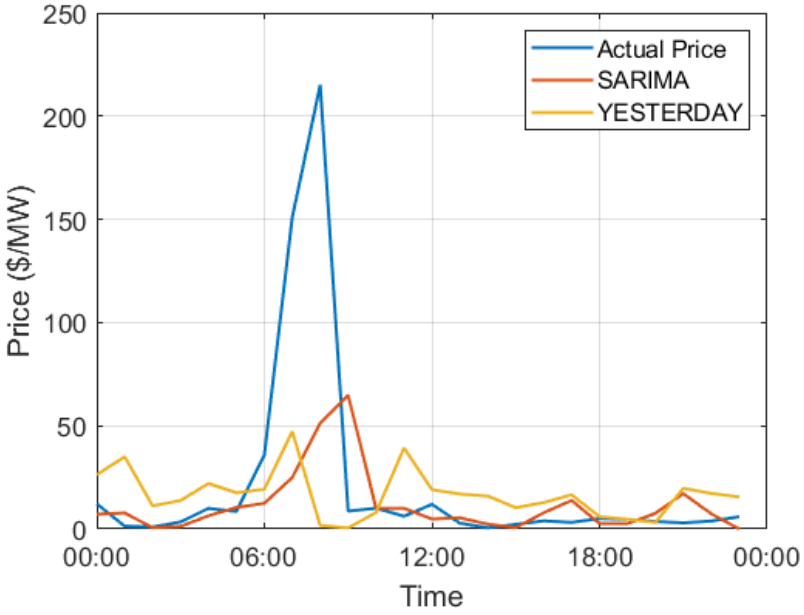

FIGURE 6.10: The predicted CCP on February 4, 2021.

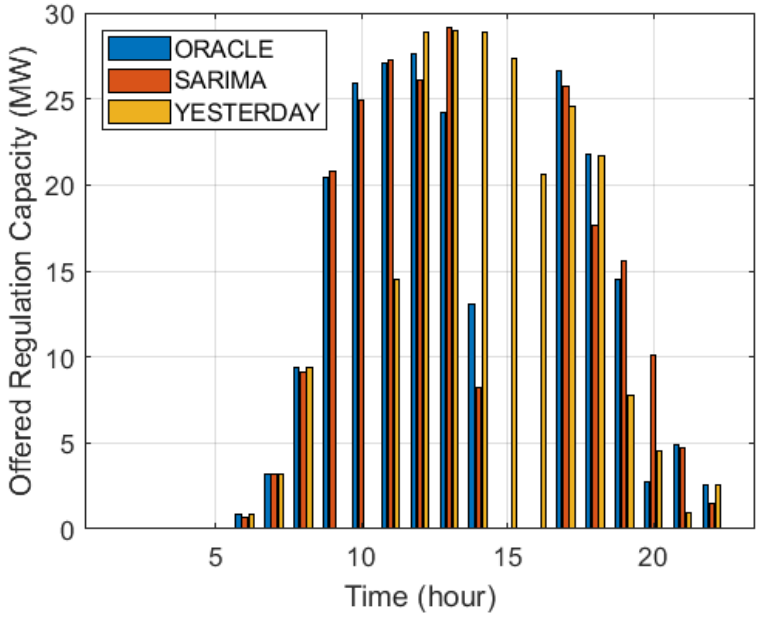

FIGURE 6.11: The offered capacity on February 4, 2021.

user's requirement. There are a few times that the departure SOC does not meet the requirement. This is due to that some EVs plug in with a low initial SOC but only park for a short time. The SOC cannot reach the requirement even though they are charging at full power during their parking. Hence, in normal situations, the proposed MPC scheme can satisfy

the users' requirement on departure SOC.

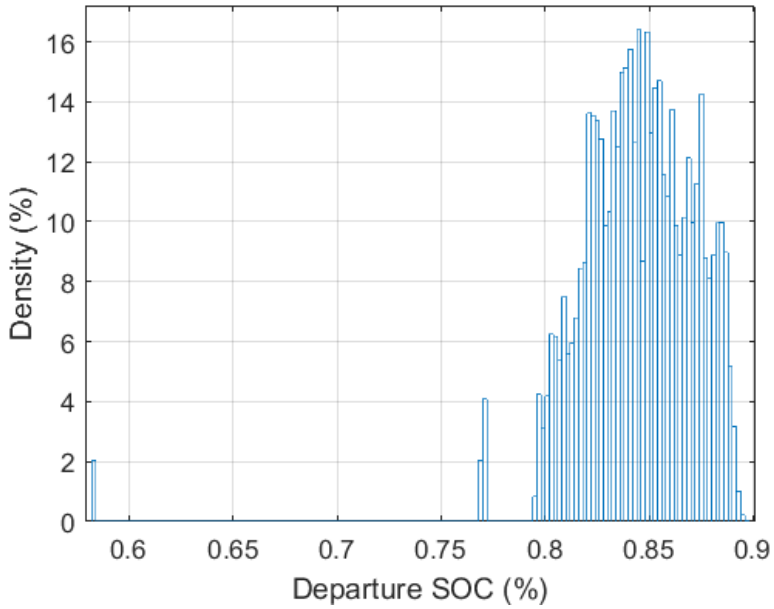

FIGURE 6.12: The distribution of the departure SOC with the proposed MPC scheme from July 4, 2020 to March 1, 2021.

6.2 Corporation of Delay Compensation and Optimal Dispatching

The overall controller design with delay compensation and optimal dispatching is illustrated in Figure 6.13. In real-time operation, the EV aggregator applies optimal dispatching control in the MPC scheme with SARIMA prediction on the CCP to determine the capacity offer Cap_{bid} in each market time-step Δt_m and the participation factors p_k for each EV in each control time-step Δt_c. The delay compensation control in the EV side reconstructs the dispatched LFC signal to improve the frequency regulation performance of the EV.

A simulation is run for 1 day to demonstrate the performance of the proposed controller as an example. The EV aggregator is the same as the one in Section 5.4.1, and the EVs are parking in 3 different locations with total communication delays of $d_1 = 8$, $d_2 = 11$, and $d_3 = 13$ as assumed in Section 4.4. The performance of the EV aggregator is evaluated by the total payment from the target LFC market. The CCP and PCP are the actual clearing price

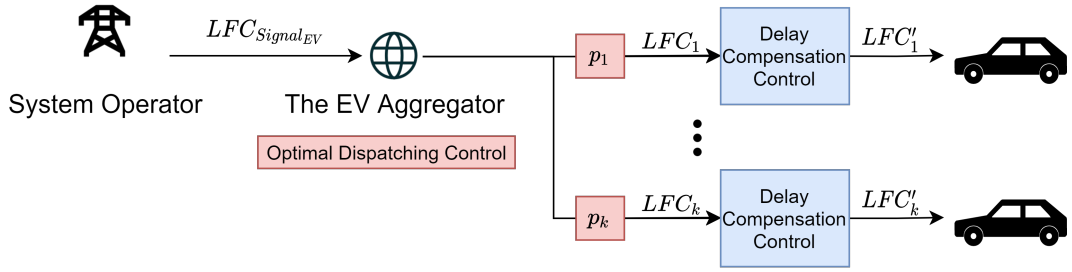

FIGURE 6.13: The overall controller design.

from PJM on March 1, 2021 [153]. The CCP and PCP are shown in Figure 6.14 and Figure 6.15 respectively. The power system model is the AGC30 Model introduced in Section 2.5. The noise level of the frequency measurement x is set to be 0.2. The parameters of the proposed controllers are basically the same as those in previous simulations and can be found in Table 6.3.

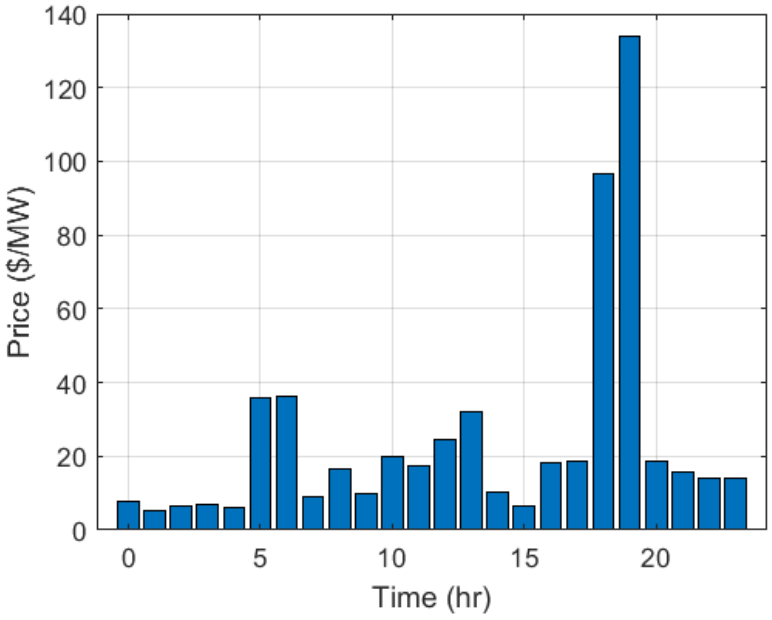

FIGURE 6.14: The CCP on March 1, 2021.

The total LFC payment is calculated according to (2.12) and the detailed results are presented in Table 6.4. 4 scenarios are set up according to whether the proposed delay compensation controller and optimal dispatching controller are implemented or not. Precisely, not implementation of the proposed optimal dispatching control indicates that the EV aggregator applies long control time-steps ($\Delta t_c = \Delta t_m$) and the simple YESTERDAY prediction on the CCP.

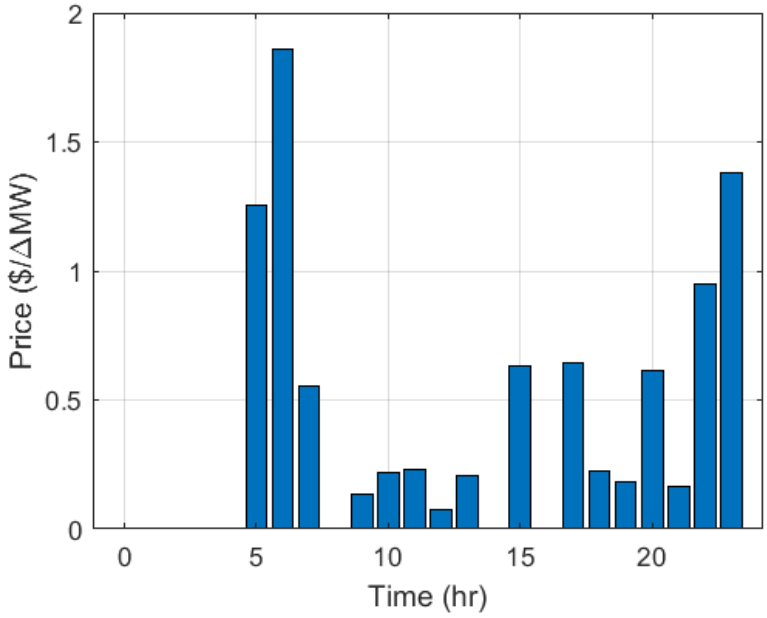

FIGURE 6.15: The PCP on March 1, 2021.

TABLE 6.3: The parameters of the proposed controllers.

	Parameter	Value
	Adaptive Parameter Estimation	
Delay	κ	1
Compensation	P_0	$5 \times 10^5 I$
Control	m'	20
	n'	20
Optimal	Δt_c	15min
Dispatching	GA Tuning	Same as Table 5.2
Control	SARIMA Order	$(1,0,1)(3,0,3)_{24}$

TABLE 6.4: The total LFC payment.

Scenario	Delay Compensation	Optimal Dispatching	Performance Score	Capacity Payment	Mileage Payment	LFC Payment
1	×	×	0.796	6.07×10^3\$	3.72×10^3\$	7.79×10^3\$
2	×	O	0.797	7.18×10^3\$	3.67×10^3\$	8.64×10^3\$
3	O	×	0.948	6.07×10^3\$	3.39×10^3\$	8.97×10^3\$
4	O	O	0.947	7.18×10^3\$	3.35×10^3\$	9.97×10^3\$

The implementation of the delay compensation controller raises the performance score to around 0.95 while the optimal dispatching controller increases the capacity payment by 18.3%. However, the mileage payment

decreases with the proposed controller implemented. This phenomenon is due to that the calculation of the mileage payment does not consider the performance of the resources. Worse performance of the LFC resources will incentive more LFC regulation requirement in the system, therefore the mileage of the LFC signal increases, and the resources can receive more mileage payment, as pointed out in [132]. The delay compensation control improves the performance more than the optimal dispatching control, so the reduce in mileage payment is larger when adopting the delay compensation control. Hence, it is crucial to consider the actual performance of the regulation resource when determining mileage payment. The presence of the performance score in the LFC payment formula (2.12) addressed this problem. The actual mileage payment, which is the product of the mileage payment and the performance score, will be penalized if the performance of a regulation resource is bad. The actual mileage payment of scenario 4 increases by 7% compared to scenario 1. Overall, with both of the proposed controllers implemented, the total LFC payment increases by 28%.

6.3 Other Discussions

6.3.1 Estimated Payback Time

The payback time of the initial installation cost of V2G equipment is roughly estimated in this subsection for the target EV aggregator.

The total capacity payment in 240 days with SARIMA prediction is 9.10×10^5\$ according to the simulation results in Section 6.1.3. The mileage payment is estimated via the *Mileage Ratio* mentioned in Section 2.4.1 since it is difficult to perform system simulation for 240 days to obtain the actual mileage:

$$\overset{Estimated\ Mileage\ Payment}{}(\$) = \overset{Capacity\ Offer}{}(\text{MW}) \times \overset{Mileage\ Ratio}{}(\Delta\text{MW/MW}) \times \overset{Mileage\ Price}{}(\$/\Delta\text{MW}) \quad (6.5)$$

The *Mileage Ratio* is the ratio between the mileage and the capacity offer of a resource. Although the typical mileage of RegD resources with battery systems is around 15 in PJM, the requirement for fast regulation resources is not so urgent in PJM. In the AGC30 Model where the RES penetration is high, the average *Mileage Ratio* of the EV aggregator with the overall controller

during the 24-hour simulation is around 55. Hence, the mileage payment is estimated to be 5.09~20.35$\times 10^5$\$ in 240 days.

The annual total payment with the overall proposed controller is estimated as

$$\frac{365}{240} \times {}^{Performance}_{Score} \times (1.1 \times {}^{Capacity}_{Payment} + {}^{Mileage}_{Payment}) \tag{6.6}$$

The coefficient of 1.1 denotes the expected increase of 10% in capacity payment by the optimal dispatching control with Δt_c=15min according to the simulation results in Section 5.4.2 and Section 6.2.

The performance score with the overall controller is 0.947 as given in Table 6.4. With the above assumptions, the estimated annual payment for each EV is 443.83~892.35\$. If the unit investment for a slow V2G charger and its ancillary equipment is 2000~3000\$ [155], the target EV aggregator is expected to payback the initial investment in 3 to 6 years.

6.3.2 Uncertainty Margin for the Unexpected Departure of EVs

So far, the unexpected departure of the EVs is not considered in this dissertation. It is assumed that all the EV owners will leave at the time as they informed in advance. In the realistic situation, it is inevitable that the some EVs might have to leave earlier than scheduled. To ensure that the offer capacity can still be satisfied even if some EVs suddenly leave, $Cap_{bid}(t_m)$ should be reduced by a small margin. In this subsection, a simple method is proposed to determine this uncertainty margin for the EV aggregator.

To determine the uncertainty margin, the EV aggregator needs to know the leaving probability $p_k^{leave}(t_m)$ for each EV at each time-step. This information can be obtained via surveying the participating EV users or statistical data. In this dissertation, the leaving probability $p_k^{leave}(t_m)$ of the k^{th} EV is simply modeled as:

$$p_k^{leave}(t_m) = \begin{cases} p_k^{promise} & \text{if } t_m \geq t_k^{leave} \\ \frac{2(1-p_k^{promise})(t_m - t_k^{arrive}+1)}{(t_k^{leave}-t_k^{arrive})(t_k^{leave}-t_k^{arrive}-1)} & \text{if } t_k^{arrive} \leq t_m < t_k^{leave} \end{cases} \tag{6.7}$$

$p_k^{promise}$ is the probability that the EV will not leave earlier that scheduled. The rest of the probability is the probability of unexpected departure and

is distributed during the parking period. The leaving probability increases linearly as the EV parks, as illustrated in Figure 6.16. For example, if an EV arrives during 14:00 to 15:00 and plans to leave during 18:00 to 19:00 with $p_k^{promise} = 0.9$, the distribution of the leaving probability p_k^{leave} is given in Table 6.5.

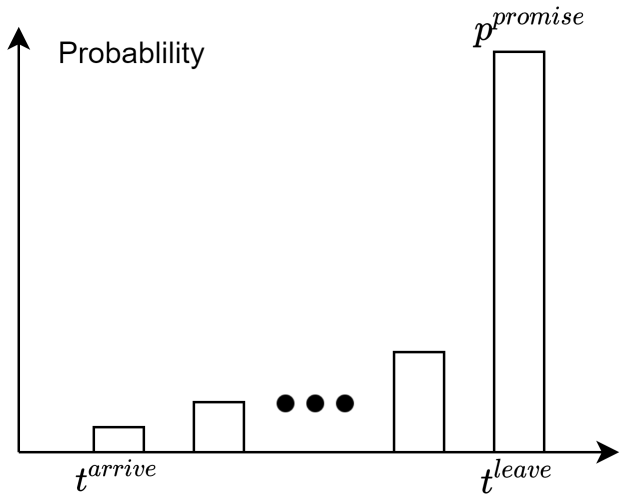

FIGURE 6.16: The distribution of the leaving probability p_k^{leave}.

TABLE 6.5: The distribution of the leaving probability p_k^{leave}: an example.

	14:00-15:00	**15:00-16:00**	**16:00-17:00**	**17:00-18:00**	**18:00-19:00**
p_k^{leave}	0.01	0.02	0.03	0.04	0.9

At time-step t_m, the uncertainty margin is determined by the following steps:

Step 1: Schedule the EVs according to the proposed optimal dispatching control

Step 2: Calculate the cumulative probability of $Cap_{bid}(t_m)$ according to the optimal dispatching schedule and the leaving probability of each EV at t_m.

Step 3: Determine the uncertainty margin via the cumulative probability of $Cap_{bid}(t_m)$.

To provide an example, the uncertainty margin at $t_m = 12$ (11:00-12:00) in the simulation in Section 6.2 is calculated. The optimal dispatching schedule is listed in Table 6.6. Without considering the unexpected departure, an LFC capacity of 29.05MW can be provided by the EV aggregator. It is extremely difficult to derive the analytical solution for the cumulative probability of $Cap_{bid}(12)$ with the probability model (6.7), therefore Monte Carlo simulation is performed 100,000 times to derive the numerical result.

TABLE 6.6: The optimal dispatching schedule at $t_m = 12$.

t_m		**12**			
t_c		**45**	**46**	**47**	**48**
Number of EVs	**State (a)**	4120	4140	4120	4120
	State (b)	60	20	60	60
	State (c)	0	60	40	60
	Not Parking	720	680	680	660
$Cap(t_c)$ **(kW)**		29050	29050	29050	29050
$Cap_{bid}(t_m)$ **(kW)**		29050			

The cumulative probability with $p_k^{promise} = 0.9$ is shown in Figure 6.17. The horizontal length of the steps is $0.5P^{max}$. The probability that $Cap_{bid}(12)$ is smaller than 28.7MW is close to 0. Therefore, it is pretty safe for the EV aggregator to submit $Cap_{bid}(12)$ =28.7MW to the LFC market. The uncertainty margin is 0.35MW, which is 1.21% of the offer capacity without considering the unexpected departure of EVs.

Another example of the cumulative probability with $p_k^{promise} = 0.7$ is shown in Figure 6.18. The safe value for capacity bidding is 28.2MW. The uncertainty margin increases to 0.85MW, namely 2.93% of the offer capacity without considering the unexpected departure of EVs. Apparently, the uncertainty margin is affected by the $p_k^{promise}$, and the EV aggregator should try to avoid unexpected departure of the participants, i.e. reduce the discount of parking fee if an EV leaves earlier than schedule.

Additionally, since the horizontal length of the steps represents the charging power of the EVs, if an EV aggregator adopts fast-charging infrastructures, the uncertainty margin will be affected more severely by the unexpected departure. The target EV aggregator is modified into aggregating 245 EVs with $P^{max} = 50$kW. With other conditions remain the same, the cumulative probability with $p_k^{promise} = 0.9$ is shown in Figure 6.19.

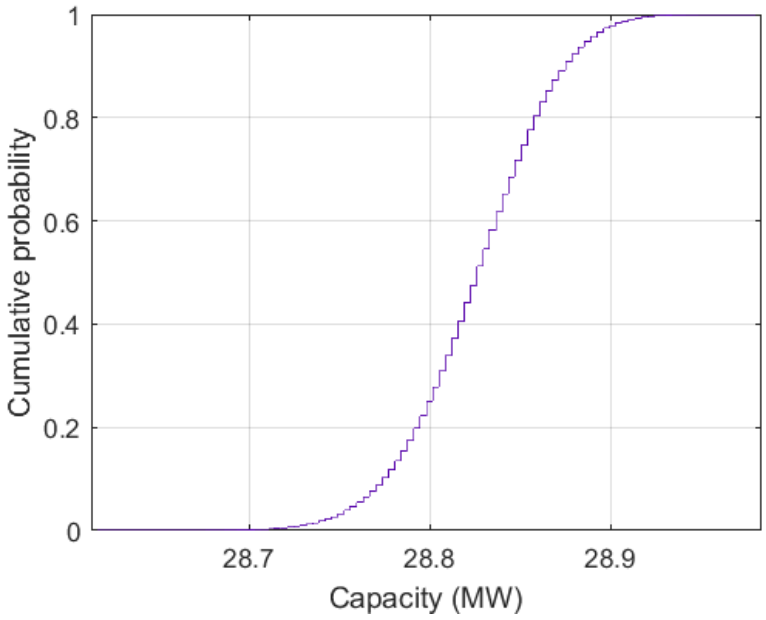

FIGURE 6.17: The cumulative probability of $Cap_{bid}(12)$: $p_k^{promise} = 0.9$.

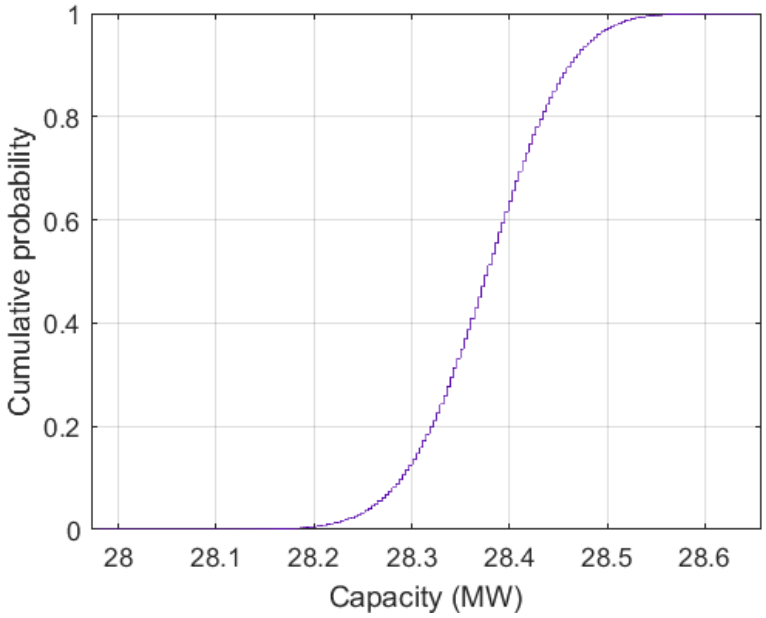

FIGURE 6.18: The cumulative probability of $Cap_{bid}(12)$: $p_k^{promise} = 0.7$.

The offer capacity without considering the unexpected departure of EVs is 10.38MW, and the safe bidding value is 10MW. The uncertainty margin is

0.38MW, which is 3.6% of the original value. Compared to the case of slow-charging with $p_k^{promise} = 0.9$ in Figure 6.17, the uncertainty margin increases by 3 times.

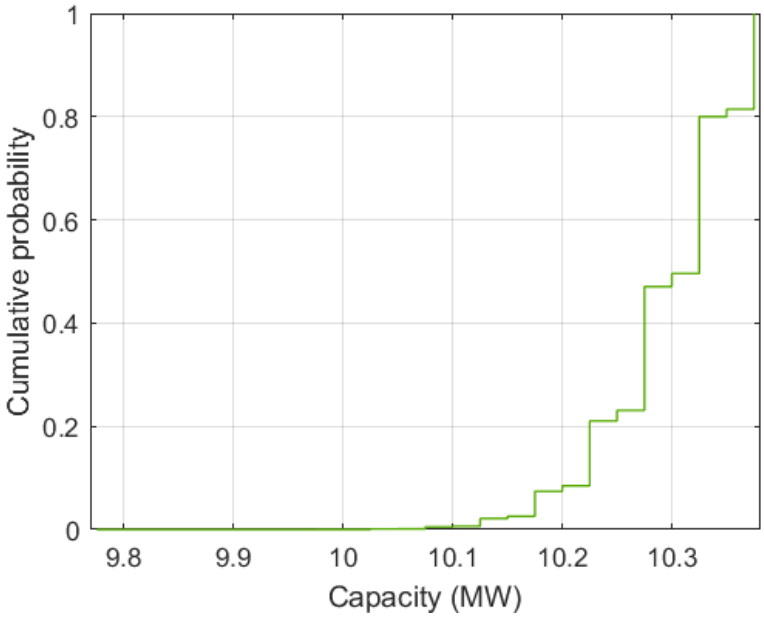

FIGURE 6.19: The cumulative probability of $Cap_{bid}(12)$: fast-charging.

Chapter 7

Conclusion and Future Works

7.1 Conclusion

In this dissertation, a novel controller is designed for EV aggregators participating in LFC. The overall controller is comprised of two parts: a delay compensation controller and an optimal dispatching controller. Cooperatively, the two parts of the proposed controller can improve the performance of the EV aggregator and boost the LFC payment in a performance-based frequency regulation market, such as the existing PJM regulation market or the future Synchronized Frequency Restoration Reserve market in the Electricity Demand & Supply Market in Japan.

The delay compensation controller reconstructs an LFC signal without delay directly from the EV side based on real-time system frequency deviation in a power system operating at FFC mode. Two different algorithms, linear regression and adaptive parameter estimation, are applied to discover the relationship between the received LFC signal and the system frequency fluctuation for the reconstruction of the signal. Compared to the linear regression algorithm, the adaptive parameter estimation algorithm provides a more precise estimation result with less calculation burden and has stronger resistance to the nonlinearity in the LFC system and the noise in the frequency measurement. With the proposed controller, the output of the EV aggregator can follow the LFC signal closely. The simulation results show that the proposed controller can not only improve the performance score of the EV aggregator but also help to suppress the system frequency deviation under a practical noise level. Besides, the cost of a proper frequency measurement device, i.e. a household multimeter, is low, indicating that the proposed delay compensation controller is feasible economically.

The optimal dispatching controller operates at a fast control time-step to

utilize the aggregated EVs more efficiently. With a fast control time-step, the optimization of the dispatching control becomes nonlinear and nonconvex. A GA with 3 variable states is specifically designed to search for the optimal dispatching schedule that the capacity payment of the EV aggregator can be maximized while the EV users' traveling requirement is not violated. A 10% increase in the capacity payment can be observed from the simulation results and the deviation of departure SOC due to the energy change by providing LFC regulation is suppressed. Meanwhile, an extremely short time-step is not recommended for the normal EV aggregators since the benefit is relatively small. In real-time operation, the optimal dispatching controller is implemented in an MPC scheme with SARIMA prediction on the CCP. The SARIMA prediction is implemented in a way that cooperates with the MPC scheme and the CCP is predicted in real-time with the latest information. The capacity payment of the EV aggregator increased by 4.3% with the SARIMA prediction results compared to that with simple YESTERDAY prediction. Although the SARIMA model cannot predict the actual price precisely, it successfully predicts the overall trend of the price, which is more meaningful and valuable to the EV aggregator.

The proposed controller increases the LFC payment of the target EV aggregator by 28% in the simulation. The performance score is improved by the delay compensation control while the optimal dispatching control boosts the capacity payment. At first glance, the mileage payment seems to drop because of the proposed controller. However, the real mileage payment actually increases by 7% due to the improved performance score.

Finally, an extra discussion on the payback time and the uncertainty margin are given. A rough estimation of the payback time for the target EV aggregator is examined. Under the assumed background and performance-based LFC market, the EV aggregator is expected to have the initial investment of V2G infrastructures paid back in 3 to 6 years. A simple method is proposed to determine the uncertainty margin for the unexpected departure of EVs. The method requires the knowledge of the EVs' leaving probabilities and the uncertainty margin is determined by the cumulative probability of the offer capacity. The uncertainty margin obviously affects the payment of the EV aggregator, and simple analysis shows the fast-charging of EV batteries has a more significant influence on the uncertainty margin compared to the regular slow-charging.

7.2 Future Works

A HIL simulation involving EVs is a good way to demonstrate the practical application of the proposed controller in this dissertation. The hardware experiment can explore the potential problems and challenges in the following aspects:

- How to setup a practical communication network for the EV aggregator
- How does the cost and the topology of the communication network affect the communication delay
- Quantitative evaluation on the EV battery degradation due to providing frequency regulation

On the other hand, surveys or statistical analyses of the EV users' behavior are also important. The feasible business scheme of the EV aggregator is affected by the willingness of the EV owners to participate in LFC regulation, the probability of unexpected departure, etc. A more detailed analysis of the practical EV aggregator business scheme can be one of the relative future research topics.

Last but not least, technical improvements such as:

- Improve the adaptive parameter algorithm for stronger noise tolerance
- Improve the GA design for faster and more accurate convergence on the global optimum
- Improve the precision of the SARIMA prediction on CCP by introducing an extra artificial neural network for additional information input such as real-time weather conditions and the system load demand.

can be considered for future researches as well.

In general, these directions for future researches will be beneficial and help to expand the business of the EV aggregators. The EV aggregators will be able to provide better LFC regulation service to the system, and the system can become more reliable and stable with a large amount of RES generation.

Bibliography

[1] IEA. Key world energy statistics 2020. IEA, Paris. [Online]. Available: https://www.iea.org/reports/key-world-energy-statistics-2020

[2] F. Zabihian and A. Fung, "Fuel and ghg emission reduction potentials by fuel switching and technology improvement in the iranian electricity generation sector," *International Journal of Engineering (IJE)*, vol. 3, no. 2, p. 159, 2009.

[3] "Energy consumption trends and their linkages with renewable energy policies in east and southeast asian countries: Challenges and opportunities," *Sustainable Environment Research*, vol. 28, no. 6, pp. 257–266, 2018.

[4] IEA. Global share of electricity generation. IEA, Paris. [Online]. Available: https://www.iea.org/data-and-statistics/charts/global-share-of-electricity-generation-2018

[5] A. Qazi, F. Hussain, N. A. Rahim, G. Hardaker, D. Alghazzawi, K. Shaban, and K. Haruna, "Towards sustainable energy: A systematic review of renewable energy sources, technologies, and public opinions," *IEEE Access*, vol. 7, pp. 63 837–63 851, 2019.

[6] IRENA (2018), "Renewable capacity statistics 2018," International Renewable Energy Agency (IRENA), Abu Dhabi, Tech. Rep., 2018.

[7] "Energy white paper 2018," Agency for Natural Resources and Energy, Japan, Tech. Rep., 2018.

[8] "5th basic energy plan," Agency for Natural Resources and Energy, Japan, Tech. Rep., 2018.

[9] State Grid Corporation of China, 2017, http://www.sgcc.com.cn/html/sgcc_main_en/col2017112619/column_2017112619_1.shtml, Last accessed on 2021-03-20.

[10] "Short-term energy outlook," U.S. Energy Information Administration, U.S., Tech. Rep., March 2021.

[11] I. Vieto and J. Sun, "Small-signal impedance modelling of type-iii wind turbine," in *2015 IEEE Power & Energy Society General Meeting*. IEEE, 2015, pp. 1–5.

[12] ——, "Sequence impedance modeling and analysis of type-iii wind turbines," *IEEE Transactions on Energy Conversion*, vol. 33, no. 2, pp. 537–545, 2017.

[13] ——, "Refined small-signal sequence impedance models of type-iii wind turbines," in *2018 IEEE Energy Conversion Congress and Exposition (ECCE)*. IEEE, 2018, pp. 2242–2249.

[14] U. Princy, S. Jaseena, S. Sreedharan, and S. Sreejith, "Voltage stability analysis of power system network integrated with renewable source and svc," in *2017 Innovations in Power and Advanced Computing Technologies (i-PACT)*. IEEE, 2017, pp. 1–6.

[15] P. Kundur, J. Paserba, V. Ajjarapu, G. Andersson, A. Bose, C. Canizares, N. Hatziargyriou, D. Hill, A. Stankovic, C. Taylor *et al.*, "Definition and classification of power system stability ieee/cigre joint task force on stability terms and definitions," *IEEE transactions on Power Systems*, vol. 19, no. 3, pp. 1387–1401, 2004.

[16] P. Tielens and D. Van Hertem, "The relevance of inertia in power systems," *Renewable and Sustainable Energy Reviews*, vol. 55, pp. 999–1009, 2016.

[17] C. Seneviratne and C. Ozansoy, "Frequency response due to a large generator loss with the increasing penetration of wind/PV generation–a literature review," *Renewable and Sustainable Energy Reviews*, vol. 57, pp. 659–668, 2016.

[18] T. Alquthami, H. Ravindra, M. Faruque, M. Steurer, and T. Baldwin, "Study of photovoltaic integration impact on system stability using custom model of PV arrays integrated with PSS/E," in *North American Power Symposium 2010*. IEEE, 2010, pp. 1–8.

[19] G. Strbac, A. Shakoor, M. Black, D. Pudjianto, and T. Bopp, "Impact of wind generation on the operation and development of the UK electricity systems," *Electric power systems research*, vol. 77, no. 9, pp. 1214–1227, 2007.

[20] T. Ackermann and P. E. Morthorst, "Economic aspects of wind power in power systems," *Wind power in power systems*, p. 383, 2005.

[21] Z. Ming, Z. Kun, and D. Jun, "Overall review of china's wind power industry: Status quo, existing problems and perspective for future development," *Renewable and Sustainable Energy Reviews*, vol. 24, pp. 379–386, 2013.

[22] J. Rogers, S. Fink, and K. Porter, "Examples of wind energy curtailment practices," National Renewable Energy Lab.(NREL), Golden, CO (United States), Tech. Rep., 2010.

[23] A. Bunodiere and H. S. Lee, "Renewable energy curtailment: Prediction using a logic-based forecasting method and mitigation measures in kyushu, japan," *Energies*, vol. 13, no. 18, p. 4703, 2020.

[24] C. Li, H. Shi, Y. Cao, J. Wang, Y. Kuang, Y. Tan, and J. Wei, "Comprehensive review of renewable energy curtailment and avoidance: a specific example in china," *Renewable and Sustainable Energy Reviews*, vol. 41, pp. 1067–1079, 2015.

[25] C. Fernandes, P. Frías, and J. M. Latorre, "Impact of vehicle-to-grid on power system operation costs: The spanish case study," *Applied Energy*, vol. 96, pp. 194–202, 2012.

[26] M. C. Falvo, R. Lamedica, R. Bartoni, and G. Maranzano, "Energy management in metro-transit systems: An innovative proposal toward an integrated and sustainable urban mobility system including plug-in electric vehicles," *Electric Power Systems Research*, vol. 81, no. 12, pp. 2127–2138, 2011.

[27] IEA. Global EV Outlook 2020. IEA, Paris. [Online]. Available: https://www.iea.org/reports/global-ev-outlook-2020

[28] J. Dai, M. Dong, R. Ye, A. Ma, and W. Yang, "A review on electric vehicles and renewable energy synergies in smart grid," in *2016 China International Conference on Electricity Distribution (CICED)*. IEEE, 2016, pp. 1–4.

[29] P. Kundur, *Power system stability and control*. New York: McGraw-Hill, 1994.

[30] S. Takayama, "Design and evaluation of a electric power supply and demand control system considering large penetration of renewable energy (再生可能エネルギー大量連系を考慮した需給制御システムの設計と評価)," Master's thesis, The Universit of Tokyo, Japan, 2016.

[31] The Ministry of Electric Industry of the People's Republic of China, "Business Standard for Power Supply, Order 53," 1996.

[32] O. I. Elgerd and C. E. Fosha, "Optimum megawatt-frequency control of multiarea electric energy systems," *IEEE transactions on power apparatus and systems*, no. 4, pp. 556–563, 1970.

[33] T. E. Bechert and N. Chen, "Area automatic generation control by multi-pass dynamic programming," *IEEE Transactions on Power Apparatus and Systems*, vol. 96, no. 5, pp. 1460–1469, 1977.

[34] D. Das, J. Nanda, M. Kothari, and D. Kothari, "Automatic generation control of a hydrothermal system with new area control error considering generation rate constraint," *Electric Machines & Power Systems*, vol. 18, no. 6, pp. 461–471, 1990.

[35] R. R. Shoults and J. J. Ibarra, "Multi-area adaptive LFC developed for a comprehensive agc simulator," *IEEE Transactions on Power Systems*, vol. 8, no. 2, pp. 541–547, 1993.

[36] C. Liaw, "Design of a reduced-order adaptive load-frequency controller for an interconnected hydrothermal power system," *International Journal of Control*, vol. 60, no. 6, pp. 1051–1063, 1994.

[37] A. Rubaai and V. Udo, "Self-tuning load frequency control: multilevel adaptive approach," *IEE Proceedings-Generation, Transmission and Distribution*, vol. 141, no. 4, pp. 285–290, 1994.

[38] M. Azzam and Y. S. Mohamed, "Robust controller design for automatic generation control based on q-parameterization," *Energy conversion and management*, vol. 43, no. 13, pp. 1663–1673, 2002.

[39] M. Karrari, H. Shayeghi, M. Abedi, and M. Menhaj, "Design of H_∞ controller load frequency control in electrical power systems," *Amirkabir Journal of Science & Technology*, vol. 11, no. 41, pp. 79–88, 1999.

[40] H. Zeynelgil, A. Demiroren, and N. Sengor, "The application of ann technique to automatic generation control for multi-area power system," *International journal of electrical power & energy systems*, vol. 24, no. 5, pp. 345–354, 2002.

[41] E. Yeşil, M. Güzelkaya, and İ. Eksin, "Self tuning fuzzy pid type load and frequency controller," *Energy Conversion and Management*, vol. 45, no. 3, pp. 377–390, 2004.

[42] C. Chang, W. Fu, and F. Wen, "Load frequency control using genetic-algorithm based fuzzy gain scheduling of pi controllers," *Electric Machines and power systems*, vol. 26, no. 1, pp. 39–52, 1998.

[43] I. Avramiotis-Falireas, P. Zolotarev, A. Ahmadi-Khatir, and M. Zima, "Analysis and comparison of secondary frequency control reserve activation rules: Pro-rata vs. merit order," in *2014 Power Systems Computation Conference*. IEEE, 2014, pp. 1–7.

[44] N. P. Padhy, "Unit commitment-a bibliographical survey," *IEEE Transactions on power systems*, vol. 19, no. 2, pp. 1196–1205, 2004.

[45] Q. P. Zheng, J. Wang, and A. L. Liu, "Stochastic optimization for unit commitment—a review," *IEEE Transactions on Power Systems*, vol. 30, no. 4, pp. 1913–1924, 2014.

[46] J. Wang, M. Shahidehpour, and Z. Li, "Security-constrained unit commitment with volatile wind power generation," *IEEE Transactions on Power Systems*, vol. 23, no. 3, pp. 1319–1327, 2008.

[47] R. Billinton, B. Karki, R. Karki, and G. Ramakrishna, "Unit commitment risk analysis of wind integrated power systems," *IEEE Transactions on Power Systems*, vol. 24, no. 2, pp. 930–939, 2009.

[48] J. F. Restrepo and F. D. Galiana, "Assessing the yearly impact of wind power through a new hybrid deterministic/stochastic unit commitment," *IEEE Transactions on Power Systems*, vol. 26, no. 1, pp. 401–410, 2010.

[49] A. Botterud, H. Keko, V. Miranda, J. Wang, and J. Sumaili, "Clustering-based wind power scenario reduction technique," 2011.

[50] J. Dupacová, N. Gröwe-Kuska, and W. Römisch, *Scenario reduction in stochastic programming: An approach using probability metrics*. Humboldt-Universität zu Berlin, Mathematisch-Naturwissenschaftliche Fakultät ⋯, 2000.

[51] N. Growe-Kuska, H. Heitsch, and W. Romisch, "Scenario reduction and scenario tree construction for power management problems," in *2003 IEEE Bologna Power Tech Conference Proceedings*, vol. 3. IEEE, 2003, pp. 7–pp.

[52] S. Takayama and R. Matsuhashi, "Development of model for load frequency control in power system with large-scale integration of renewable energy," in *2016 IEEE Power and Energy Conference at Illinois (PECI)*. IEEE, 2016, pp. 1–8.

[53] J. P. Deane, B. Ó. Gallachóir, and E. McKeogh, "Techno-economic review of existing and new pumped hydro energy storage plant," *Renewable and Sustainable Energy Reviews*, vol. 14, no. 4, pp. 1293–1302, 2010.

[54] F. Mohamad and J. Teh, "Impacts of energy storage system on power system reliability: A systematic review," *Energies*, vol. 11, no. 7, p. 1749, 2018.

[55] M. A. Crew, C. S. Fernando, and P. R. Kleindorfer, "The theory of peak-load pricing: A survey," *Journal of regulatory economics*, vol. 8, no. 3, pp. 215–248, 1995.

[56] P. Samadi, A.-H. Mohsenian-Rad, R. Schober, V. W. Wong, and J. Jatskevich, "Optimal real-time pricing algorithm based on utility maximization for smart grid," in *2010 First IEEE International Conference on Smart Grid Communications*. IEEE, 2010, pp. 415–420.

[57] M. Perez, R. Perez, K. R. Rábago, and M. Putnam, "Overbuilding & curtailment: The cost-effective enablers of firm PV generation," *Solar Energy*, vol. 180, pp. 412–422, 2019.

[58] P. L. Joskow, "Lessons learned from electricity market liberalization," *The Energy Journal*, vol. 29, no. Special Issue# 2, 2008.

[59] Federal Energy Regulatory Commission, "Order No. 888. Promoting Wholesale Competition Through Open Access Non-discriminatory

Transmission Services by Public Utilities; Recovery of Stranded Costs by Public Utilities and Transmitting Utilities," 1996.

[60] A. M. Pirbazari, "Ancillary services definitions, markets and practices in the world," in *2010 IEEE/PES Transmission and Distribution Conference and Exposition: Latin America (T&D-LA)*. IEEE, 2010, pp. 32–36.

[61] F. E. R. Commission *et al.*, "Order No. 755. Frequency Regulation Compensation in the Organized Wholesale Power Markets," 2011.

[62] Y. Makarov, S. Lu, J. Ma, and T. Nguyen, "Assessing the value of regulation resources based on their time response characteristics," 2008.

[63] A. D. Papalexopoulos and P. E. Andrianesis, "Performance-based pricing of frequency regulation in electricity markets," *IEEE Transactions on Power systems*, vol. 29, no. 1, pp. 441–449, 2012.

[64] Z. Wang and J. Zhong, "Procuring and pricing performance-based frequency regulation services in the electricity market," *IET Generation, Transmission & Distribution*, vol. 11, no. 10, pp. 2633–2642, 2017.

[65] Z. Wang, J. Zhong, and J. Li, "Design of performance-based frequency regulation market and its implementations in real-time operation," *International Journal of Electrical Power & Energy Systems*, vol. 87, pp. 187–197, 2017.

[66] Z. Zhou, T. Levin, and G. Conzelmann, "Survey of us ancillary services markets," Argonne National Lab.(ANL), Argonne, IL (United States), Tech. Rep., 2016.

[67] P. Manual 11, "Energy & ancillary services market operations," 2012.

[68] P. Manual 12, "Balancing operations," 2012.

[69] Y. Xiao, Q. Su, F. S. S. Bresler, R. Carroll, J. R. Schmitt, and M. Olaleye, "Performance-based regulation model in pjm wholesale markets," in *2014 IEEE PES General Meeting | Conference & Exposition*. IEEE, 2014, pp. 1–5.

[70] Ministry of Economy, Trade and Industry (METI), Electricity and Gas Market Surveillance Commission, "Information on Electricity Demand & Supply Market and the Estimation on the Tie-line Capacity Requirement of Replacement Reserve for FIT (需給調整市場における情報公表及

び三次調整力 2 の連系線容量確保に係る試算について)," https://www.emsc.meti.go.jp/activity/emsc_system/pdf/041_06_00.pdf, 9 2019.

[71] Ministry of Economy, Trade and Industry (METI), Agency for Natural Resources and Energy, "About Electricity Demand & Supply Market (需給調整市場について)," https://www.meti.go.jp/shingikai/enecho/denryoku_gas/denryoku_gas/seido_kento/pdf/043_04_01.pdf, 10 2020.

[72] R. Furuta, "Analysis and stabilization on frequency regulation prices after the establishment of Electricity Demand & Supply Market. (需給調整市場設立後を想定した電力システムにおける調整力価格の分析と安定化方策に関する研究)," Master's thesis, The Universit of Tokyo, Japan, 2020.

[73] R. Furuta and R. Matsuhashi, "A study on analysis of reserve prices assuming the power system structure after the establishment of the balancing market in japan," *Journal of Japan Society of Energy and Resources*, vol. 41, no. 5, pp. 166–175, 2020.

[74] T. Kato, "Preface to special issue on " simulation technologies by using ieej agc30 model for automatic generation control analysis "," *IEEJ Transactions on Power and Energy*, vol. 140, no. 5, pp. 350–350, 2020.

[75] Y. Yamamoto, "Design and Economic Evaluation of a novel Frequency Regulation Market Taking Use of Existing Power Generations and Electric Vehicles into Consideration (既存電源および電気自動車の活用を考慮した周波数調整市場の設計とその経済性評価)," Master's thesis, The Universit of Tokyo, Japan, 2016.

[76] G. Fujita, G. Shirai, and R. Yokoyama, "Automatic generation control for dc-link power system," in *IEEE/PES Transmission and Distribution Conference and Exhibition*, vol. 3. IEEE, 2002, pp. 1584–1588.

[77] P. F. De Toledo, J. Pan, K. Srivastava, W. Wang, and C. Hong, "Case study of a multi-infeed HVDC system," in *2008 Joint International Conference on Power System Technology and IEEE Power India Conference*. IEEE, 2008, pp. 1–7.

[78] S. Sterpu and M. N. Tuan, "Sharing frequency response between asynchronous electrical systems," in *2009 IEEE Power Energy Society General Meeting*, 2009, pp. 1–6.

[79] Y. Phulpin, "Communication-free inertia and frequency control for wind generators connected by an HVDC-link," *IEEE Transactions on Power Systems*, vol. 27, no. 2, pp. 1136–1137, 2011.

[80] M. Guan, J. Cheng, C. Wang, Q. Hao, W. Pan, J. Zhang, and X. Zheng, "The frequency regulation scheme of interconnected grids with VSC-HVDC links," *IEEE Transactions on Power Systems*, vol. 32, no. 2, pp. 864–872, 2016.

[81] J. Cho, S. Jeong, and Y. Kim, "Commercial and research battery technologies for electrical energy storage applications," *Progress in Energy and Combustion Science*, vol. 48, pp. 84–101, 2015.

[82] N.-K. C. Nair and N. Garimella, "Battery energy storage systems: Assessment for small-scale renewable energy integration," *Energy and Buildings*, vol. 42, no. 11, pp. 2124–2130, 2010.

[83] A. Poullikkas, "A comparative overview of large-scale battery systems for electricity storage," *Renewable and Sustainable Energy Reviews*, vol. 27, pp. 778–788, 2013.

[84] X. Luo, J. Wang, M. Dooner, and J. Clarke, "Overview of current development in electrical energy storage technologies and the application potential in power system operation," *Applied energy*, vol. 137, pp. 511–536, 2015.

[85] H. Chen, T. N. Cong, W. Yang, C. Tan, Y. Li, and Y. Ding, "Progress in electrical energy storage system: A critical review," *Progress in natural science*, vol. 19, no. 3, pp. 291–312, 2009.

[86] Y. Yang, S. Bremner, C. Menictas, and M. Kay, "Battery energy storage system size determination in renewable energy systems: A review," *Renewable and Sustainable Energy Reviews*, vol. 91, pp. 109–125, 2018.

[87] R. Kempener and E. Borden, "Battery storage for renewables: Market status and technology outlook," *International Renewable Energy Agency, Abu Dhabi*, p. 32, 2015.

[88] K. Divya and J. Østergaard, "Battery energy storage technology for power systems—an overview," *Electric power systems research*, vol. 79, no. 4, pp. 511–520, 2009.

[89] M. Belouda, A. Jaafar, B. Sareni, X. Roboam, and J. Belhadj, "Design methodologies for sizing a battery bank devoted to a stand-alone and electronically passive wind turbine system," *Renewable and Sustainable Energy Reviews*, vol. 60, pp. 144–154, 2016.

[90] T. Khatib, I. A. Ibrahim, and A. Mohamed, "A review on sizing methodologies of photovoltaic array and storage battery in a standalone photovoltaic system," *Energy Conversion and Management*, vol. 120, pp. 430–448, 2016.

[91] A. Berrada and K. Loudiyi, "Operation, sizing, and economic evaluation of storage for solar and wind power plants," *Renewable and sustainable energy Reviews*, vol. 59, pp. 1117–1129, 2016.

[92] O. Ma, N. Alkadi, P. Cappers, P. Denholm, J. Dudley, S. Goli, M. Hummon, S. Kiliccote, J. MacDonald, N. Matson *et al.*, "Demand response for ancillary services," *IEEE Transactions on Smart Grid*, vol. 4, no. 4, pp. 1988–1995, 2013.

[93] R. Menke, E. Abraham, P. Parpas, and I. Stoianov, "Demonstrating demand response from water distribution system through pump scheduling," *Applied Energy*, vol. 170, pp. 377–387, 2016.

[94] T. Masuta, A. Yokoyama, and Y. Tada, "System frequency control by heat pump water heaters (HPWHs) on customer side based on statistical hpwh model in power system with a large penetration of renewable energy sources," in *2010 International Conference on Power System Technology*. IEEE, 2010, pp. 1–7.

[95] M. Motalleb, M. Thornton, E. Reihani, and R. Ghorbani, "Providing frequency regulation reserve services using demand response scheduling," *Energy Conversion and Management*, vol. 124, pp. 439–452, 2016.

[96] H. Shahinzadeh, J. Moradi, G. B. Gharehpetian, H. Nafisi, and M. Abedi, "Iot architecture for smart grids," in *2019 International Conference on Protection and Automation of Power System (IPAPS)*. IEEE, 2019, pp. 22–30.

[97] W. Kempton and J. Tomić, "Vehicle-to-grid power fundamentals: Calculating capacity and net revenue," *Journal of power sources*, vol. 144, no. 1, pp. 268–279, 2005.

[98] E. Sortomme and M. A. El-Sharkawi, "Optimal charging strategies for unidirectional vehicle-to-grid," *IEEE Transactions on Smart Grid*, vol. 2, no. 1, pp. 131–138, 2010.

[99] T. K. Kristoffersen, K. Capion, and P. Meibom, "Optimal charging of electric drive vehicles in a market environment," *Applied Energy*, vol. 88, no. 5, pp. 1940–1948, 2011.

[100] R. J. Bessa, M. A. Matos, F. J. Soares, and J. A. P. Lopes, "Optimized bidding of a EV aggregation agent in the electricity market," *IEEE Transactions on Smart Grid*, vol. 3, no. 1, pp. 443–452, 2011.

[101] W. Kempton and J. Tomić, "Vehicle-to-grid power fundamentals: Calculating capacity and net revenue," *Journal of power sources*, vol. 144, no. 1, pp. 268–279, 2005.

[102] ——, "Vehicle-to-grid power implementation: From stabilizing the grid to supporting large-scale renewable energy," *Journal of power sources*, vol. 144, no. 1, pp. 280–294, 2005.

[103] W. Kempton, V. Udo, K. Huber, K. Komara, S. Letendre, S. Baker, D. Brunner, and N. Pearre, "A test of vehicle-to-grid (v2g) for energy storage and frequency regulation in the pjm system," *Results from an Industry-University Research Partnership*, vol. 32, 2008.

[104] S. Vandael, T. Holvoet, G. Deconinck, S. Kamboj, and W. Kempton, "A comparison of two giv mechanisms for providing ancillary services at the university of delaware," in *2013 IEEE international conference on smart grid communications (SmartGridComm)*. IEEE, 2013, pp. 211–216.

[105] C. Marnay, T. Chan, N. DeForest, J. Lai, J. MacDonald, M. Stadler, T. Erdmann, A. Hoheisel, M. Mueller, S. Sabre *et al.*, "Los angeles air force base vehicle to grid pilot project," Lawrence Berkeley National Lab.(LBNL), Berkeley, CA (United States), Tech. Rep., 2013.

[106] N. B. Arias, S. Hashemi, P. B. Andersen, C. Træholt, and R. Romero, "V2G enabled evs providing frequency containment reserves: Field results," in *2018 IEEE International Conference on Industrial Technology (ICIT)*. Ieee, 2018, pp. 1814–1819.

[107] Tokyo Electricity Consortium, "A Demonstration Experiment of Open Platform EV Aggregation Business," 2020, https://sii.or.jp/vpp02/uploads/B2_tepco.pdf, Last accessed on 2021-04-28.

[108] J. J. Escudero-Garzás, A. García-Armada, and G. Seco-Granados, "Fair design of plug-in electric vehicles aggregator for V2G regulation," *IEEE Transactions on Vehicular Technology*, vol. 61, no. 8, pp. 3406–3419, 2012.

[109] W. Choi, W. Lee, and B. Sarlioglu, "Reactive power control of grid-connected inverter in vehicle-to-grid application for voltage regulation," in *2016 IEEE Transportation Electrification Conference and Expo (ITEC)*. IEEE, 2016, pp. 1–7.

[110] I. S. Bayram and I. Papapanagiotou, "A survey on communication technologies and requirements for internet of electric vehicles," *EURASIP Journal on Wireless Communications and Networking*, vol. 2014, no. 1, pp. 1–18, 2014.

[111] H. Bevrani and T. Hiyama, "On load-frequency regulation with time delays: design and real-time implementation," *IEEE transactions on energy conversion*, vol. 24, no. 1, pp. 292–300, 2009.

[112] E. Ancillotti, R. Bruno, and M. Conti, "The role of communication systems in smart grids: Architectures, technical solutions and research challenges," *Computer Communications*, vol. 36, no. 17-18, pp. 1665–1697, 2013.

[113] K. Wada and A. Yokoyama, "Load frequency control using distributed batteries on the demand side with communication characteristics," in *2012 3rd IEEE PES Innovative Smart Grid Technologies Europe (ISGT Europe)*. IEEE, 2012, pp. 1–8.

[114] K. Wada, A. Yokoyama, S. Kawauchi, and F. Ishikawa, "Frequency control using fast demand response in power system with a large penetration of renewable energy sources," in *2014 International Conference on Power System Technology*. IEEE, 2014, pp. 1150–1156.

[115] K. Shimizu, T. Masuta, Y. Ota, and A. Yokoyama, "Load frequency control in power system using vehicle-to-grid system considering the customer convenience of electric vehicles," in *2010 International Conference on Power System Technology*. IEEE, 2010, pp. 1–8.

[116] ——, "A new load frequency control method in power system using vehicle-to-grid system considering users' convenience," in *Proceedings of the 17th Power System Computation Conference, Stockholm, Sweden*, 2011, pp. 22–26.

[117] T. Adachi and A. Yokoyama, "System frequency control by LFC signal equipartition method based on slow smart charging of electric vehicle," in *2015 IEEE Eindhoven PowerTech*. IEEE, 2015, pp. 1–6.

[118] E. Sortomme and M. A. El-Sharkawi, "Optimal scheduling of vehicle-to-grid energy and ancillary services," *IEEE Transactions on Smart Grid*, vol. 3, no. 1, pp. 351–359, 2011.

[119] S. I. Vagropoulos and A. G. Bakirtzis, "Optimal bidding strategy for electric vehicle aggregators in electricity markets," *IEEE Transactions on power systems*, vol. 28, no. 4, pp. 4031–4041, 2013.

[120] S. I. Vagropoulos, D. K. Kyriazidis, and A. G. Bakirtzis, "Real-time charging management framework for electric vehicle aggregators in a market environment," *IEEE Transactions on Smart Grid*, vol. 7, no. 2, pp. 948–957, 2015.

[121] A. Aldik, A. T. Al-Awami, E. Sortomme, A. M. Muqbel, and M. Shahidehpour, "A planning model for electric vehicle aggregators providing ancillary services," *IEEE Access*, vol. 6, pp. 70 685–70 697, 2018.

[122] R. Dey, S. Ghosh, G. Ray, and A. Rakshit, "H_∞ load frequency control of interconnected power systems with communication delays," *International Journal of Electrical Power & Energy Systems*, vol. 42, no. 1, pp. 672–684, 2012.

[123] X. Yu and K. Tomsovic, "Application of linear matrix inequalities for load frequency control with communication delays," *IEEE transactions on power systems*, vol. 19, no. 3, pp. 1508–1515, 2004.

[124] L. Jiang, W. Yao, Q. Wu, J. Wen, and S. Cheng, "Delay-dependent stability for load frequency control with constant and time-varying delays," *IEEE Transactions on Power systems*, vol. 27, no. 2, pp. 932–941, 2011.

[125] K. Warwick and D. Rees, *Industrial digital control systems*. IET, 1988, no. 37.

[126] T. Lee, "Exploring frequency regulation market transformation," 2017.

[127] H. Toda, Y. Ota, T. Nakajima, K.-i. Kawabe, and A. Yokoyama, "Hil test of power system frequency control by electric vehicles," *Transfer*, vol. 1, no. T1, p. 1, 2017.

[128] ——, "Implementation and verification of V2G control schemes on multiple electric vehicles," in *2nd E-Mobility Power System Integration Symposium*, 2018.

[129] G. Song, G. Tao, and C. Tan, "A unified discrete-time model reference adaptive control scheme," in *2018 IEEE 14th International Conference on Control and Automation (ICCA)*. IEEE, 2018, pp. 106–111.

[130] G. Tao, *Adaptive control design and analysis*. John Wiley & Sons, 2003, vol. 37.

[131] N. Manual 14, "Accounting and billing manual," 2020.

[132] K. S. Ko, S. Han, and D. K. Sung, "A new mileage payment for EV aggregators with varying delays in frequency regulation service," *IEEE Transactions on Smart Grid*, vol. 9, no. 4, pp. 2616–2624, 2016.

[133] C. Le Floch, E. C. Kara, and S. Moura, "Pde modeling and control of electric vehicle fleets for ancillary services: A discrete charging case," *IEEE Transactions on Smart Grid*, vol. 9, no. 2, pp. 573–581, 2016.

[134] M. Wang, Y. Mu, Q. Shi, H. Jia, and F. Li, "Electric vehicle aggregator modeling and control for frequency regulation considering progressive state recovery," *IEEE Transactions on Smart Grid*, vol. 11, no. 5, pp. 4176–4189, 2020.

[135] E. L. Karfopoulos, K. A. Panourgias, and N. D. Hatziargyriou, "Distributed coordination of electric vehicles providing V2G regulation services," *IEEE Transactions on Power Systems*, vol. 31, no. 4, pp. 2834–2846, 2015.

[136] G. Wenzel, M. Negrete-Pincetic, D. E. Olivares, J. MacDonald, and D. S. Callaway, "Real-time charging strategies for an electric vehicle aggregator to provide ancillary services," *IEEE Transactions on Smart Grid*, vol. 9, no. 5, pp. 5141–5151, 2017.

[137] H. Liu, Z. Hu, Y. Song, J. Wang, and X. Xie, "Vehicle-to-grid control for supplementary frequency regulation considering charging demands," *IEEE Transactions on Power Systems*, vol. 30, no. 6, pp. 3110–3119, 2014.

[138] H. Liu, J. Qi, J. Wang, P. Li, C. Li, and H. Wei, "EV dispatch control for supplementary frequency regulation considering the expectation of EV owners," *IEEE Transactions on Smart Grid*, vol. 9, no. 4, pp. 3763–3772, 2016.

[139] P. Chatupromwong, A. Yokoyama, and Y. Ota, "Suppression of system frequency fluctuation by smart charging of electric vehicles considering customer's convenience," *IEEJ Transactions on Power and Energy*, vol. 134, no. 7, pp. 579–585, 2014.

[140] M. Angelova and T. Pencheva, "Tuning genetic algorithm parameters to improve convergence time," *International Journal of Chemical Engineering*, vol. 2011, 09 2011.

[141] D. E. Goldberg and J. H. Holland, "Genetic algorithms and machine learning," 1988.

[142] D. E. Goldberg, *Genetic Algorithms in Search, Optimization, and Machine Learning*. New York: Addison-Wesley, 1989.

[143] Z. Michalewicz, *Genetic algorithms+ data structures= evolution programs*. Springer Science & Business Media, 2013.

[144] T. Back, "Selective pressure in evolutionary algorithms: A characterization of selection mechanisms," in *Proceedings of the first IEEE conference on evolutionary computation. IEEE World Congress on Computational Intelligence*. IEEE, 1994, pp. 57–62.

[145] K. Jebari and M. Madiafi, "Selection methods for genetic algorithms," *International Journal of Emerging Sciences*, vol. 3, no. 4, pp. 333–344, 2013.

[146] Statistics Bureau of Japan. "2016 survey on time use and leisure activities," sept. 15, 2017. [Online]. Available: https://www.e-stat.go.jp

[147] ISO New England. "final five-minute regulation clearing prices," feb. 20, 2021. [Online]. Available: https://www.iso-ne.com/isoexpress/web/reports/pricing/-/tree/ancillary-final-five-minute-rcp

[148] T. Masuta and A. Yokoyama, "Supplementary load frequency control by use of a number of both electric vehicles and heat pump water heaters," *IEEE Transactions on smart grid*, vol. 3, no. 3, pp. 1253–1262, 2012.

[149] E. F. Camacho and C. B. Alba, *Model predictive control*. Springer science & business media, 2013.

[150] T. Jakaša, I. Andročec, and P. Sprčić, "Electricity price forecasting - ARIMA model approach," in *2011 8th International Conference on the European Energy Market (EEM)*. IEEE, 2011, pp. 222–225.

[151] A. J. Conejo, M. A. Plazas, R. Espinola, and A. B. Molina, "Day-ahead electricity price forecasting using the wavelet transform and ARIMA models," *IEEE transactions on power systems*, vol. 20, no. 2, pp. 1035–1042, 2005.

[152] D. Singhal and K. Swarup, "Electricity price forecasting using artificial neural networks," *International Journal of Electrical Power & Energy Systems*, vol. 33, no. 3, pp. 550–555, 2011.

[153] PJM Interconnection. "ancillary service market results," april. 15, 2021. [Online]. Available: https://dataminer2.pjm.com/feed/reserve_market_results/

[154] G. E. Box, G. M. Jenkins, G. C. Reinsel, and G. M. Ljung, *Time series analysis: forecasting and control*. John Wiley & Sons, 2015.

[155] E. Mortaz and J. Valenzuela, "Optimizing the size of a V2G parking deck in a microgrid," *International Journal of Electrical Power & Energy Systems*, vol. 97, pp. 28–39, 2018.

Research Achievements

Conference Presentations & Proceedings

1. S. Cai, and R. Matsuahshi,“A Compensation Method for Electric Vehicle Aggregators with Communication Delays in Frequency Regulation Service,” *UT-SNU Joint Seminar in Electrical Engineering*, Seoul, South Korea, May, 2019.

2. S. Cai, and R. Matsuahshi,“A Control Method for Compensating Communication Delays in Load Frequency Control,”第 *38* 回エネルギーシステム・経済・環境コンファレンス, Tokyo, Japan, Aug. 2019.

3. S. Cai, and R. Matsuahshi,“Communication Delay Compensation by Adaptive Parameter Estimation for Electric Vehicle Aggregators Joining Load Frequency Control,” *2020 IEEE 8th International Conference on Smart Energy Grid Engineering (SEGE)*, Oshawa, ON, Canada, Aug. 2020, pp. 33-38.

Publications

1. S. Cai, and R. Matsuahshi,“A Control Method for Compensating Communication Delays in Load Frequency Control,” *Journal of Society for Energy and Resources*, vol. 41, no.1, pp. 1-10, Jan. 2020.

2. S. Cai, and R. Matsuahshi,“Model Predictive Control for EV Aggregators Participating in System Frequency Regulation Market,” in *IEEE ACCESS*, vol. 9, pp. 80763-80771, Jun. 2021.

3. S. Cai, and R. Matsuahshi,“Optimal Dispatching Control of EV Aggregators for Load Frequency Control with High Efficiency of EV Utilization,” in *Applied Energy* (Under review).

Patent Application

1. 電気自動車が系統負荷周波数制御を参加する場合で起きた通信遅延を補償する制御方法の設計 (出願済).

2. EV への周波数制御信号の配分方法 (出願中).